FLOW PATTERNS OF OIL-WATER IN PRODUCTION PIPELINES AND EFFECT OF INTERNAL TURBULATORS

BY

ABDULLAH MISFER AL-OTAIBI

A Thesis Presented to the

DEANSHIP OF GRADUATE STUDIES

KING FAHD UNIVERSITY OF PETROLEUM & MINERALS

DHAHRAN, SAUDI ARABIA

In Partial Fulfillment of the
Requirements for the Degree of

MASTER OF SCIENCE

In

MECHANICAL ENGINEERING

JULY, 2011

KING FAHD UNIVERSITY OF PETROLEUM & MINERALS
DHAHRAN, SAUDI ARABIA

DEANSHIP OF GRADUATE STUDIES

This thesis, written by **ABDULLAH MISFER AL-OTAIBI** under the direction of his Thesis Advisor and approved by his Thesis Committee, has been presented to and accepted by the Dean of Graduate Studies, in partial fulfillment of the requirements for the degree of **MASTER OF SCIENCE IN MECHANICAL ENGINEERING.**

Thesis Committee

Dr. Mohamed A. Habib
Thesis Advisor

Dr. Rached Ben-Mansour
Co-advisor

Dr. Amro A. Al-Qutub
Department Chairman

Dr. Zuhair M. Gasem
Member

Dr. Salam Zummo
Dean of Graduate Studies

Dr. Abdelsalam AL-Sarkhi
Member

18/7/2011
Date

Dr. Wael Ahmed
Member

In the Name of Allah, Most Gracious, Most Merciful

Dedicated to My Beloved Family (Wife, Sons: Turki and Talal, and Daughters: Arwa and Shadha)
whose constant prayers, sacrifice and inspiration led to this wonderful accomplishment

ACKNOWLEDGEMENTS

In the name of Allah, Most Gracious, Most Merciful

All praise and gratitude are due to Allah (subhana wa taala) for bestowing me with health, knowledge and patience to complete this work.

I would like to extend my appreciation and my gratitude to all those who contributed to the completion of this work. First, I am grateful to my advisor Dr. Mohamed A. Habib and the co-advisor Dr. Rached Ben-Mansour for their continuous personal support and advices in the development of this study. Thanks are also due to Dr. Abdelsalam AL-Sarkhi, Dr. Wael Ahmed and Dr. Zuhair Gasem for being my thesis committee and for their valuable support and suggestions.

Thanks are due to KFUPM for facilities and available resources. Thanks are to the ME department Chairman Dr. Amro A. Al-Qutub for his usual support. I am also thankful to the department secretaries: Lateef, Thomas and Jameel for their assistance

Great thanks are extended to Saudi Aramco presented in the Career Development Department (CDD) and the Consulting Services Department (CSD) employees and management for allowing study time, continuous support and appreciation. Special thank is due to the previous Manager of CSD, Mr. Nasser A. Al-Wohaibi who really provided wonderful support and good memories of encouragements.

Finally, thanks are due to my Father, Mother, Brothers and Sisters. Special thanks are to my Wife and my Children for their emotional and moral support throughout my academic and work career and also for their love, patience, encouragement and prayers.

TABLE OF CONTENTS

LIST OF TABLES

LIST OF FIGURES

THESIS ABSTRACT (English)

Name: **ABDULLAH MISFER AL-OTAIBI**

Title: Flow Patterns of Oil-Water in Production Pipelines and Effect of Internal Turbulators

Major Field: **MECHANICAL ENGINEERING**

Date of Degree: **May, 20011**

Oil-water two-phase flows are commonly found in petroleum industry with the possibility of having dissolved corrosive gases. Even though oil and water transport simultinously, they natuarally get separated in the pipelines before reaching the separation plant and cause internal pipelines corrosion. The objective of the present research is to numerically evaluate some design and operation parameters effecting the separation of oil and water and measure their effect in terms of water holdup and flow patterns change.

The evaluation covered the pipe length to diameter ratio (L/D) in the range from 29.7 to 58.8 and the Reynolds numbers for the inlet mixture in the range from $6.37x10^3$ to $1.59 x10^5$ based on different variables related to operation, oil properties and piping geometries. The work is compared to a base case selected according to normal operation and design application in Saudi Arabian Oil Company (Saudi Aramco). The base case has an oil and water mixture flow in a horizontal pipe of 15.4 cm (6 inch) inner diameter. The mixture is of Arabian oil of API 39 and 30% water cut. The oil density is 830 kg/m^3 and the viscosity is 2.0 cP. The water density is 998.2 kg/m^3 and the viscosity is 1.0 cP. The inlet mixture flow rate is assumed to be at a velocity of 1.0 m/s minimum velocity as recommended by Saudi Aramco standards. The different variables are: operating conditions including: mixture inlet velocities

of 0.5, 1.0 and 2.0 m/s and water cuts of 20, 30 and 50% WC, oil physical properties including: densities of 662, 830 and 998.2 Kg/m^3 and viscosities of 2.0, 15.0 and 30.0 cP and pipeline geometry including: inner diameter size of 10.2, 15.4 and 20.2 cm, pipe inclinations of 0, 15^o upward and 15^o downward and two types of internal turbulators (Type A and B).

The outcomes of the present research are compared to the available experimental data that are conducted for identical design conditions as the present work as applicable to show good agreement in terms of different flow patterns and water holdup. The present research show that increasing mixture velocity, oil viscosity and pipe diameter results in more mixing area of oil and water and less water holdup. It also shows that increasing water cuts and upward inclined flow result in more water holdup. The downward inclined flow shows less water holdup. The reported flow patterns in the present work range are: Segregated, Semi-segregated, Semi-mixed, and Semi-dispersed. As free water at the pipe bottom is a source of corrosion, all operation and design parameters that can enhance water separation should be considered in the design stage and controlled during normal operation. One method of mitigating corrosion is to use inhibitors. However, different inhibitors require different specific flow pattern for better effectiveness. Internal turbulators might be a good tool to create certain flow patterns that can be suitable to inject the right inhibitors at the right environment and that requires conducting further investigation in this field. Mitigating corrosion will contribute in reducing the corrosion that costs the Kingdom of Saudi Arabia industry about $1.4 billion a year [Tems and Al Zahrani, (2006)].

MASTER OF SCIENCE DEGREE
KING FAHD UNIVERSITY OF PETROLEUM AND MINERALS
Dhahran, Saudi Arabia

THESIS ABSTRACT (Arabic)

الملخص

الاسم: عبدا لله مسفر العتيبي

عنوان الرسالة: أنماط مزيج النفط و الماء الجاري في الأنابيب المستخدمة للإنتاج وتأثير أدوات الخلط الداخلية

التخصص: الهندسة الميكانيكية

تاريخ منح الدرجة: جمادى الثاني 1432هـ

يُضخ الزيت الخام (النفط) والماء غالباً معاً في أنابيب الحديد من أبار و حقول النفط المختلفة بالإضافة إلى ما تحمله من بعض الغازات المسببة لتأكل الحديد كممارسة شائعة في صناعة البترول. بالرغم من ضخ النفط والماء معاً إلا أن الخليط يبدأ بالانفصال تلقائياً داخل الأنابيب قبل وصولها المعمل المخصص لفصل كل مادة على حدة , إلى زيت, ماء, غازات, الخ. هذا الانفصال المبكر للخليط داخل الأنابيب يتسبب في تأكل الأنابيب من الداخل مما أدى إلى إجراء هذه البحث الذي يهدف إلى دراسة بعض العوامل ومعرفة مدى تأثيرها على تسارع انفصال الماء عن الزيت و تجمعه في قاع الأنابيب مستخدماً الحسابات العددية. يقاس تأثير كل عامل عن طريق حساب كمية الماء المتجمع في قاع الأنبوب و تغير أنماط الخليط تبعاً لتغير العوامل.

غطت الدراسة الأنابيب التي نسبة قطرها إلى طولها (ط/ ق) يتراوح بين 29.7 إلى 58.8. كما شملت الدراسة عدد تمييز ديناميكية السوائل (رقم رينولدز) للخليط عند مدخل الأنبوب والذي يتراوح بين 6.37×10^3 إلى 1.59×10^5 وذلك من خلال التطرق لثلاثة أنواع من المتغيرات لتشمل حالة التشغيل ، الخصائص الفيزيائية للنفط و الأنابيب الحاملة للنفط. وتم التحقق من أثر هذه

المتغيرات بمقارنتها بالحالة التي تم تحديدها كحالة أساسية وفقا للاستخدامات في المعامل النفطية كما في شركة آرامكو السعودية. تستخدم الحالة الأساسية لنقل النفط والماء أنبوب أفقي قطره الداخلي 15.4 سم (6 بوصة). كما أُختير الخليط من الزيت العربي الخام الخفيف ذو معامل درجة كثافة 39 API ويحتوي على نسبة من الماء تقدر بـ 30٪. حيث أن كثافة الزيت تقدر بـ830 كجم/ م^3 واللزوجة 2.0 ملي باسكال.ث. وتقدر كثافة الماء تقدر بـ998.2 كجم/ م^3 واللزوجة 1.0 ملي باسكال.ث. كما حُددت سرعة الخليط عند مدخل الأنبوب بـ 1.0 م/ث كأقل سرعة لهذا النوع من السوائل تبعاً للمراجع الخاصة بآرامكو السعودية. المتغيرات المختلفة التي من خلالها تم التحقق من تغيرات أنماط الخليط تكون تبعاً للآتي: ظروف التشغيل و تشمل: سرعة الخليط الداخل (0.5, 1.0 و 2.0 م/ث) و نسبة الماء الداخل (20, 30 و 50 %). وكذلك الخواص الفيزيائية للنفط وتشمل: الكثافة (662, 830 و 998.2 كجم/ م^3) و اللزوجة (2.0, 15.0 و 30.0 ملي باسكال.ث). وأخيراً هندسة الأنابيب وتشمل: مقاس القطر الداخلي (10.2, 15.4, 20.2 سم) , انحدار الأنابيب ليشمل:(أنبوب أفقي (0 درجة),أنبوب مائل إلى الأعلى (15 درجة), و إلى الأسفل (15 درجة). كذلك تمت دراسة تأثير نوعين من أجهزة الخلط (نوع A ونوع B) المثبتة داخل الأنابيب.

تمت مقارنة نتائج هذا البحث مع الأعمال العملية السابقة المتواجدة للحالات المماثلة. بالرغم من ندرة الاعمال المماثل التي تهتم بتأثير كل عامل على حدة. ألا إن النتائج الحالية كانت مطابقة إلى حد كبيرا للأعمال العملية المتواجدة للحالات المماثلة حول ما تم التوصل إليه من نتائج متعلقة بأنماط الخليط وكمية الماء المتجمع في قاع الأنابيب. الدراسة الحالية بينت إن زيادة سرعات الخليط الداخل, زيادة لزوجة النفط وزيادة قطر الأنابيب يزيد منطقة التمازج بين الماء و النفط وتقليل إمكانية انفصال الماء وتجمعه في قاع الأنبوب. وتبين أيضا أن كلاً من زيادة نسبة المياه الداخلة مع النفط وتدفق الخليط باتجاه ميلان الأنبوب للأعلى يزيد تراكم المياه في قاع الأنابيب. بينما تبين إن تدفق

الخليط للأسفل باتجاه ميلان الأنبوب يقلص تكدس المياه في قاع الأنابيب. بين العمل الحالي شكل أنماط الخليط المختلفة والتي قد تحدد سلوكيات تدفق الخليط بناءَ على ظروف التشغيل و حالات التصاميم المختلفة والتي يمكن تلخيصها كالأتي: أنماط منفصلة, شبه منفصلة وشبه مختلطة, و أنماط ممزوجة. وبما إن انفصال المياه في قاع الأنابيب يكون مصدراً أساسيا لتآكل الأنابيب فيجب العمل على تخفيضها وعمل الاحتياطات الأزمة إثناء التصميم لاستيعاب جميع احتمالات التشغيل المختلفة التي قد تسبب انفصال الماء في الأنابيب. هناك مواد معروفة في الصناعة يمكن استخدامها لحماية الأنابيب ضد التآكل ولكن تحتاج البيئة (النمط) المناسبة للتمكن من حُسن فعاليتها. حيث اظهر استخدام أدوات الخلط الثابتة أنه من الممكن خلق بعض أنماط المزج التي يمكن الاستفادة منها كبيئة مناسبة لإضافة مواد حماية الأنابيب ضد التآكل و هذا ما قد يتطلب إجراء بعض التجارب في هذا المجال. أهمية البحث في عملية نقل الماء و الزيت الخام تهدف إلى السيطرة على انفصال الماء في الأنابيب و تخفيف تكلفة التآكل الناتج عن هذا الانفصال حيث يكلف التآكل الصناعة في المملكة العربية السعودية ما يقارب 1.4 مليار دولار سنوياً.

هذه الدراسة أعد ت لنيل درجة الماجستير في العلوم
جامعة الملك فهد للبترول والمعادن
الظهران, المملكة العربية السعودية

NOMENCLATURE

a	Arc length
A	Pipe cross-sectional area of inner diameter, D, (= $A_o + A_w$)
A_b	Cone base area
A_o	Pipe cross-sectional area occupied by oil phase
A_{r2}	Area outside the outer hollow cone
A_{r3}	Area inside the outer hollow cone
A_w	Pipe cross-sectional area occupied by water phase
A_{sw_n}, A_{sw_b}	Surface area wetted with free water, n: any case, b: base case
A1	Cross section area upstream turbulator
B	Pipe inclinations from horizontal line
B1	Gap between inner diameter of the pipe and the outs side diameter hollow cone, fixed to 10 mm
c	Cord representing water to mixing zone interface
CeS-n, CeS-b	Corrosion exposed surface area to free water, n: any case, b: base case
CR	Corrosion rate
$C_{1\varepsilon}, C_{2\varepsilon}, C_{3\varepsilon}, C\mu$	Empirical constants in the $k-\varepsilon$ turbulence model
D, ID	Pipe inner diameter [m]
Do/w&w	Dispersed oil in water and water layer
Do/w&Dw/o, o/w	Dispersed oil in water and dispersed water in oil and layers of oil and water
Do/w&w/o)	Dual dispersion or dispersed flow of equal dominated
Dw/o&o	Dispersed water in oil and oil layer
D_{32}	Sauter mean diameter (SMD) of droplets

D_{pq}	Mean droplet diameter, where p and q are the parameters used depending on the type of mean diameter required, for comparison p = 3 and q = 2.
D_i^p , D_i^q	Random droplet diameter of power p or are parameters used depending on the type of mean diameter required, for comparison p = 3 and q = 2.
D_b, r_b	Cone base diameter, radius
D_{r2}	Outside diameter of the outer hollow cone
D_{r3}	Inside diameter of the outer hollow cone
D_{r3e}	Effective base diameter of D_{r3}
D_{be}	Effective base diameter
D_{ij}^L	Molecular diffusion term in equation
D_{ij}^T	Turbulent diffusion term in equation
E20/32/300	E in such designation refers to number of meshes per edge
F, D	Represent the convective mass flux per unit area and diffusion conductance at cell faces
F	Dimensionless function
f	friction factor (Fanning) [fraction]
fMs	Moody pipe static friction factor [fraction]
fMRI	Moody perforated pipe friction factor with influx [fraction]
fo	Fractional flow of oil [fraction]
$f$tp	Two-phase flow friction factor [dimensionless]
fT	Total friction factor [dimensionless]
fw	Wall friction factor [dimensionless]
fw	Fractional flow of water [fraction]
g	Acceleration due to gravity [m/s^2]
G	Mixture mass flux (W/A)
G_b	Production of turbulent kinetic energy due to buoyancy
G_k	Production of turbulent kinetic energy due to mean velocity gradient

h, h_n	Represent the water height from the pipe bottom
H_w	Water holdup (local), the amount of water separates at the bottom.
H_o	Oil holdup
k	Kinetic energy of turbulence
L	Pipe length [m]
L_f	Proposed final pipe length (m)
L_p	Location of present test planes (m)
L_1	Inlet water partition height (m)
L_2	Water accumulation height measured from the pipe bottom (m)
n	Difference between V_1 and V_2 downstream and upstream turbulator
N/A	Not applicable
N_i	Number of droplets in size range
OD	Pipe outer diameter
p	Pressure
P_n	Nodal point
P_{ij}	Stress production term in equation
p^*, p	Pressure field assumption and correction pressure field
p'	Difference pressure between the correct pressure field and the assumed pressure field, ($p = p^* + p'$)
Pr	Prandtl number
Q	Mixture volumetric rate (= Q_o + Q_w)
Q_o	Oil phase inlet volume fraction
Q_w	Water phase inlet volume fraction, called water cut (WC/100)
r	Radius of the pipe

Re_m	Mixture Reynolds number at the inlet conditions
S_ϕ	Source of ϕ per unit volume
S	Slip ratio factor based on the ratio of oil to water velocities
V	An arbitrary control volume
V_m	Mixture-averaged velocity for the mixture at the inlet
V_{wo}	Slip velocity of water in relative to oil
V_w	Average water velocity
V_o	Average oil velocity
V_{Sw}	Superficial velocity of water phases
V_{So}	Superficial velocity of oil phase
V_1	Fluid velocity upstream turbulator
V_2	Mixture velocity leaving the turbulator
$u^*,\ v^*$	Velocity components
v	Velocity vector ($u\,\hat{i} + v\,\hat{j}$)
$\bar{u}$, $\bar{v}$	Time average velocity
u' , v'	Fluctuating components of velocity
W	Mixture mass flow rate ($=W_o + W_w$)
WC	Water cut, water quantity defined at the pipeline inlet as volume percentages of the total inlet volumetric rate
W_o	Oil phase mass flow rate
W_t	Weight loss of pipe metal
W_w	Water phase mass flow rate
W, E, N, S	Nodes of the west, east, north and south, respectively.
w, e, n, s	west, east, north and south of control volume face side respectively.
x	x- co-ordinate

Xn	Portion of pipe length (m)
Xp	Proposed test location (m)
X0, X1, .. X6	Location of perpendicular planes to the flow direction at 0, 1000, …. 6000 mm from inlet

Greek Symbols

β	Inclination angle
ε	Rate of dissipation of the kinetic energy
∇	Gradient
ΔN_i	Total number of droplets in size range
$\Delta x = \delta\ x_{we}$, $\Delta y = \delta\ y_{ns}$	Widths of the control volume.
μ	Viscosity for a phase of water or oil
μ_m	Mixture viscosity at the inlet
$\mu_w\ \mu_o$	Water and oil viscosity, respectively
μ_t	Turbulent dynamic viscosity
ρ	Density for a phase of water or oil
ρ_0	A reference density at 0^o for a phase of water or oil
ρ_m	Mixture density at the inlet
ρ_{metal}	Pipe material density
ρ_w, ρ_o	Water and oil density, respectively
$\hat{\rho}_q, \rho_q$	Effective and total density of a phase (q)
ϕ	General field variable represented in the transport equations
Γ_ϕ	Diffusion coefficient for ϕ
δ	liquid film thickness (m)

δx_{WP}	Distance between the nodes W and P
μ_α	α-phase dynamic viscosity (kg/m s)
μ_e	Effective viscosity (kg/m s)
θ	Angle representing water to pipe interface
ρ_α	density of α-phase (kg/m^3)
κ	Von karman constant
μ	Laminar viscosity
μ_t	Turbulent viscosity
ν	Molecular kinematic viscosity
σ_k	Prandtl number for k
σ_ε	Prandtl number for ε
τ_w	Wall shear stress

Subscripts/superscripts

B^+	constant
F_{ij}	drag force between phases i and j (N/m^3)
i, j	Spatial coordinate indices
Grad	Gradient = ∇
o	Outlet condition
n	Nodal point
ref.	Reference

CHAPTER 1

INTRODUCTION

1.1 Background

Oil-water two-phase flows are commonly found in petroleum industry with possibility of having dissolved corrosive gases that are transferred in pipelines as a mixture flow from wells to a central gathering plant [Vedapuri et al. (1997)]. It is not practical to separate the mixture at the well site, especially for remote areas. For an economical reason, the mixture from several wells is transported to a central gathering plant where separation takes place. Corrosive gases, such as, carbon dioxide and sulfur dioxide originally exist in the reservoir specially in Arabian Gulf as reported by Nyborge (2005). However; carbon dioxide and salt water are sometimes pumped down the well to enhance oil and gas production and maintain pressure within the reservoir as the well ages. Moreover, oil and water get seperated in the pipelines before reaching the separation plant based on different parameters.

There are two definitions of water contents in the two-phase flow of oil and water. The water quantity defined at the pipeline inlet as volume percentages of the total inlet volumetric rate is called water cut (WC). Unfortunately, this water content is usually the basis for pipelines and equipment design. During transportation of the mixture, water in

the system starts separation and accumulates at the pipe bottom and that amount of water is called local water contents, local water or water holdup. Holdup is defined as the ratio of the volume of water to the total volume of the liquid as a local content at the point of concern.

So at different operating conditions, water concentrates at certain locations along the pipe which creates different water holdup profiles and pressure gradients as explained by Habib et al. (2005). The presence of water and salts as well as carbon-dioxide in petroleum products is the main cause of carbon steel pipelines corrosion during oil transportation and storage. Since H_2S and CO_2 can be dissolved in water to form weak carbonic acid and cause high corrosion rate in carbon steel pipelines. Usually at low water cut, the corrosive water does not create problems where water is fully dispersed in oil. However, it was reported by Cai et.al (2004) that there are cases with water contents of 2% where failure occurred.

Many oil wells operate at different water cuts, as high as 90%, which result in different flow structures. As water cut increases, water droplets start to coalesce and phase separation of oil and water occurs. In horizontal or near horizontal pipes, the two-phase flow along the pipe with water flowing at bottom of the pipe and oil at the top due to difference in densities. As each phase wets part of the pipe, therefore, the possibility of corrosion is high when water phase is in contact with the pipe wall. Therefore; it is important to understand the two-phase oil-water behavior in production pipelines and predict structure and the resulting (flow patterns) and consequently control the piping corrosion.

Definitions and parameters

a) Water holdup (Hw)

Water holdup (local) is the amount of water separates at the bottom of the pipe leading to localized water contents different from inlet water content. The bottom line is that with an identical inlet water cut, the local water fraction (water holdup) can vary along the pipe depending on the design and operation conditions. The water holdup contents is influenced by different factors related to fluid physical properties, operation condition and piping geometry as explained more in the following sections. Water holdup can be calculated and there are different parameters to give an indication of water holdup as coming.

- The oil and water holdups have a direct geometric relationship to the phases' height, h, inside the pipe which is defined as the vertical distance from the bottom of the pipe to different locations inside the pipe.

  ✓ In stratified flow, water holdup is the fraction of the cross section area occupied by water. The water holdup can formulated as:

$$H_W = \frac{A_w}{\frac{\pi}{4} D^2} \qquad (1.1)$$

Where, Aw, divided by the total cross-sectional area of the pipe of diameter, D.

- ✓ A similar term is the oil holdup.

$$H_o = \frac{A_o}{\frac{\pi}{4} D^2} \tag{1.2}$$

It is defined as the cross-sectional area occupied by the oil phase, Ao, divided by the total cross-sectional area of the pipe of inner diameter, D.

- For two phase flow with mixing zone, the no-slip water (WC) and the slip ratio factor which is water holdup indication (S) both are used to identify the water holdup and slip condition.
  - ✓ The relationship between local water content (holdup, Hw) and the velocity ratio between the phases (slip ratio, S) is given as:

$$H_W = \frac{\frac{WC}{100} S}{1 + \frac{WC}{100}(S-1)} = \frac{WC * S}{100 + WC(S-1)} \tag{1.3}$$

- Slip velocity is the difference between water velocity and oil velocity:

$$Vwo = Vw - Vo \tag{1.4}$$

- It is also used as an indication of water holdup. This formula is selected so that oil-water slip velocity is always positive when water holdup increases per location. Based on the pipe orientation and flow conditions, both positive and negative slip scenarios are possible regarding which phase moves faster, water or oil. In the region of dispersed flow pattern, the slip effect is negligible [Rojas-Figueroa and Fairuzov (2002)].

b) Common variable parameters

There are several common variables that are defined for multiphase flows to describe the system and the flow regimes. Here, these terms are defined as they are used or mentioned in this work.

- The mixture mass flux, G, is simply the ratio of the given mixture mass flow rate, W, to the respective pipe cross-sectional area of inner diameter, D:

$$G = \frac{W}{A} = \frac{W}{\frac{\pi}{4} D^2} \tag{1.5}$$

- The mixture volumetric rate, Q, may be composed of two volumetric rates, one for the oil phase (Q_o) and one for the water phase (Q_w), water volume fraction. The inlet water fraction called in this work water cut (WC) can be defined as:

$$WC = \frac{Q_w}{(Q_w + Q_o)} \times 100 \tag{1.6}$$

- The mixture data:

  - ✓ Mixture density: $\rho_m = (\frac{WC}{100})(\rho_w - \rho_o) + \rho_o$ (1.7)
  - ✓ Mixture viscosity: $\mu_m = (\frac{WC}{100})(\mu_w - \mu_o) + \mu_o$ (1.8)
  - ✓ Mixture velocity at the inlet:

$$V_m = \frac{WC \times \rho_w V_w + (100 - WC)\rho_o V_o}{100 \times \rho_m} \tag{1.9}$$

✓ The generalized Reynolds number at the inlet conditions is calculated as:

$$\mathrm{Re}_m = \frac{\rho_m V_m}{\mu_m} \qquad (1.10)$$

- The velocity of a particular phase can be described in different ways.

✓ The superficial velocities of the phases, water and oil, are defined as the velocities of the phases averaged over the entire cross-sectional area of the pipe, as though each phase was flowing in the pipe without the presence of the other:

➢ Water superficial velocity: $V_{Sw} = \dfrac{W_w}{\rho_w \dfrac{\pi}{4} D^2}$ (1.11)

➢ Oil superficial velocity: $V_{So} = \dfrac{W_o}{\rho_o \dfrac{\pi}{4} D^2}$ (1.12)

✓ The mean velocities of the phases, water and oil, are averaged over the cross-sectional area of the relevant phase: where $A = A_o + A_w$.

Along the pipe:

➢ Water velocity or average velocity:

$$V_w = \frac{W_w}{\rho_w A_w} = \frac{V_{Sw}}{H_w} \qquad (1.13)$$

➢ Oil velocity or average velocity:

$$V_o = \frac{W_o}{\rho_o A_o} = \frac{V_{So}}{H_o} = \frac{V_{So}}{1 - H_w} \qquad (1.14)$$

At pipe inlet:

- Water velocity or average velocity:

$$V_w = \frac{W_w}{\rho_w A_w} = \frac{100 V_{Sw}}{WC} \tag{1.15}$$

- Oil velocity or average velocity:

$$V_o = \frac{W_o}{\rho_o A_o} = \frac{V_{So}}{H_o} = \frac{100 V_{So}}{100 - WC} \tag{1.16}$$

c) Flow patterns and flow patterns map

Name of flow patterns of two-phase flow oil-water flowing in pipelines can change from researchers to others. However, the definition of each flow pattern is the same for all. The flow structure map is a map built as a result of multiphase contours that presents the flow pattern change according to different parameters. Some definitions of different type of flow patterns in the field of oil-water two-phase flow are as follows:

1. **Annular flow**: one fluid forms an annular film on the pipe wall and the other flows in the pipe centre. This flow structure is common when the two liquids have equal densities or when one liquid has large viscosity.
2. **Continuous phase**: the phase that coats the pipe wall in a continuous pure layer.
3. **Dominant phase**: equivalent to the continuous phase.
4. **Dispersed flow**: one fluid is continuous and the other is in the form of drops dispersed in it. The phase that is entrained in the continuous phase, is called a

"dispersed" or the "internal" phase, (Do/w&w, Dw/o&o, Do/w&Dw/o, o/w or w/o flows). Oil and water are totally mixed (though concentration gradients may persist).

5. **Dual continuous flow**: This pattern is known as 3L and appeared at intermediate mixture velocities between stratified and dispersed flows and resulted in pressure gradients less than those of single phase oil flow (Lovick and Angeli 2004).
6. **Dual dispersion (D o/w&w/o), or dispersed flow of equal dominated**: in this flow pattern, two different layers occur. Both phases are present across the entire pipe, but at the top the continuous-phase is the oil, containing droplets of water. In the lower region of the pipe, the continuous-phase is water and the oil exists as dispersed droplets.
7. **Emulsion**: a dispersion of droplets of one liquid in another one with which it is incompletely miscible. In emulsions the droplets often exceed the usual limits for colloids in size.
8. **Fully dispersed**: the oil and water become fully dispersed and the mixture flows as a homogeneous phase without appreciable changes in concentration in pipeline.
9. **Homogeneous:** at high mixture velocity, oil and water flow as a homogeneous phase without appreciable variation in concentration across the pipe diameter.
10. **Fully dispersed = homogeneous.**
11. **Mixed flow**: occurs when the oil-water dispersion occupies more than half the pipe volume.
12. **Segregated flow**: the flow of the liquids in two distinct layers. Segregated flow patterns include:
    - **Stratified flow and stratified flow with some mixing at the interface**.

13. **Semi-dispersed:** at high mixture velocity, oil and water are totally mixed with some sharp steep gradient of fluid concentration in the mixture.
14. **Semi-segregated flow**: as the mixture velocity is increased, some mixing occurs at the interface giving rise to semi-segregated flow.
15. **Semi-mixed flow**: the flow is said to be semi-mixed when there is a segregated flow of dispersion and a 'free' phase and the dispersion volume is less than half the total pipe volume. The flow can be in three segregated layers, with dispersion in the middle and two pure phases at the top (oil) and the bottom (water). Or it is segregated into dispersion and a pure phase. In both cases the dispersion volume is less than half of the total pipe volume.
16. **Stratified flow (ST):** In this flow pattern the two liquid phases flow as layers with the heavier (usually water) at the bottom and the lighter (usually oil) at the top.
17. **Stratified flow with mixing at the interface (ST&MI):** In this flow pattern the system tends to be stratified, but interface instability generates a mixing zone. The mixing zone at the interface can be significant, but still pure fluids exist at the top and the bottom of the pipe. So it can named segregated flow.
18. **3L phase**: Increasing velocity beyond ST flow results in interfacial waves appears at the interface to form water droplets in the oil layer and oil droplets in the water layer. This pattern is known as dual continuous flow or (3L).
19. **Wavy flow**: similar to stratified flow, but with a wavy interface resulting from a higher slip velocity between the two phases.

1.2 Design of Production Pipelines

Production pipelines consist of pipelines above ground, as shown in Figure 1.1, that are used to transport oil-water two phase flows from the well-head to the central gathering plant. The oil-water is usually transported through two parallel types of pipelines; one for products testing and the other for product processing. The typical crude oil production systems from the wells to the separation plants are shown in Figure 1.2 and have the following special features:

- The lines run horizontally on the surface of the ground most of the time.
- The lines are normally of large diameter
- The lines run normally at low pressures and temperature.
- The lines have special configuration and names as follows:
    - The main lines run in parallel for long distance and collect the wells' production even from different reservoirs. These lines are called trunk-lines and test-lines.
    - The lines carrying the production from the wells to the trunk-lines or test lines are called flow-lines.
    - Different trunk-lines are connected into a line existing in each separation plant called header-line or production line.

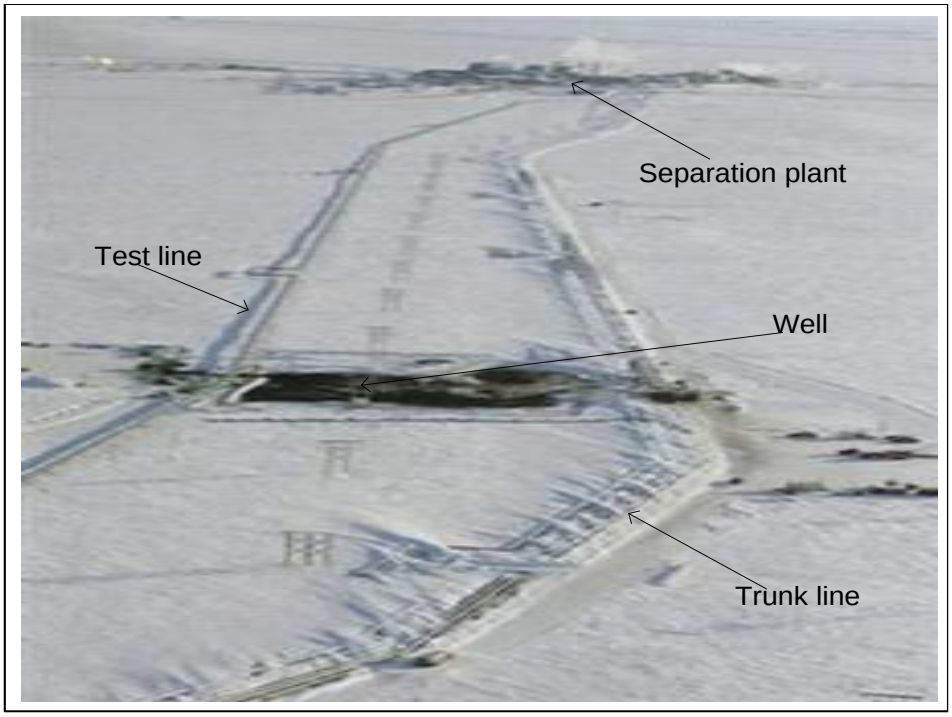

Figure 1.1: Actual oil production pipeline from well to separation plant (Doyle, 2006)

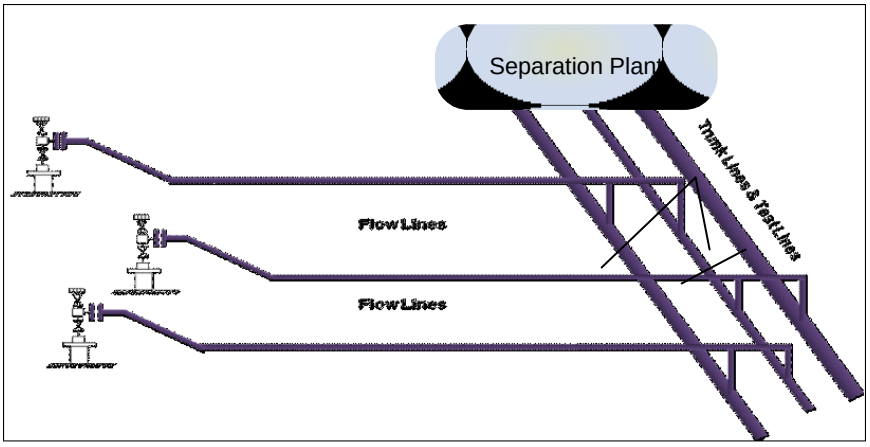

Figure 1.2: Oil pipelines from wells to separation plant (Saudi Aramco, 2005)

1.3 Flow Patterns and Influencing Parameters

Different operating conditions result in different oil-water flow patterns. The existing flow pattern in a given system depends on different parameters. The different parameter can be related to operation variables, piping geometry and fluid physical properties [Angeli & Hewitt (2000) and Bannwart et al. (2004)]. The operation variables can include volume fractions of each phase, inlet mixture velocity, pressure, temperature, etc. The geometrical variables are such as; pipe diameter, piping configurations, etc. The fluid physical properties include oil density, oil viscosity, etc. There is high contribution of these parameters affecting the multiphase flow patterns where the research in this field is not yet understood.

The majority of previous studies focused on gas-liquid flows behavior. However; the built models for the gas-liquid flows cannot be extended to the liquid-liquid flow [Shi et al (2002)]. There are differences in flow patterns between gas-liquid flows and liquid-liquid flows. The differences can be summarized in large difference between the phase's fluid densities and viscosities, and the complexity of liquid-liquid interface surface tension as highlighted by Shi et al. (2002). As gas-liquid flows have been studied extensively to produce large data sets, the two-phase liquid-liquid flows not yet being extensively studied [Shi et al. (2002)]. Concentration on stratified flow patterns due to possibility of controlling the flow and well defined interface appeared in the previous researches. The previous work published about liquid-liquid flows in horizontal pipelines shows that the dynamic characteristics of oil-water behavior are not yet fully understood. There are some studies about creating dispersed phases in pipes using direct external

stirring. However, due to its installation difficulty and high required energy, the research has not yet identified all parameters that may control the flow patterns and optimize the piping design to lower corrosion failures [Atmaca et al. (2008)].

Liquid-liquid flow patterns

As this work is to cover oil-water flows in horizontal and near horizontal pipelines, the two phases will be distributed into various flow patterns based on the different design and operation variables. Oil-water flows can generally be classified into two principal flow patterns, namely stratified (oil and water as separate layers) and mixed (the oil and water mixture flows as dispersion). As the transition occurs from stratified to completely mixed flow, different flow patterns are observed. Mixture velocity has a direct effect on the flow pattern type. Four flow patterns were observed by Ayello et al. (2008) such as; stratified flow, stratified flows with mixing layer, semi dispersed flows and fully dispersed flow. Continuous water layer is observed at low velocity which is disappeared or reduced by increasing the mixture velocity due to water entrainment to oil.

Oil-water contents

As oil-water production is the subject of this work, it is worth highlighting important factors that affect the design parameters of the piping and separation plant. There are certain factors that could play major roles to classify processing requirements, equipment type and material selection and installation for oil production; such as, oil density and viscosity, and sulfur content as well as water cut.

Physical properties of oil

The first two factors of oil are density and viscosity. The density is usually referred to degree API and specific gravity of oil. The term degree API is a scale that is established by the American Petroleum Institute and is expressed either in degree API or ^{o}API. The ^{o}API is related to the specific gravity, SG, and defined at temperature of 60^{o}F as per the following relation (1.17) [Maxwell (1975)].

$$^{o}API = \frac{141.5}{SG_{@60^{o}F/60^{o}F}} - 131.5 \qquad (1.17)$$

Accordingly, the crude oil is defined as heavy and light crude oil. The heavy crude oil is any type of crude oil which does not flow easily. It is referred to as "heavy" because its density is high. Heavy crude oil has been defined as any liquid petroleum with an API gravity less than 22°, meaning that its specific gravity is greater than 0.92. On the other hand, light crude oil is liquid petroleum that has a low density and flows freely at room temperature. It has a low viscosity, low specific gravity and high API gravity. It generally has low wax content with an API gravity exceeding 38 degrees, meaning that its specific gravity is less than 0.835. There are also extra heavy and super light crude oil. The crude oils with API gravity between 22 and 38 degrees are generally referred to as medium crude oils. The viscosity is another feature of oil. It is a measure of a fluid's resistance to flow due to the internal friction of the moving oil. Usually the heavy crude oil is very viscous. However, there is no direct relation between density and viscosity of oil due to including the oil to many substances.

Sulfur content

Sulfur content is very important factor from corrosion point of view. It is undesirable property when it appears in large quantities. Crude oil is classified as “sweet” when the sulfur content by weight is less than 0.5% and as “sour” when sulfur content by weight is greater than 0.5%.

Water Cut

The last mentioned important factor in oil production is the percentage water content or water cut (WC). The WC increase is attributed to production practice of maintaining reservoir internal pressure. As oil is produced, reservoir gets aging, and the pressure inside the reservoir drops which requires re-injecting the produced water, or injecting fresh or sea water, into the reservoir to maintain its internal pressure for stable operation. That process is called Enhanced Oil Recovery (EOR) process. CO_2 and water are found naturally in the reservoir; however; sometimes CO_2 is dissolved in water that is pumped into oil wells to enhance oil recovery.

1.4 Research Motivations

More water can be produced and the WC may reach high values ranging between 80-95% or higher depending on the production economics. Since most of wells are located in remote areas, the cost of repair, maintenance, clean up or replacement of the related pipelines is extremely high. Most of these pipelines run several hundred kilometers where the use of corrosion resistant pipe materials is not economically

feasible. Moreover, the high WC places a great economic load on oil-water separation facilities. So these facilities are subjected to internal corrosion due to corrosive water and ends with high corrosion cost due to failure as shown in Figure 1.3. The total annual cost of corrosion in oil and gas production industry in Kingdom of Saudi Arabia is estimated to be $1.4 billion that is in parallel with industrial countries [Tems and Al Zahrani (2006) and Koch et al. (2001)].

Figure 1.3: Internal pipeline corrosion

This high impact cost of wells' products transportation, operation and maintenance urgently requires great attention to reduce factors increasing water separation in the production pipelines which starts from identifying flow patterns and water holdup at different location. By considering the effect of the corrosive gases from corrosion point of view and neglect the effect of the corrosive gases on the mixture flow patterns, the oil-water flow patterns and water holdup can be identified and have an indication of controlling them by studying the effect of the following variables:

- Operation variables:
    - Water cut
    - Mixture inlet velocity
- Oil physical properties
    - Oil density
    - Oil viscosity
- Geometrical variables:
    - Pipe diameter
    - Pipe inclination
    - Internal turbulator devices

1.5 Objectives of the Present Work

The main objective of the present study is to numerically predict flow pattern type at different location that can assist mitigating internal corrosion of piping system carrying two-phase flow of oil-water for certain design variables including: operation, oil physical properties and piping geometry variables.

1.6 Thesis Organization

The thesis is organized into six (6) chapters. Chapter 1 is introduction. It includes background about multiphase flow, production pipelines, flow patterns and characteristic of oil-water flow, research motivations and the objective of this work. Chapter 2 is a literature review. It presents a brief about the research carried out in the field of oil-water flow for similar operation and design conditions. Chapter 3 is a problem description. It states the

problem and identifies the operation and design conditions for the present work. It also shows the approach and methodology of the present work to cover numerical calculation of water-and-oil separation in the pipeline, potential local water concentration (holdup) and its condition, and corrosion rate estimation.

Chapter 4 covers the result and discussions. It reviews the design parameters, grid independence and result analysis and validation with exiting experimental work. Chapter 5 covers turbulator device design and operation. It covers the type selection and design, testing and investigation of the flow patterns using the turbulators. Chapter 6 presents the conclusions and recommendations. It covers the outcome conclusions and recommendations resulted from the present work.

CHAPTER 2

LITERATURE REVIEW

Oil-water flows can be generally classified into two principal flow patterns, namely stratified (oil and water as separate layers) and mixed (the oil and water mixture flows as dispersion). As the transition occurs from stratified to completely mixed flow, temporary flow patterns are observed [Ayello et al. (2008)] as detailed below. The flow patterns were observed by Trallero et al. (1997) for different experimental oils. Mixture velocity has a direct effect on the flow pattern type. Four flow patterns were observed by Ayello et al. (2008) such as; stratified flow, stratified flows with mixing layer, semi dispersed flows and fully dispersed flow. Continuous water layer is observed at low velocity which is disappeared or reduced by increasing the mixture velocity due to water entrainment to oil.

Determination of the flow patterns is a critical problem in two-phase flow. Oil-water flow has the oil with a wide range of properties. Previous investigations in this area have been reviewed extensively by Valle (1998). The available data do not show a close agreement among the different flow patterns observed. In early experimental studies of oil-water flow in horizontal pipes, 14 different flow patterns has been reported, whereas others described only three to four different flow patterns [Russel et al. (1959), Charles et al. (1961) and Arirachakaran et al. (1989)] as reported by Xu (2007). Many researchers considered water holdup in their experimental work as a source of flow patterns changes and considered it as the

corrosion source. Coming paragraphs give an idea about previous work in the field of oil-water phase flow and how the flow patterns change based on different parameters that can be related to the fluid physical properties, piping geometries or operation conditions.

2.1 Experimental Work

Russel et a1. (1959) studied oil-water flow in a transparent horizontal pipeline using white mineral oil with a viscosity of 18 cP. They found three distinct flow patterns: bubble flow, stratified, and mixed flow. Charles et al. (1961) defined four flow patterns in their equal density oil-water flow in 2.5 cm pipes as water droplets in oil, concentric water with oil flowing in the core, oil slugs in water, and oil bubble in water. Three different oils with viscosity of 6.29, 16.8 and 65 cP were used in their studies. They found that the resulting oil-water flow patterns were mostly independent of the oil viscosities.

Arirachakaran et al. (1989) conducted extensive experimental work of oil-water flow in horizontal pipes of two different pipe sizes (25.4 mm & 38.1 mm diameter) for a very wide range of oil viscosity (4.7 to 2116-cP) to have a total of 1199 oil-water tests. The tests have mixture velocities varied from 0.46 m/s to 3.66 m/s while input water fractions ranged from 5% to 90%. The study shows different flow patterns developed for the range of different viscosity. The reported flow patterns resulted from low viscous tests as stratified phase with some mixing at the interface, mixed phase with separated layer of a dispersion and ‘free” phase, intermittent phases alternately occupying the pipe as a free phase or as dispersion and Dispersed phase flow patterns.

Vedapuri et al. (1997) studied experimentally oil-water flow in horizontal and slightly inclined (+/-2 degree) plexiglas pipes of 10 cm diameter with oil viscosity of (2 and 90 cP) and ASTM standard water. The study covered the mixture velocity from 0.1 to 2 m/s with water cut 20, 40, 60 and 80%. Different flow patterns were reported based on the viscosity of oil, flow condition and pipe orientation to have the following flow patterns: semi-segregated flow pattern, semi-mixed flow pattern and semi-dispersed. They summarized the cross-section flow patterns of three layers as shown in Figure 2.1. The semi-flow patterns (semi-segregated, semi-mixed and semi-dispersed) are called by other authors as stratified flow with mixing at the interface ST&MI or three-layer (3L).

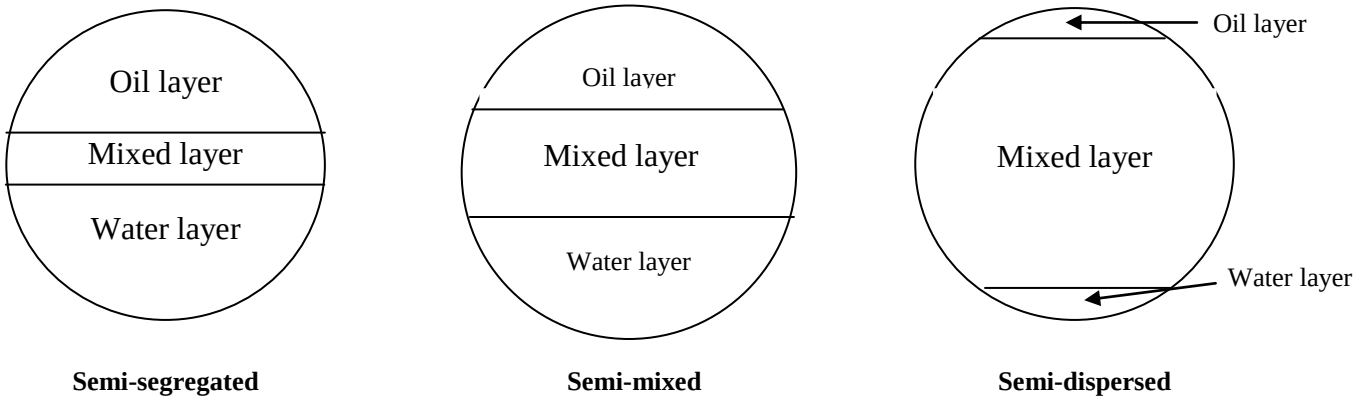

Figure 2.1: Analysis of the cross section for the three flow patterns (Vedapuri, 1997)

Shi (2001) studied experimentally the behavior of two-phase flow in a pipe (101 mm ID) of oil (820 kg/m^3 and 3cP) and water (1024 kg/m^2) and the impact of velocity (0.4 – 3.0 m/s) and water cut (0% - 100%) on local holdup and corrosion rate. The investigation of Angeli & Hewitt (2000) for the experimental work conducted for oil with 1.6 mPa.s viscosity

and 801 kg/m^3 density and water flowing in a 25.4-mm tube of stainless-steel and acrylic resin material defined a new intermediate regime, called three layers (3L) flow in which a mixed layer of oil and water is located in between the separate phases, oil and water.

Ayello et al. (2008) experimentally investigated the internal corrosion that occurs for transportation pipelines and highlighted that it is usually related to the phase wetting the pipe wall. The problem extensively studied with crude oils by identifying comprehensive flow pattern as a function of water cut, up to 20%, and flow velocities, from 0.5 to 3 m/s in a 4 inch pipe diameter. The study was based on different flow conditions for model oil and crude oil of 825 and 830 kg/m^3 respectively and different pipe inclinations in the range of 0^o to +/- 90^o. Three main flow patterns were observed for the crude oil as a function of the velocity and water cut: stratified, stratified flow with mixing layer and dispersed flow. They considered the 1.5 m/s as a critical velocity for oil-water two-phase flowing in a horizontal pipe as stratified layers disappeared. It is noticed that as velocity increases, oil wetting increases. On the other hand as water cut increases, water wetting increases. Moreover, as the pipe inclined up, the oil wetting increases accordingly the required critical velocity decreases. That is opposite to the operation in the present work and many of previous works. They justified this difference by having more mixing that reduces the effect of gravity force.

Nadler and Mewes (1997) experimentally investigated the flow of two immiscible liquids in a horizontal pipe with an inner diameter of 59 mm for oil viscosities of 22, 27 and 35 mPas. The observed flow patterns are listed below in Figure 2.2.

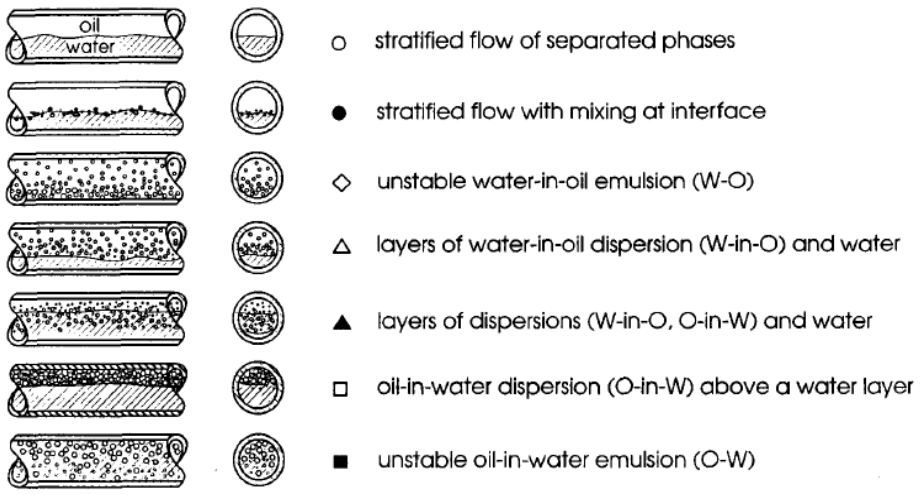

Figure 2.2: Typical flow patterns observed in the multiphase pipeline (Nadler and Mewes, 1997)

Lum et al. (2006) experimentally investigated the effect of upward ($+5^{o}$, $+10^{o}$) and downward (-5^{o}) pipe inclinations on the flow patterns, holdup and pressure gradient during oil-water phase flows for mixture velocities between 0.7 and 2.5 m/s and water fractions between 10% and 90% with oil of 5.5 mPa.s viscosity and 828 kg/m^3 density in a 38-mm tube. The investigations were to identify the different flow patterns compared to horizontal flow. A new flow pattern, like oil plug flow, appeared at both $+5^{o}$ and $+10^{o}$ inclination while the stratified wavy pattern disappeared at (-5^{o}) inclination. Moreover, they showed that the small inclination in the pipeline, as well as the size of the inclination affect the flow patterns observed in horizontal flows.

Hussain et al. (2008) experimentally studied the phase fraction of oil-water flowing in horizontal tube 25.4-mm, at certain distances from inlet for a specific range of mixture velocity and specific water volume fraction. The study reported different flow patterns of water dispersed in oil or oil dispersed in water and some entrainment in the form of drops of

phase into the other. Mandal et al. (2007) carried out experimental work to understand the influence of pipe size on the flow patterns of two immiscible liquids (water and kerosene) flowing in a horizontal pipe with indicating a marked influence of conduit size on flow patterns.

Al-Yaari et al. (2009) conducted an experimental work for oil–water flowing in a horizontal 25.4 mm pipe. Different flow patterns were observed for a wide range of mixture velocities (0.5–3.5 m/s) and input water cut (WC) on the range of 10%–90%. Six flow patterns are reported as shown in the following flow patterns map in Figure 2.3. The present work is reflected on Al-Yaari's flow pattern map in the shaded area for the velocity in the range from 0.5 to 2.0 m/s and WC in the range of 20 to 50%. The present flow patterns show good agreement to Al-Yaari' work in this range of operation.

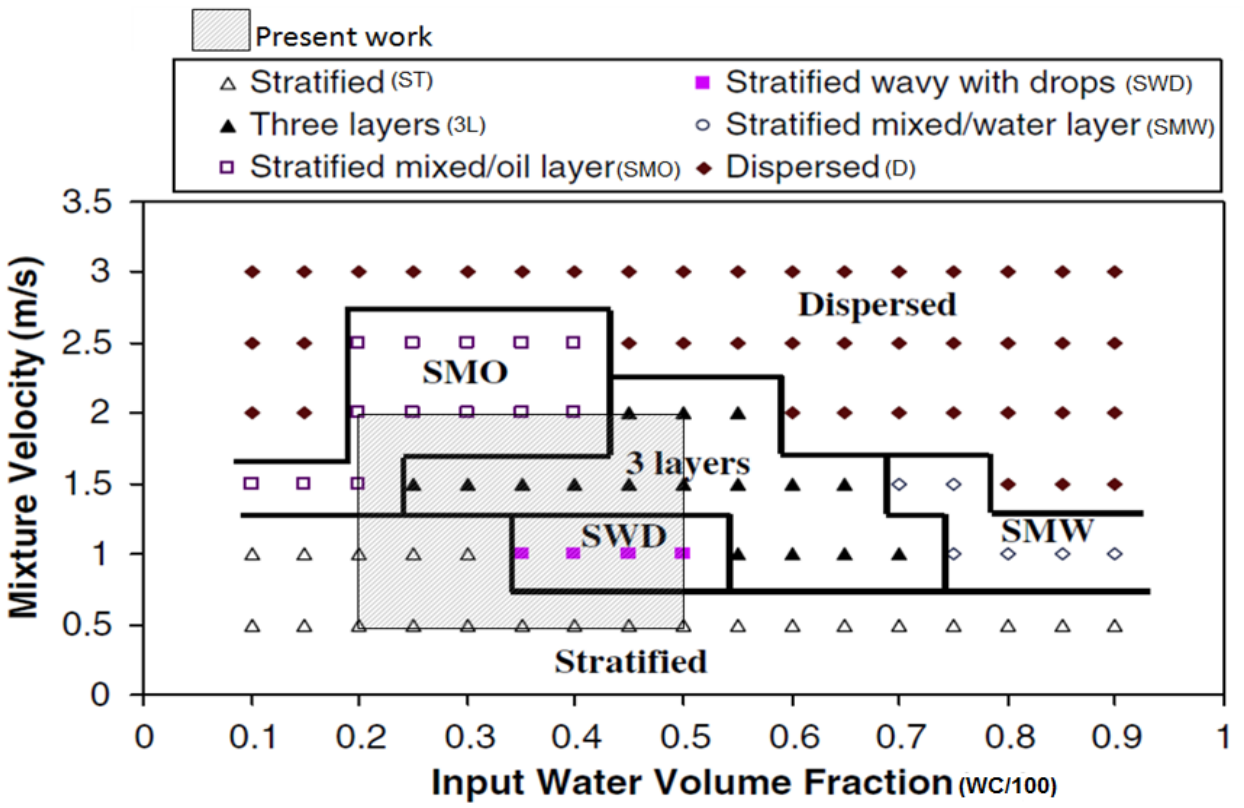

Figure 2.3: Flow patterns map of oil-and-water flow (Al-Yaari et al., 2009)

Kumara et al. (2010) conducted experimental work of oil (density790 kg/m3 and viscosity1.64mPas) and water (density 996kg/m^3 and viscosity 1.00 mPas) in a pipe (56 mm ID) horizontal and slightly inclined (5 to -5 degree). The test was conducted at a mixture velocity of 0.50 and 1.00 m/s and water cut of 50%. Stratified flow with mixing at the interface is observed at mixture velocity of 0.50 m/s. Interfacial waves were observed in upwardly and downwardly inclined flows. At mixture velocity 1.00 m/s, interfacial mixing is increased and dual continuous flows are observed.

Based on the selected work in the literature review above, the flow patterns of oil-water phase flow in horizontal and inclined pipelines can be summarized as follows:

1. Segregated flow includes:
    a. Stratified flow (ST): In this flow pattern the two liquid phases flow as layers with the heavier (usually water) at the bottom and the lighter (usually oil) at the top.
    b. Stratified flow with mixing at the interface (ST&MI): In this flow pattern the system tends to be stratified, but interface instability generates a mixing zone. The mixing zone at the interface can be significant, but still pure fluids exist at the top and the bottom of the pipe.
2. Dispersed flow includes:
    a. Water dominated
        i. Dispersion of oil in water and water layer (Do/w & w): The water is distributed across the entire pipe. A layer of clean water flows at the bottom and dispersed droplets of oil in water flow at the top.
        ii. Oil in water emulsion (Do/w): In this case, the entire pipe cross sectional area is occupied by water containing dispersed oil droplets.
    b. Oil dominated
        - Water in oil emulsion (Dw/o): The oil is the continuous-phase and the water is present as droplets across the entire pipe cross sectional area.
3. Dispersed flow of equal dominated: Dual dispersion (D o/w&w/o), in this flow pattern, two different layers occur. Both phases are present across the entire pipe, but at the top the continuous-phase is the oil, containing droplets of water. In the lower region of the pipe, the continuous-phase is water and the oil exists as dispersed droplets.

The previous experimental work can be summarized and categorized based on the influence of each design variable on the change of flow patterns as follows:

Effect of inlet conditions

The water volume percentage (water cut) plays a key role in creating different flow patterns change, per the study of Arirachakaran et al. (1989), the flow patterns in oil-water mixture depend primarily on mixture velocity and water fraction. Angeli and Hewitt (2000) showed in their experimental work that the phase volume fraction different from the input ones since the local average velocities of the phases are not necessarily the same. Based on the input oil/water volumetric ratio, the local oil/water volume ratio in most cases is higher than the input ratio.

The experimental work done by Hussain et al. (2008) is to examine the effect of input water fraction and velocity on the water holdup flowing in horizontal tubes of 25.4-mm diameter. Starting from stratified flows of different phase fraction of oil-water (WC: 40, 46, and 60%) and different mixture velocity in the range of 1.8 – 2.76 m/s, the phase fraction distribution was determined. The work showed that at low water fractions, oil is the continuous phase while at high water fractions, water is the continuous phase. The study showed that the local holdup and water slip velocity increases with increasing inlet water concentration.

In multiphase flows, the actual velocities of the individual phases are, in general, not the same and usually do not correspond to their velocities at inlet conditions. Higher viscosity oil is observed to move slower than water. Meanwhile, some researchers believe that under

most oil-water flow situations, the oil phase flows faster than the water phase resulting in accumulation or holdup of water [Flores et al. (1997)]. Per the study of Arirachakaran et al. (1989), the flow patterns in oil-water mixture depend primarily on mixture velocity and water fraction and may on oil viscosity when oil is the continuous phase. Hussain et al. (2008) experiment showed also that the higher the mixture inlet velocity, the more water entrainment and the less in-situ water holdup concentration and the less velocity slip is.

Effect of oil properties

According to the study of Arirachakaran et al. (1989), the flow patterns in oil-water mixture depend primarily on mixture velocity, water fraction and oil viscosity when oil is the continuous phase. Shi (2001) highlighted that high viscous oil moves slowly resulting in higher cross section area than water's that leads to an increase in local water velocity. Accordingly, corrosion rate estimation shall be based on the local water velocity not on the inlet mixture velocity. The reason is that the viscose oil is difficult to break down to small droplets. So the flowing oil plugs the cross-section area of the pipe causing velocity increase of the water layer.

The comprehensive review of Yeo et al. (2000) that was to study the effect of various physical properties, geometry and flow patterns on phase inversion included that the large density differences between the aqueous and continuous phases make dispersion more difficult to achieve. That means reducing density difference between oil and water, increase oil-water mixing zone.

Effect of pipeline geometry

The influence of piping diameter appears in the work of Mandal et al. (2007) where new flow patterns in small pipe sizes were reported. Lum et al. (2006) in their experimental work showed that the oil to water velocity ratio was higher for the upward than for the downward flows. However, in the majority of cases inclinations, oil was flowing faster than water. At low mixture velocities, the velocities ratio increase with oil fraction while they decrease at high velocities because separation increases with low mixture velocity and mixing increases with high mixture velocity. The increase of mixing became more significant as the degree of inclination increases.

Hussain et al. (2008) highlighted that the gravitational force acts perpendicular to the direction of flow in the horizontal pipes causing phases separation. Where the lighter phase moves upwards by buoyancy and the heavy phase moves downwards by gravity force. Kumara et al. (2010) highlighted that the degree of mixing largely depends on the pipe inclination. In general, higher water holdup values are observed for upwardly inclined flows compared to the horizontal and downwardly inclined flows. Moreover, the slip between the phases increases as the pipe inclination increases. In extensive experiments of Mandal et al. (2007), they investigated the influence of certain mixer designs to the downstream distribution of the two liquids and the flow pattern map by just changing the way of introducing the two fluids in the test rig that resulted in different flow patterns.

2.2 Numerical Investigations

There are good numbers of literature in the field of two phase flow oil-water using numerical investigation. Hussain et al. (2008) studied the oil-water dispersion numerically in a horizontal pipe under gravity effect with using advanced computational fluid dynamics, CFD software. The pipe of 25.4 mm inner diameter with mixture velocity of 1.8 and 2.76 m/s carrying oil (802 Kg/m^3 density and 1.6 cP viscosity) and water (input WC of 40, 46 and 60%). They selected Eulerian-Eulerian model with K-ε Turbulence model for liquid-liquid flow that gave fairly well-dispersed flow.

Gao et al. (2003) numerically simulated stratified oil–water turbulent flow in a horizontal tube, 55.75 mm diameter, using a volume of fluid model, VOF. The oil has a density of 790 kg/m3 and dynamic viscosity of 1.6 cP and input water cut in the range of 10 to 86%. They selected the RNG K-ε model combined with a near-wall low-Re turbulence model for each phase. The conclusion was that the prediction of the results showed acceptable agreement with experimental data.

Martinez et al. (1988) tried to characterize the rheological behavior of a fluid system using the power-law model as a function of the oil fluid to prove possibility of numerical calculation. That was confirmed by Arirachakaran et al. (1989) who calculated the mixture properties and flow behavior for different flow patterns. They highlighted that the formulated mixture viscosity does not reflect the actual complex viscosity of the actual mixture that is yet unknown.

Abdulkadir et al. (2010) numerically analyzed the characteristics of fluid flow and phase separation of oil-water flowing in a horizontal cylindrical vessel to study the effect of different velocities and droplet diameters on the separation. The simulations were carried out using the software package Fluent 6.2 using Eulerian model and turbulence of the k-ε model. The results showed that there is a strong dependency of phase separation on mixture velocity and droplet diameter. Increasing mixture velocity slows down phase separation. An increase in droplet diameter increases phase separation. The simulations showed good agreement with results reported in literature and showed that CFD can be a useful tool in studying oil-water separation.

From this literature review, it shows that full-scale experiments with sufficient instrumentation for multi-phase flows are often extremely difficult to be performed due to their size. The literature reviews give good results in using CFD/fluent to investigate the multiphase fluid and predict the related flow patterns.

Factors influence flow patterns

The literature review shows that there are different factors affecting flow patterns when utilizing CFD/fluent. The most affecting factors are water droplet size and geometry meshing. So in order to reflect the actual operating conditions using CFD/fluent, these factors shall be evaluated carefully by conducting mesh independency test and validate the work against experimental data.

a) Water droplet

The dispersed phase has certain shape based on the operation conditions. Researchers utilize droplets size distribution curves to identify the droplet size of the dispersed water in oil of two-phase flow. The transition from stratified flow to stable water-in-oil dispersion takes places when the oil phase turbulence is intense enough to maintain the water phase broken up into droplets. Oil dynamic and buoyant forces are acting simultaneously on the droplets and tend to spread the droplets throughout the pipe cross- section. They try to overcome the gravity forces that work to settle down droplets. The oil-water phase shares the dispersed droplets while flowing throughout movement in two directions: horizontal and vertical. The horizontal movement of the droplets results in the break up and coalescence of the droplets. The high velocity breaks the dispersed droplets to smaller droplets. At the same time, increasing the velocity increases water entrainment which results in bigger dispersed water droplets [Lovick and Angeli (2004)]. The vertical movements are mainly controlled by the gravity force and the turbulent dispersion force. Gravity force pulls the droplets down and turbulent dispersion force makes the droplets move upward [Shi (2001)].

Fluent requires the droplet size of the secondary phase to be determined, which is water phase in this case. The bigger the droplet size, the high rate of oil-water separation is. The droplet diameter in the present work is selected initially as 0.1 mm as the flow is fully mixed at the inlet and the water droplets are distributed across the pipe in small diameters. The simulation is run for 300 iterations then the water droplet size is increased to 1.00 mm and run the simulation until get converged. The reason of increasing droplet size is to match the normal water droplet coalescence downstream the pipe that is also supported by the

statistical data of water distribution in different works. The distribution functions of fully dispersed flow that are most frequently used in analyses of droplet size data are normal distribution, log-normal distribution, root-normal distribution, Nukiyama-Tanasawa distribution, Rosin-Rammler distribution, and upper-limit distribution. Vielma et al. (2008), in their experimental work, show droplet-size distributions for the case of Vso = Vsw = 0.75 m/s which shows good fit to the log-normal distribution as shown in Figure 2.4. Their work is equivalent to case 8 of the present work with 50% WC and 1.0 m/s.

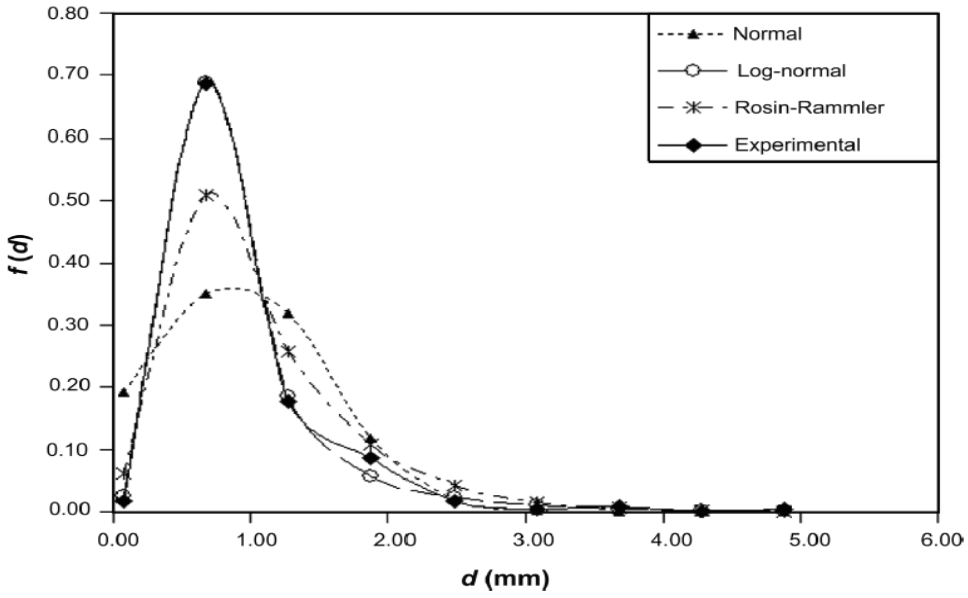

Figure 2.4: Water droplet size distributions at Usw = 0.75 m/s, Uso = 0.75 (Vielma et al., 2008)

The mixture velocity did not affect significantly the droplets size of either phase since higher velocities that would result in smaller drops are accompanied by increased entrainment of one phase dispersed into the other that resulted in larger droplets [Lovick and Angeli 2004]. Oil-water separation depends strongly on droplet size and mixture velocity [Abdulkadir et al. (2010)]. Droplet size is a function of the mixture velocity. The droplet size and distribution is a result of dynamic and buoyant forces. Morales (2009) summarized in his thesis the most followed methods to quantify and measure the size distributions of droplets. He highlighted that the most used method to characterize the droplet size distribution is the Sauter Mean Diameter (SMD). The SMD, (D_{32}) is defined as the ratio between particle cumulative volume and particle overall surface area [Morales (2009)]. The widely used definition of the mean droplet diameter is given by:

$$D_{pq} = \frac{\sum_{i=1}^{m} D_i^p \Delta N_i}{\sum_{i=1}^{m} D_i^q \Delta N_i} \qquad (2.1)$$

Where p and q are the parameters used depending on the required type of mean diameter, for comparison p = 3 and q = 2.

Al-Wahaibi and Angeli (2008) conducted experimental study investigating the size and vertical distribution of droplets during horizontal dual continuous oil–water flow. It showed that there was no clear effect of the layer velocity on the size of droplets dispersed in that layer. Moreover, per Al-Wahaibi and Angeli (2008), none of the available correlations of maximum droplet size was able to predict the present experimental data, saying that "these correlations were developed for droplet breakage in a turbulent flow field". The

investigations were carried out in a 38 mm ID stainless steel with water and oil (density 828 kg/m^3 and viscosity 5.5 mPa s). Droplets velocities and sizes were obtained with a dual impedance probe which allowed measurements at different locations in a pipe cross-section. They showed that water droplets in oil generally increase in size as the oil superficial velocity increases for certain water superficial velocity. The increase could be due to the increase in the amount of water entrained in the oil phase.

The average chord length distribution over the pipe cross-section can be calculated by averaging the droplet chord length measurements obtained at different locations from the interface to find out that water droplet is around 1.0 mm for different water cuts as shown in Figure 2.5. It shows that distribution of droplets side changes with velocity changes. The droplets size depend on water counts which is 31% water counts at Figure 2.5-a and 26% at Figure 2.5-b.

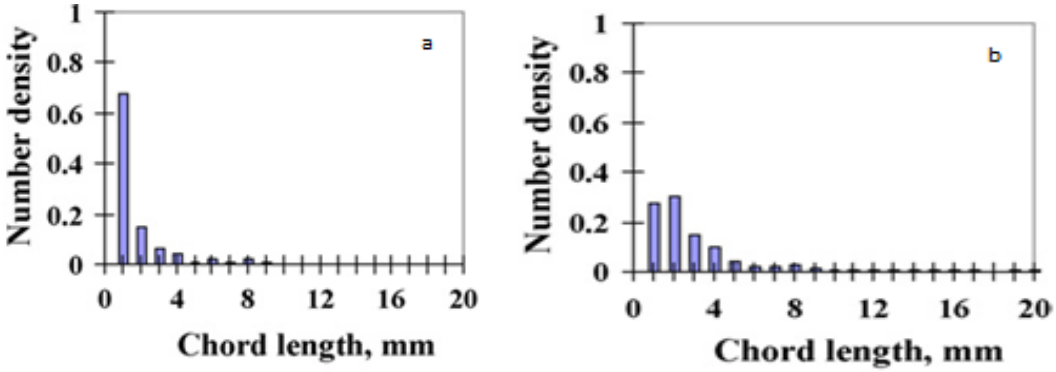

Figure 2.5: Water droplet size distributions at a) Usw = 0.5 m/s, Uso = 1.1 b) Usw = 0.5 m/s, Uso = 1.4 (Al-Wahaibi and Angeli, 2008)

b) Meshing buildup and validation

Meshing buildup requires conducting mesh dependency test in order to be high confident of result-free from the meshing effect. This certainty can be built by conducting the mesh dependency test. In order to confirm this certainty, a validation against experimental work is required.

2.3 Corrosion Mechanisms of Multiphase Flows

Part of this work is to investigate the corrosion susceptibility of piping carrying water-oil flow. The main cause of corrosion is due to the presence of free water in the system that can be measured in terms of water holdup and velocity slip between the two-phases. The related literature review shows that local water cut is not normally the same as the input water cut.

In the oil and gas production industry, internal corrosion of carbon steel pipeline is a well-known phenomenon and a serious problem. Crude oil at normal production with temperatures (less than 120 °C) without dissolved gases is not corrosive, by itself. CO_2 and H_2S gases in combination with water cause most of the corrosion problems in the oil and gas production. Different crude oil can have significant different effects on steel corrosion [Efird and Jasinski (1989)]. So it is required to identify the corrosive species in the flow, the local water concentration and expected corrosion mechanism to estimate equipments lifetime and select corrective measures. Nesic (2007), in his review of internal corrosion mechanisms, reported that multiphase flow is one of the more complex corrosion problems where different flow patterns can be found. Different flow patterns lead to a variety of corrosion mechanisms.

The internal corrosion mechanism depends on the phase in contact with the pipe wall [Shi (2001) and Ayello et al. (2008)]. Prediction of corrosion rates under these flow conditions requires knowledge of local water cut, water velocity, water film thickness and pipe surface area wetted by water. The thickness of water layer and local water velocity are two essential elements for corrosion to occur. The mixture of oil and water contains dissolved corrosive gases that results in formation of a weak carbonic acid often causing severe corrosion in carbon steel pipelines [Vedapuri, et al. (1997)]. The dissolved CO_2 in the liquid phase is distributed in the solution in the form of [H_2CO_3], [HCO_3^-], and [CO_3^-] as per the following steps, [Dayalan et el. (1998)]:

$$CO_2 + H_2O = H_2CO_3 \quad (2.2)$$

$$H_2CO_3 = H^+ + HCO_3^- \quad (2.3)$$

$$HCO_3^- = H^+ + CO_3^- \quad (2.4)$$

Shi (2001) associated the corrosion rate with the thickness of water layer and local water velocity as key factors to corrosion. Some research work reported that high viscose fluid may increase local water velocity which leads to high erosion/corrosion rate. This is the reason that most of researches use local water velocity to monitor the corrosion rate and not the mixture velocity where the corrosion rate will result in large errors [Shi (2001)]. Therefore, the local holdup of water is very important to be monitored to predict corrosion rates in oil-water flow. Shi (2001) recommended studying water distribution at low water cut even below (< 20%) since free water layer which is the source of corrosion can present at the bottom of the pipeline at any water cut. Based on Shi (2001) work, it was expected that the minimum local water percentage for corrosion to happen is about 30% local water contents.

From Shi (2001) experiment shown in Figure 2.6, the corrosion rate is a function of the bottom water fraction which presents the local water content. It is seen that up to 1.2 m/s, the local water contents reaching 100% and the corrosion rate increases sharply to almost 1.0 mm/yr. Between 1.2 m/s and 2.6 m/s, the local water contents drops sharply from 100% to 35% where the corrosion rate increases from 1.0 mm/yr to its maximum value in this figure of 1.8 mm/y. Beyond 2.6 m/s mixture velocity, the local water contents drops gradually to 30% at 3.0 m/s. However; in this range of mixture velocity, the corrosion rate drops sharply to 1.48 mm/yr. From this, Shi (2001) presented that the availability of 70% oil at the bottom of the pipe can reduce corrosion rate significantly.

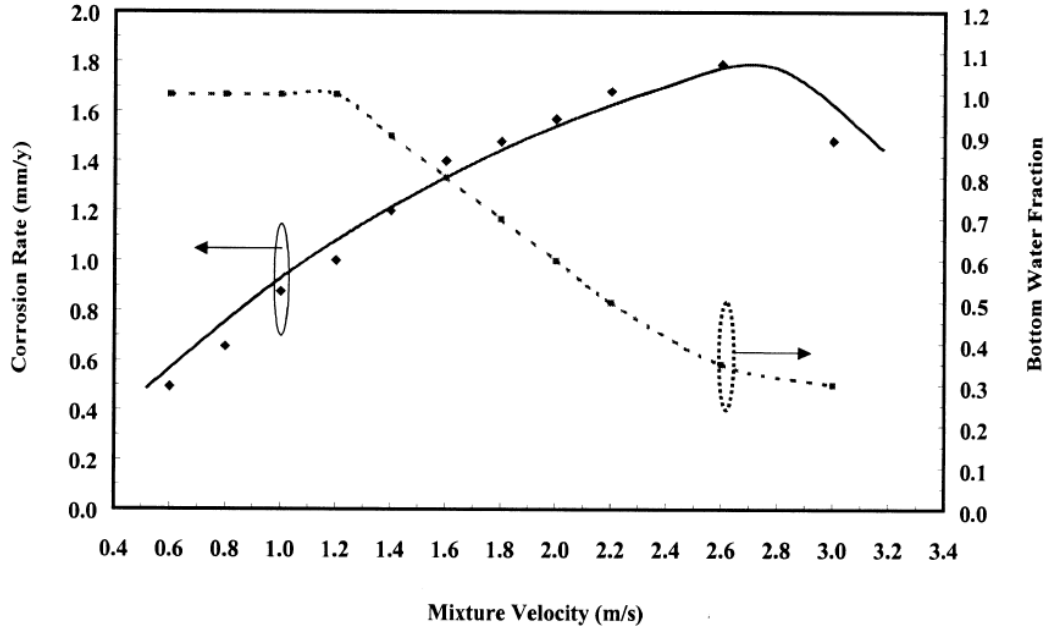

Figure 2.6: Relation between mixture velocity and corrosion rate (Shi, 2001)

Prediction of corrosion rates in oil-water flows requires knowledge of the local holdup and velocity of the water layer to predict mass transfer coefficient [Shi et el. (2002)]. As the water cut increases, water break out may occur leading to flow of a separate layer of

water. The thickness of water layer and local water velocity are two essential elements for erosion/corrosion occurrence. The corrosion rate increases as the separated water layer increases [Shi (2001) and Vedapuri et al. (1997)]. Dayalan et al. (1998) formulated the corrosion of steel with dissolved CO_2 as follows:

Cathodic reactions:

$$2\ H_2CO_3 + 2e = H_2 + 2HCO_3^- \quad (2.5)$$

$$2HCO_3^- + 2e = H_2 + 2CO_3^{2-} \quad (2.6)$$

$$2H^+ + 2e = H_2 \quad (2.7)$$

Anodic reactions:

$$Fe = Fe^{2+} + 2e \quad (2.8)$$

General reaction:

$$Fe + CO_2 + H_2O \rightarrow FeCO_3 + H_2 \quad (2.9)$$

The reported methods of mitigating pipelines corrosion in case of oil-water multiphase flow is to inject chemical inhibitors and or maintain the flow velocity above certain velocity, called critical velocity as repored by Ayello et al. (2008) in order to have complete entrainment for water in the system. The effectiveness of inhibitors depends on many factors as highlighted by Shi et al. (2002) and Nesic (2007) such as pipeline material, inhibitor composition and flow conditions. Corrosion inhibitors are substances containing organics that are adsorbed to the metal surface and form a protective film to prevent corrosion. The two most common sources of corrosion inhibition in oil-water flow are: (a)

inhibition by addition of corrosion inhibitors and (b) inhibition by components present in the crude oil, [Nesic (2007)]. For effective inhibition, inhibitor must be introduced into the phase in contact with the pipe wall by using oil or water soluble inhibitors based on the existing flow patterns [Wang et al. (2001)]. This decision can be made effectively, only if flow patterns and phase distribution under different flow conditions are known.

2.4 Turbulator Generation Devices Applications

Turbulator devices proposed in this investigation are static devices of a special geometry design. It is proposed to be used for pipelines with multiphase fluid to mix two-immiscible liquids. There are many static mixers available with different mixer configurations mainly for chemical mixing applications. The literature review shows different static mixers.

Kenics™ static mixers consists of a series of alternating left and right hand helical elements of 180 degree helices as reported in the internet website for Kenics [Kenics (1998)] that is shown in Figure 2.7.

Figure 2.7: Kenics static mixer (Kenics, 1998)

GV static mixer is also available on the website of Stamixco [Stamixco (2006)]. It is to mix low viscosity liquids and gases and contacting of immiscible fluids to enhance mass transfer in pipelines. It is made of corrugated plates that are stacked on top of each other in an

alternating-crossing fashion to form open intersecting channels that are at a 45^{o} angle relative to the pipe axis. Adjacent mixing elements are oriented 90^{o} relative to each other to create 3-dimensional mixing. The GV mixer is shown in Figure 2.8.

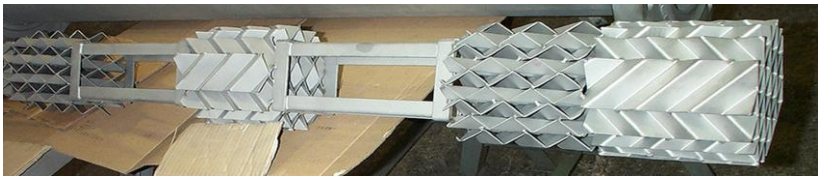

Figure 2.8: GV static mixer (Stamixco, 2006)

Mandal et al. (2007) conducted extensive experiments on horizontal pipes of diameters 12 mm and 25 mm using two immiscible liquids (water and kerosene). They reported that mixer design influences the distribution of the two liquids and a properly designed mixer can increase or decrease the range of existence of any flow pattern.

The problem with the existing mixers is that they have large area of contacts with the internal surface of the pipe. The contact areas to the pipe create stagnant flow that can lead to corrosion due to many reasons. Two-phase flow separate in the stagnant areas and the sludge start build up behind the contact areas that causes corrosion and plug the flow area. The target of this work for this part is to use turbulator device that has different design from the reported mixers, Kenics™ static mixers and GV static mixer. It is expected to have low energy impact resulting from the geometry itself. The purpose of this device is to investigate the possibility of creating specific flow pattern by installing the turbulator device inside the pipe with different dimensions. Moreover, the study is targeting to mitigate the corrosion by getting specific flow patterns at specific locations. Since the effective inhibition requires

introducing the right phase that depends on whether to use oil or water soluble inhibitors, and amount of inhibitor. This condition can be met effectively, only if the flow patterns and the phase distribution under different flow conditions are known.

CHAPTER 3

MATHEMATICAL FORMULATION AND NUMERICAL ANALYSIS

3.1 Problem Statement

This work is to numerically simulate oil-water phase flow in horizontal and slightly inclined pipelines as shown in sketches per Figure 3.1. The flow enters the pipe based on two cases as shown in Figure 3.2 for different test applications as summarized below.

a) Mixed flow

The flow enters as a mixed flow, Figure 3.2-a, of oil-and-water in a horizontal or slightly inclined pipe to investigate the effect of some parameters on the flow patterns at certain operation conditions. These parameters consist of variables covering piping geometry, operation and fluid physical properties:

- Operation variables: water concentration, and mixture inlet velocity.
- Fluid physical properties: oil density and oil viscosity.
- Geometrical variables: pipe diameter, pipe inclination and internal turbulator device.

b) Segregate flow:

The flow enters as a separate flow in a horizontal pipe, Figure 3.2-b, by dividing the inlet to equivalent portions to the volume fractions. Oil enters into the top while water enters into the bottom portion. The two flows move as stratified flows with some interfaces mixing until they hit a turbulator device downstream. The flows then get mixed with different degrees of mixing. This part is to investigate the effect of the turbulator on the streams and evaluate possibility of controlling flow patterns. Since flows are get mixed downstream the pipe in both cases, the flows are considered mixed flows and accordingly the numerical formulations are selected to be exchangeable fluids as Eulerian model of fluent can be used .

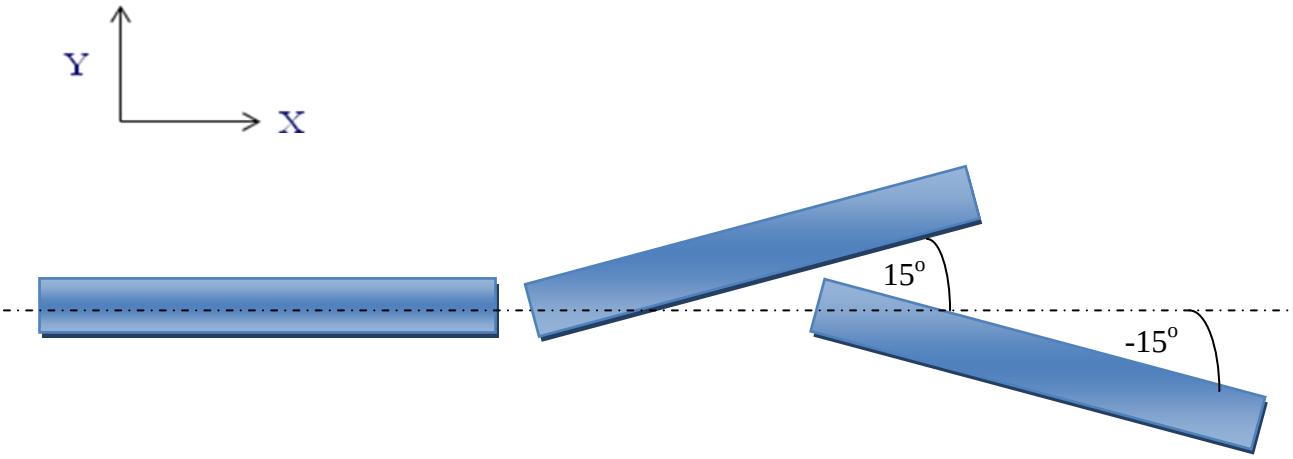

Figure 3.1: Different orientations of pipelines: horizontal, inclined up, and inclined down

Figure 3.2: Different inlet flow condition: a) fully mixed and b) fully separated

3.2 Numerical Calculation Tool

The present work utilizes the Computational Fluid Dynamics CFD, fluent package, as the numerical tool. CFD/fluent operates on quite simple laws such as laws of thermodynamics, conservation, momentum, energy, and Euler equations. The partial differential equations known as Navier-Stokes equations resulting from these laws are

what govern fluid dynamics. Solving the Navier-Stokes equations involves the use of sophisticated solution algorithms. It is more suited to steady state flow which is less demanding for the computer and enables solution to be achieved within a reasonable number of iterations.

General governing equations

All the flow variables such as pressure, velocities etc. are defined as volume average. The phases are assumed to share space in proportion to their volume fractions to satisfy the total continuity relation. Volume fractions represent the space occupied by each phase, and the laws of conservation of mass and momentum are satisfied by each phase individually [ANSYS (2002)]:

a) Multiphase modeling

Among the different multiphase models in Fluent application for oil-water two-phase flow, multiphase Eulerian-Eulerian was selected based on its ability to handle high water cut of the two fluid phases with different flow patterns as in this case. Moreover, Eulerian models assist to identify water holdup. An implicit, steady-state and segregated 3D solver are selected to solve the Fluent's built-in conservation of mass and momentum equations for the specified models. CFD has further features as follows [ANSYS (2002)]:

- A single pressure is shared by all phases.
- Momentum and continuity equations are solved for each phase.

- All of the k-ε turbulence models are available, and may apply to all phases or to the mixture.

i) Conservation of mass (Continuity):

For any phase, the mass conservation equation can be written as:

$$\frac{\partial\left(\rho\bar{u}\right)}{\partial x}+\frac{\partial\left(\rho\bar{v}\right)}{\partial y}=0 \tag{3.1}$$

ii) Conservation of x-momentum:

$$\frac{\partial}{\partial x}\left(\rho\bar{u}\bar{u}\right)+\frac{\partial}{\partial y}\left(\rho\bar{u}\bar{v}\right)=-\frac{\partial p}{\partial x}+\frac{\partial}{\partial x}\left[\left(\mu+\mu_t\right)\frac{\partial\bar{u}}{\partial x}\right]+\frac{\partial}{\partial y}\left[\left(\mu+\mu_t\right)\frac{\partial\bar{u}}{\partial y}\right]-\frac{2}{3}\rho\frac{\partial k}{\partial x} \tag{3.2}$$

iii) Conservation of y-momentum:

$$\frac{\partial}{\partial x}\left(\rho\bar{u}\bar{v}\right)+\frac{\partial}{\partial y}\left(\rho\bar{v}\bar{v}\right)=-\frac{\partial p}{\partial y}+\frac{\partial}{\partial x}\left[\left(\mu+\mu_t\right)\frac{\partial\bar{v}}{\partial x}\right]+\frac{\partial}{\partial y}\left[\left(\mu+\mu_t\right)\frac{\partial\bar{v}}{\partial y}\right]-\frac{2}{3}\rho\frac{\partial k}{\partial y}+\left(\rho-\rho_0\right)g \tag{3.3}$$

The above governing equations are time averaged; however, they no longer form a closed set due to the additional terms representing the transport of momentum and heat of the fluctuating motion. Equations governing these fluctuating motions introduce additional unknown quantities and can only be solved when the turbulence correlations are used.

b) Turbulence modeling

The Realizable k-ε model is used with the following transport equations as per fluent manual [ANSYS (2002)]:

$$\frac{\partial}{\partial t}(\rho k)+\frac{\partial}{\partial x_j}(\rho k u_j)=\frac{\partial}{\partial x_j}[\eta+\frac{\mu_t}{\sigma_k})\frac{\partial k}{\partial x_j}]+G_j+G_b-\rho\varepsilon-Y_M+S_k \tag{3.4}$$

$$\frac{\partial}{\partial t}(\rho\varepsilon)+\frac{\partial}{\partial x_j}(\rho\varepsilon u_j)=\frac{\partial}{\partial x_j}[\eta+\frac{\mu_t}{\sigma_\varepsilon})\frac{\partial\varepsilon}{\partial x_j}]+\rho C_1 S_\varepsilon-\rho C_2\frac{\varepsilon^2}{k+\sqrt{\upsilon\varepsilon}}+C_{1\varepsilon}\frac{\varepsilon}{k}C_{3\varepsilon}G_b+S_\varepsilon \tag{3.5}$$

Where

$$C_1=Max[0.43,\frac{\mu}{\mu+5}],\qquad \eta=S\frac{k}{\varepsilon},\qquad S=\sqrt{2S_{ij}}S_{ij}$$

$$\mu_t=\rho C_\mu\frac{k^2}{\varepsilon},\qquad C_\mu=\frac{1}{A_0+A_s\frac{ku^*}{\varepsilon}},\qquad u^*=\sqrt{S_{ij}S_{ij}+\tilde{\Omega}_{ij}\tilde{\Omega}_{ij}}$$

$$\tilde{\Omega}_{ij}=\Omega_{ij}-2\varepsilon_{ij}\varepsilon_{ijk}\omega_k,\qquad \Omega_{ij}=\Omega_{ij}-\varepsilon_{ijk}\omega_k,\ A_0=4.04,\ A_s=\sqrt{6}\cos\Phi$$

$$\Phi=\frac{1}{3}\cos^{-1}(\sqrt{6}W),\qquad W=\frac{S_{ij}S_{jk}S_{ki}}{\tilde{S}^3},\ \tilde{S}=\sqrt{S_{ij}S_{ij}},\ S_{ij}=\frac{1}{2}(\frac{\partial u_j}{\partial x_i}+\frac{\partial u_i}{\partial x_k})$$

$$G_b=-g_i\frac{\mu_t}{\rho\,\mathrm{Pr}_t},\qquad C_N=0.09,\qquad \mathrm{Pr}=0.85,\qquad Y_M=2\rho\varepsilon M_t^2,\qquad M_t=\sqrt{\frac{k}{a^2}},\qquad a=\sqrt{\gamma RT}$$

$$C_{1\varepsilon}=1.44,\quad C_2=1.9,\qquad \sigma_k=1.0,\qquad \sigma_\varepsilon=1.2$$

In equations (3.2)-(3.3), μ_t is the turbulent dynamic viscosity that is to be predicted from the knowledge of the kinetic energy of turbulence, k, and turbulent kinetic energy dissipation rate, ε. Note that in the above formulation, the governing equations are solved for incompressible flow with Boussinesq approximation.

Water holdup (Hw) and slip calculation

The slip or relative velocity is determined from where the water hold-up can be estimated in terms of the velocity of the secondary phase, in this case, is water (w) relative to the velocity of the primary phase (o). There are different methods to show the phases. One way is to calculate the relative velocity of the two phases as per equation (1.4). The other way is to calculate the slip ratio factor (S). It is the ratio of average velocity of oil divided by average velocity of water. In the present work, the velocities are taken at 90% contents for both oil and water along the vertical radial line passing a cross the plane X5.5. The slip ratio factor is calculated as per equation (3.6):

$$S = \frac{V_o}{V_w} \tag{3.6}$$

If the ratio is unity, the velocity is equal for both phases. If the ratio is less than unity, that means water travels faster than oil and the opposite is true if the ratio is greater than unity. The water holdup (H_w) is calculated based on the slip ratio factor per equation (1.3).

Boundary condition assumptions

In order to set the problem, some assumptions need to be set up as shown in Figure 3.3 and listed below:

a) Steady-state flow.

b) Adiabatic flow, i.e. no heat transfer throughout the flow.

c) Isothermal flow, i.e. no temperature change during flow.

d) Neglect pipe roughness.

e) Fully mixed or fully segregated inlet flow.

f) Same inlet velocity for both oil and water of mixture or segregated flow.

g) Zero static pressure (gauge) at the outlet of the pipe which is equal to the atmospheric pressure.

h) No chemical reaction taking place throughout the flow.

i) No diffusion or phase generation throughout the flow.

j) Considering the gravity affect downward.

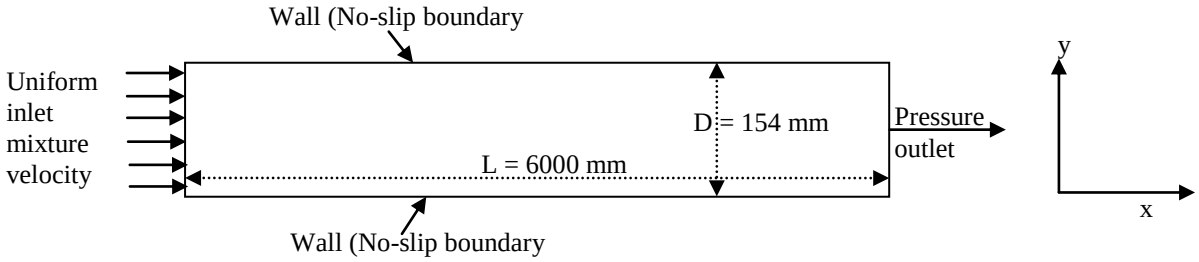

Figure 3.3: Schematic representation of pipe flow

3.3 Corrosion Calculation

There is specific ingredient of the environment required for the piping system internal corrosion to occur; such as available of corrosive gases, free water layer, pressure, temperature, etc. In the present work, it is assumed that required conditions for corrosion to occur are satisfied. The target is to determine the corroded surface area wetted with the free water layer for different flow patterns. The corrosion surface area is determined by locating the height of the water layer for each pipe size at different operating conditions. The surface area wetted with the free water layer is determined by referring to Figure 3.4 as follows:

- The surface area (A_{sw}) wetted with free water below the cord (c), representing water to mixing zone interface, is calculated per equation (3.7):

  $$A_{sw} = a \times L \tag{3.7}$$

  where (a) = arc length and (L) = pipe length.

- Arc length (a) of angle (θ), representing water to pipe interface per equation (3.8):

  $$\text{a} = \frac{r\theta\pi}{180} \tag{3.8}$$

  where (r) = radius of the pipe with inner diameter (D).

- The arc angle (θ) is calculated as per equation (3.9):

  $$\theta = 2(\frac{180}{\pi})\cos^{-1}(\frac{r - L_2}{r}) = 2(\frac{180}{\pi})\cos^{-1}(\frac{D - 2L_2}{D}) \tag{3.9}$$

  where (L_2) = water accumulation height measured from the pipe bottom in the simulation in the present work.

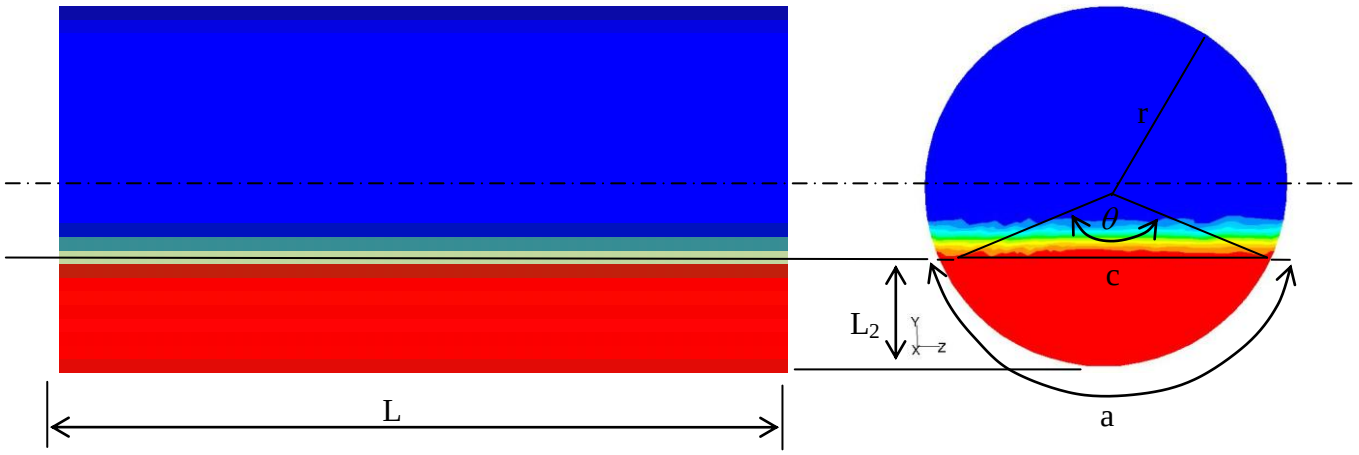

Figure 3.4: Calculation of surface area wet with water

The corrosion rate (CR) is then calculated based on the loss in weight from the given surface area during a given time interval as follows:

$$CR = \frac{Weight\ loss/time}{Wetted\ area \times density\ of\ metal} = \frac{W_t}{A_{sw} \times \rho_{metal} \times time} \qquad (3.10)$$

In the present work, the corrosion calculation is not absolute for each case and is based on the following assumptions:

- Corrosion comparison is in reference to the base case.
- Assuming corrosive environment for operation of different inlet conditions where the internal corrosion can occur due to availability of free water layer.
- Metal loss is based on the surface area wetted by 90% water content and more.
- No other considerations for metal loss source in the present work, such as erosion/corrosion due to high velocity of both or one phase.

Steps of calculating the wetted-water surface area:

- The corroded surface area is determined by locating the height of the water layer for each pipe size as shown in Figure 3.4.
- The wetted surface area (A_{rw}) with at least 90% free water below the cord (c) is considered as the affected area that will get corroded.
- The corrosion for any variable (n) referring to the base case (b) can be related to the surface area exposed to water and consider that corrosion takes place uniformly for the whole surface.
- Accordingly, the corrosion ratio based on the exposed surface area (CeS) is calculated as follows:

$$\frac{CeS_n}{CeS_b} = \frac{A_{sw-n}}{A_{sw-b}} = \frac{\cos^{-1}(\frac{D-2L_2}{D})_n}{\cos^{-1}(\frac{D-2L_2}{D})_b} \qquad (3.11)$$

To simplify equation (3.11), equation (3.12) can be utilized to calculate the corrosion rate for any case (n) as a percentage of the base case (b) corrosion rate as a wetted surface area.

$$\frac{CeS_n}{CeS_b} = \frac{A_{sw-n}}{A_{sw-b}} = \frac{\cos^{-1}(\frac{D(1-\frac{2L_2}{D})}{D})_n}{\cos^{-1}(\frac{D(1-\frac{2L_2}{D})}{D})_b} = \frac{\cos^{-1}(1-\frac{2L_2}{D})_n}{\cos^{-1}(1-\frac{2L_2}{D})_b}$$

By letting $\frac{2L_2}{D} = 2h$, so $\quad \frac{CeS_n}{CeS_b} = \frac{A_{sw-n}}{A_{sw-b}} = \frac{\cos^{-1}(1-2h_n)}{\cos^{-1}(1-2h_b)}$ (3.12)

Where (h) and (h_n) are the same and represent the water height from the pipe bottom.

3.4 Numerical Analysis

The numerical solution of a differential equation consists of a set of numbers from which the distribution of the dependent variable, ϕ, can be constructed. A numerical method treats the values of the dependent variable as its basic unknowns at a finite number of locations called the grid points in the computational domain where the numerical method implemented in the CFD/Fluent is Finite-Volume Method (FVM). The flow variables are approximated using different discretization processes. The discretization process is essentially an exercise of engineering judgment. The general objective of such a discretization is to divide the body into finite control volumes sufficiently small so that the simple models can adequately approximate the true solution. At the same time, too fine subdivisions lead to extra computational effort. For a given differential equation, the discretization equations can be derived using finite volume formulation that is integrated over each control volume to yield the discretization equation. Thus, the discretization equation represents the same conservation principle over a finite region as the differential equation over an infinitesimal region. This direct interpretation of the discretization equation makes the method easy to understand in physical terms; the coefficients in the equation can be identified, even when they appear in a computer program, as familiar quantities such as flow rate, conductance, areas, volumes, diffusivities, etc. The control volume approach can be regarded as a special case of the method weighted residuals [Patankar (1980)] in which the weighted function is chosen to be unity over a control volume and zero everywhere else.

a) Discretization of the governing transport equations

Discretization of the governing equations can be illustrated most easily by considering the steady-state conservation equation for transport of a scalar quantity ϕ. This is demonstrated by the following equation written in integral form for an arbitrary control volume V as follows:

$$\oint \rho\phi v \cdot dA = \oint \Gamma_\phi \nabla\phi \cdot dA + \int_V S_\phi dV \tag{3.13}$$

where ρ is the density, v is the velocity vector ($u\,\hat{i} + v\,\hat{j}$), A is the surface area vector, Γ_ϕ is the diffusion coefficient for ϕ, S_ϕ is the source of ϕ per unit volume and $\nabla\phi$ is given by

$$\nabla\phi = \left(\partial\phi / \partial x\right)\hat{i} + \left(\partial\phi / \partial y\right)\hat{j} \tag{3.14}$$

The above equation is applied to each control volume or cell in the computation domain. The two-dimensional cell shown in the Figure 3.5 is an example of such a control volume. Discretization of the above equation (3.14) for a steady state convection-diffusion equation for the transport of general property ϕ is given by

$$\nabla \cdot (\rho u \phi) = \nabla \cdot (\Gamma\ grad\ \phi) + S_\phi \tag{3.15}$$

The integration over a control volume gives

$$\int_{CA} n \cdot (\rho\phi u) dA = \int_{CA} n \cdot (\Gamma\ grad\ \phi) dA + \int_{CV} S_\phi dV \tag{3.16}$$

This equation represents the flux balance in a control volume. The principal problem in the discretisation of the convection terms is the calculation of the value of transported property ϕ at the control volume faces and its convective flux across these boundaries.

Applying the divergence theorem to the above equation, we get

$$\frac{\partial}{\partial x}(\rho u\phi)+\frac{\partial}{\partial y}(\rho v\phi)=\frac{\partial}{\partial x}\left(\Gamma\frac{\partial\phi}{\partial x}\right)+\frac{\partial}{\partial y}\left(\Gamma\frac{\partial\phi}{\partial y}\right)+S \qquad (3.17)$$

A portion of the two dimensional grid used for the discretisation is shown in Figure 3.5.

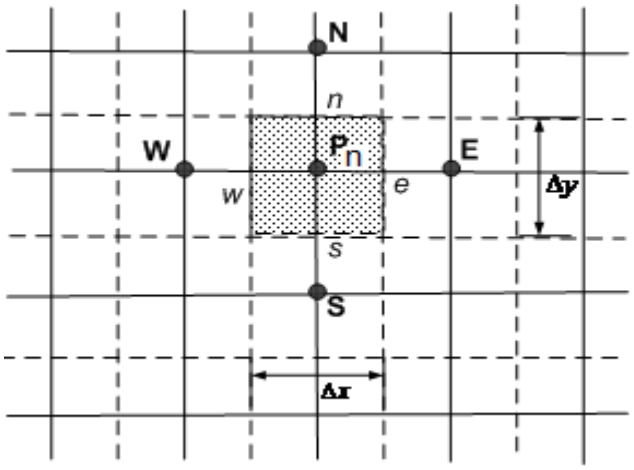

Figure 3.5: Part of the two-dimensional control volume grid

b) Domain discretization

The first step in the finite volume method is to divide the domain into discrete control volumes. The boundary of control volumes are positioned mid way between adjacent nodes. Thus, each node is surrounded by a control volume or cell. It is common practice to set up control volumes near the edge of the domain in such a way that the physical boundaries coincide with the control volume boundaries.

A general nodal point is identified by 'Pn' and its neighbors in two-dimensional geometry. The nodes of the west and east are identified by 'W' and 'E' and the nodes of the north and south by 'N' and 'S' respectively. The west side face of the control volume is referred to by 'w' and other corresponding faces on east, north and south of the control volume by 'e', 'n', 's' respectively. The distance between the nodes W and Pj is identified by δx_{WP} and between face w and Pj by δx_{wP}. Similarly, the other distances are computed. The widths of the control volume is given by $\Delta x = \delta x_{we}$ and $\Delta y = \delta y_{ns}$.

The key step of the finite volume method is the integration of the governing equation (or equations) over a control volume to yield a discretized equation at its nodal point P. For the above defined control volume this integration gives,

$$\int_{\Delta V} \frac{\partial}{\partial x}(\rho u \phi) dx.dy + \int_{\Delta V} \frac{\partial}{\partial y}(\rho v \phi) dx.dy = \int_{\Delta V} \frac{\partial}{\partial x}\left(\Gamma \frac{\partial \phi}{\partial x}\right) dx.dy + \int_{\Delta V} \frac{\partial}{\partial y}\left(\Gamma \frac{\partial \phi}{\partial y}\right) dx.dy + \int_{\Delta V} S_{\phi} dV \tag{3.18}$$

Noting that $A_e=A_w=\Delta y$ and $A_n=A_s=\Delta x$, we obtain

$$\left[(\rho u A\phi)_e - (\rho u A\phi)_w\right] + \left[(\rho v A\phi)_n - (\rho v A\phi)_s\right] = \left[\left(\Gamma A \frac{\partial \phi}{\partial x}\right)_e - \left(\Gamma A \frac{\partial \phi}{\partial x}\right)_w\right] + \left[\left(\Gamma A \frac{\partial \phi}{\partial x}\right)_n - \left(\Gamma A \frac{\partial \phi}{\partial x}\right)_s\right] + \bar{S}\Delta V \tag{3.19}$$

The flow must also satisfy continuity and accordingly,

$$\frac{\partial(\rho u)}{\partial x}+\frac{\partial(\rho v)}{\partial y}=0 \tag{3.20}$$

and its integration over the control volume gives

$$\left[(\rho uA)_e-(\rho uA)_w\right]+\left[(\rho vA)_n-(\rho vA)_s\right]=0 \tag{3.21}$$

The nonlinearity of the source term can be removed by representing it in a linear form.

$$\overline{S}\Delta V=S_u+S_p\phi_P \tag{3.22}$$

Using linear central differencing approximation we can write expressions for the flux through the control volume faces as:

$$\text{Flux across the west face}=\Gamma_w A_w\left.\frac{\partial\phi}{\partial x}\right|_w=\Gamma_w A_w\frac{(\phi_P-\phi_W)}{\delta\, x_{WP}} \tag{3.23}$$

Similar expressions can be written for flux through other faces.

To obtain discretized equations for the convection / diffusion problem the, ϕ is approximate at all terms in above equation (3.19) as follows. It is convenient to define two variables F and D to represent the convective mass flux per unit area and diffusion conductance at cell faces: $F=\rho u$ and $D=\frac{\Gamma}{\delta x}$.

The cell face values of the variables F, D and P_e can be written as

$$F_w=(\rho u)_w,\ D_w=\frac{\Gamma_w}{\delta\, x_{WP}}\ \text{and}\ P_W=\frac{F_W}{D_W} \tag{3.24}$$

For the convective terms for a uniform grid, we can write the cell face values of property ϕ as $\phi_e = \phi_P - \phi_E/2$ and similarly for other face values.

The general discretized equation form for interior nodes reduces to

$$a_P\phi_P = a_W\phi_W + a_E\phi_E + a_N\phi_N + a_S\phi_S + S_u \tag{3.25}$$

and from conservation equation we have $(F_E - F_W) + (F_N - F_S) = 0$

where $a_W = D_W A(|P_W|) + \lceil |F_W, 0| \rceil$

$a_E = D_E A(|P_E|) + \lceil |-F_E, 0| \rceil$

$a_S = D_S A(|P_S|) + \lceil |F_S, 0| \rceil$

$a_N = D_N A(|P_N|) + \lceil |-F_N, 0| \rceil$

and $a_P = a_W + a_E + a_S + a_N - S_P A$

The value of $A(|P|)$ for the upwind scheme is 1.0 [Patankar (1980)].

In the present work, the first and second order upwind schemes have been used.

i. First-Order Upwind Scheme

In the first-order upwind scheme, quantities at cell faces are determined by assuming that the cell-center values of any field variable represent a cell-average value and hold throughout the entire cell; the face quantities are identical to the cell quantities. Thus in first-order upwind, the face value ϕ_f is set equal to the cell-center value of ϕ in the upstream cell.

ii. Second-Order Upwind Scheme

In second-order upwind scheme, quantities at cell faces are computed using a multidimensional linear reconstruction approach [Barth and Jespersen (1989)]. In this approach, higher-order accuracy is achieved at cell faces through a Taylor series expansion of the cell-centered solution about the cell centroid. Thus, when second-order upwinding is selected, the face value ϕ_f is computed using the following expression:

$$\phi_f = \phi + \nabla\phi \cdot \Delta s \tag{3.26}$$

where ϕ and $\nabla\phi$ are the cell-centered value and its gradient in the upstream cell, and Δs is the displacement vector from the upstream cell centroid to the face centroid. This formulation requires the determination of the gradient $\nabla\phi$ in each cell. This is computed using the divergence theorem, which in discrete form can be written as

$$\nabla\phi = \frac{1}{V}\sum_{f}^{N_{faces}} \tilde{\phi}_f A \tag{3.27}$$

Here the face values $\tilde{\phi}_f$ are computed by averaging ϕ from the two cells adjacent to the face. Finally, the gradient $\nabla\phi$ is limited so that no new maxima or minima are introduced.

c) Grid generation

A uniform grid arrangement is used for numerical simulation of fluid flow in a pipe using Gambit 2.2 as shown in Figure 3.6.

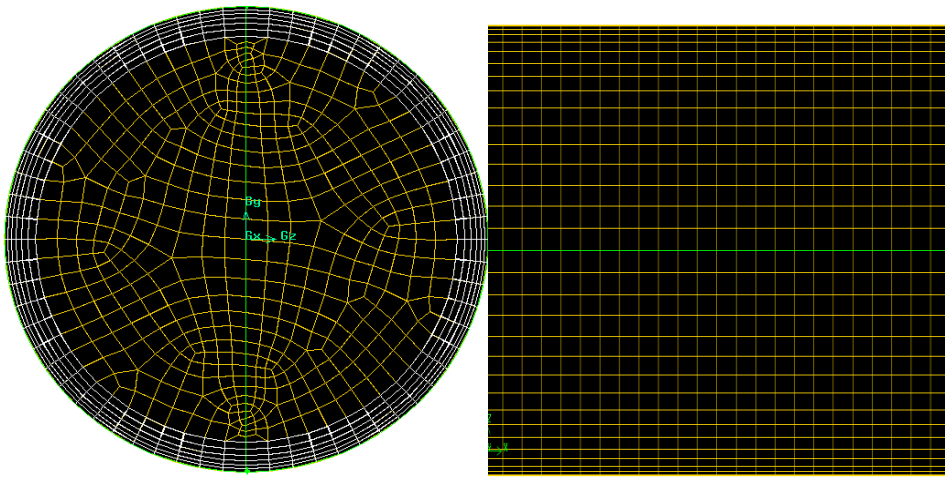

Figure 3.6: Grid generation for the test pipe for front and side view

d) Solution Algorithms for pressure-velocity coupling

If the pressure field, which appears as a major part of the source term is unknown, then equations (3.14) and (3.15) are applied at all the nodal points to yield a set of algebraic equations but the resulting velocity field may not satisfy the continuity equation. The problems of determining the pressure and satisfying continuity are overcome by adjusting the pressure field using pressure-velocity coupling by following the SIMPLE algorithm for the pressure-velocity coupling wherethe acronym SIMPLE stands for Semi-Implicit Method for Pressure-Linked Equations [Patankar and Spalding (1972)].

e) Calculation procedure

In this procedure, the governing equations are solved sequentially (i.e., segregated from one another). Since the equations are non-linear (and coupled), several iterations of the solution loop must be performed before a converged solution is obtained. The

iterations include: Fluid properties updated, based on the current values of pressure and temperature and solving the *u* and *v* momentum equations using current values for pressure and face mass fluxes in order to update the velocity field. Checks for convergence of the equation set are made and continue the above steps until the convergence criteria are met.

f) Convergence criterion

The use of an iterative solution method requires the definition of a convergence and stopping criteria to terminate the iteration process. The measure of convergence is a norm on the change in the solution vector between successive iterations. The iterative algorithm is terminated after a fixed number of iterations if the convergence has not been achieved. This criterion is used to prevent slowly convergent or divergent problems as per each scheme explained above. The convergence in the present study is defined to be obtained after all the following criteria are achieved.

- Changes in the continuity are less than 1x10-3
- Changes in the x - and y - velocity component are less than 1x10-3
- Change in the turbulence is less than 1x10-3

The discretization scheme of the present work for: momentum, volume fraction, turbulent kinetic energy and turbulent dissipation rate all are initially run at 1st order scheme until getting convergence criteria. After that all are changed to 2nd order scheme (momentum, turbulent kinetic energy and turbulent dissipation rate) except volume fraction is changed to QUICK. Finally the case is run again until getting convergence criteria.

CHAPTER 4

RESULTS AND DISCUSSIONS

4.1 Summary of Parametric Study

The objective of the present work is to numerically simulate oil-water two-phase flowing in a horizontal and slightly inclined pipe using the commercial package Computational Fluid Dynamics (CFD)/Fluent. The applied fluent modeling technique for multiphase is Eulerian model. The Realizable K-ε mixture model was selected with default related factors for turbulent. An implicit steady-state of segregated 3D solver is selected to solve the Fluent's built-in conservation of mass and momentum equations for the specified models. Oil is set as a primary continuous phase and water as a secondary phase with droplet diameter of 0.001 m.

Pipe orientation and flow direction are shown in sketches of Figure 4.1. The flow operation conditions for different variables are based on data summarized in Table 4.1. The flow is designed to enter the pipe at different variable parameters for base case and alternative cases with a total of fifteen (15) cases based on three (3) different parameters: operation conditions, fluid physical properties and piping geometry. The selection of the piping size as a conventional types used in production lines are based on the design summarized in Table 4.2. The base case selection is based on the design criteria per Saudi Aramco references [Saudi Aramco (2005)] for Arabian oil 39 ^{o}API and 30% water cut.

The mixture inlet velocity is set at 1.0 m/s as the recommended minimum velocity per Saudi Aramco standards to minimize deposition of solids and debris at the bottom of the pipe.

a) Operation conditions

Operation is simulated with two different inlet conditions as follows:

- Different inlet mixture velocity: 0.5, 1.0 and 2.0 m/s.
- Different inlet water content (WC): 20, 30 and 50%.

b) Different oil physical properties

The oil properties used in this research are based on two variables referring in the base case to specific properties of oil production at Saudi Aramco.

- Different viscosity ratio of oil to water: 2.0 / 1.0, 15.0 / 1.0 and 30 / 1.0 cP.
- Different density ratio of oil to water: 662/998.2, 830/998.2 and 998.2/998.2 kg/m^3.

c) Piping geometry

The proposed pipes have nominal diameter and standard schedule as tabulated in Table 4.2. The base case pipe is with an inner diameter of 154 mm. The alternative pipe sizes are 102 mm and 202 mm inner diameter. The selection of these sizes is based on the most used pipelines for oil-water production to transport oil-water from wells to separation plants. Moreover, since the production pipelines are never be horizontal for the total length, different inclinations are selected arbitrary to represent expected piping orientations. As part of the geometry test, effects of internal turbulator devices are tested which are detailed below. The summery of the geometry effect is as follows:

- Different pipe inner diameter; 102, 202 and 154 mm.
- Different pipe inclinations (β): -15, 0 and +15 degree from horizontal line.
- Different internal turbulators: detail is available in Chapter 5.

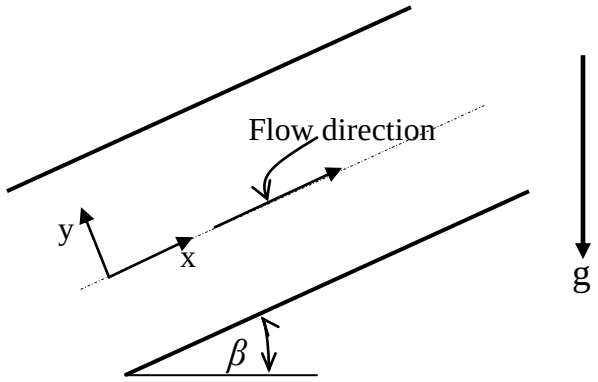

Figure 4.1: Piping orientation and flow direction

Table 4.1: Cases of different variable conditions

Variables	Base case	Case 1	Case 2	Case 3	Case 4	Case 5	Case 6	Case 7	Case 8	Case 9	Case 10	Case 11	Case 12	Case 13	Case 14
Inlet flow pattern	Mixed	Mixed	Mixed	Mixed	Mixed	Mixed	Mixed	Mixed	Mixed	Mixed	Mixed	Mixed	Mixed	Segregated Flow	
Mixture velocity (m/s)	1	0.5	2	1	1	1	1	1	1	1	1	1	1	1	1
Oil viscosity (cP)	2	2	2	15	30	2	2	2	2	2	2	2	2	2	2
Oil density (kg/m3)	830	830	830	830	830	830	830	830	830	830	830	998.2	662	830	830
Pipe inner Diameter (mm)	154	154	154	154	154	102	202	154	154	154	154	154	154	100	154
WC%	30	30	30	30	30	30	30	20	50	30	30	30	30	20	30
Inclination (Degree)	0	0	0	0	0	0	0	0	0	15	-15	0	0	0	0
Length (m)	6	6	6	6	6	6	6	6	6	6	6	6	6	6	6
Turbulator	NA	NA	NA	NA	NA	NA	NA	NA	NA	NA	NA	NA	NA	A	B

Table 4.2: Pipelines design information

Pipe Sizes & Schedules						
Nominal Dia.		**O.D.**	**Wall Thickness**	**Mass**	**Identification**	
inches	mm	mm	mm	Kg/m	Designation	Schedule Number
4	100	114.3	6.02	16.06	STD	40
6	150	168.3	7.1	28.23	STD	40
8	200	219.1	8.2	42.49	STD	40

Dimensionless pipe

To generalize this work, the result is reported in terms of dimensionless pipe geometry for length over inner diameter (L/D). This work covers up to 58.82 of L/D as per Table 4.3 that contains portion length (x_n) of the total pipe length (L).

Table 4.3: Dimensionless length of pipes used in this work (L/D)

x_n	0	1	2	3	4	5	6	D
x_n/D	0.00	9.80	19.61	29.41	39.22	49.02	58.82	0.102
x_n/D	0.00	6.49	12.99	19.48	25.97	32.47	38.96	0.154
x_n/D	0.00	4.95	9.90	14.85	19.80	24.75	29.70	0.202

Reynolds number

To generalize this work, the Reynolds numbers are calculated based on the mixture properties (Table 4.4) and piping different geometries (Table 4.2) to cover the range of Reynolds Numbers from $6.37x10^3$ to $1.59\ x10^5$.

4.2 Grid Independence Tests

The numerical solution requires building grids of the pipe geometry as cells of meshing. The numerical model can be reliable only if it is tested to be independent of the meshing dimensions. The meshing density selection is validated by comparing different parameters for different cases.

Boundary conditions

The fluid properties to investigate the meshing affect are based on the base case as shown in Table 4.1. The mixture inlet velocity is 1.0 m/s with inlet water cut of 30%. Oil has viscosity of 2.0 cP and density of 830 kg/m^3. The internal surface of the pipe is considered smooth surface.

Piping geometry building

The test is done using straight pipe configurations of inner diameter, 154 mm, and total straight length of 6000 mm. The meshing is evaluated by comparing four stages of meshing densities based on the count number of meshing per edge, center line and pipe length. The circumferential edge is divided to two parts each part has a count number of 20, 24, 32 and 40 or a circumferential counts of 40, 48, 64 and 80

with count number of 32, 38, 48 and 55 for previous edges counts respectively. The meshing has 6 layers of boundary layers based on 1.0 mm and an increment of 1.2 factors. The pipe has a longitudinal split to two parts. The longitudinal meshing is 300, 400, 500 and 550 count points for previous edges counts respectively.

The cases are named based on the count number of meshing for each stage as edges count number of meshing for one-half circumferential, center-line and length for each stage. The cases of each stage are E20/32/300, E24/38/400, 32/48/500 and 40/56/550 respectively. For simplification, the cases can be called E20, E24, E32 and E40. The different stage shows the geometry volume of total element, skewness and aspect ratio as shown in the related figures as highlighted below in Figure 4.2, Figure 4.3, Figure 4.4 and Figure 4.5.

E20/32/300-meshing: total element, skew and aspect ratio: 121200 / 42% / 20.1

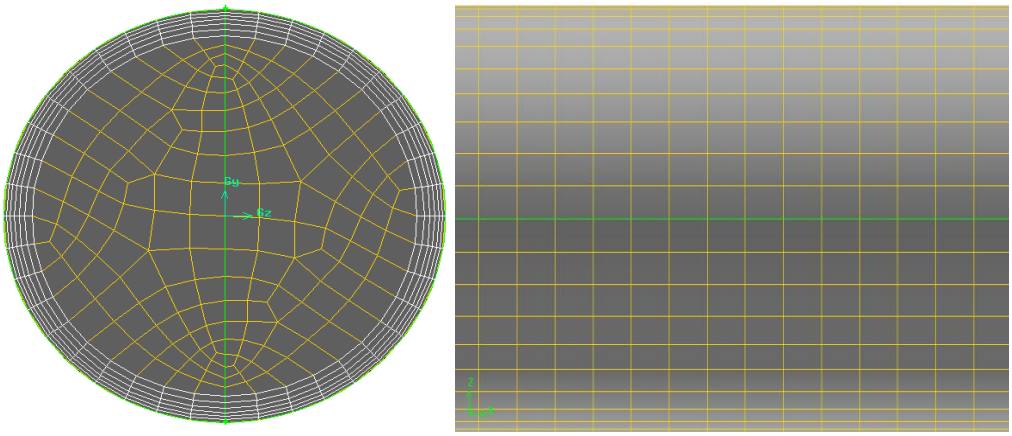

Figure 4.2: Cross section and longitudinal meshing for E20/32/300

E24/38/400-meshing: total element, skew and aspect ratio: 224000 / 48% / 15.2

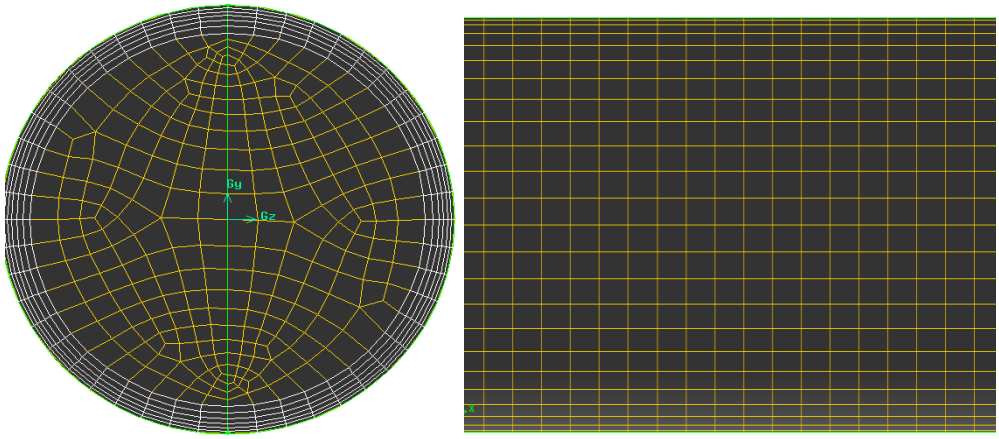

Figure 4.3: Cross section and longitudinal meshing for E24/38/400

E32/48/500-meshing: total element, skew and aspect ratio: 425000 / 69% / 12.2

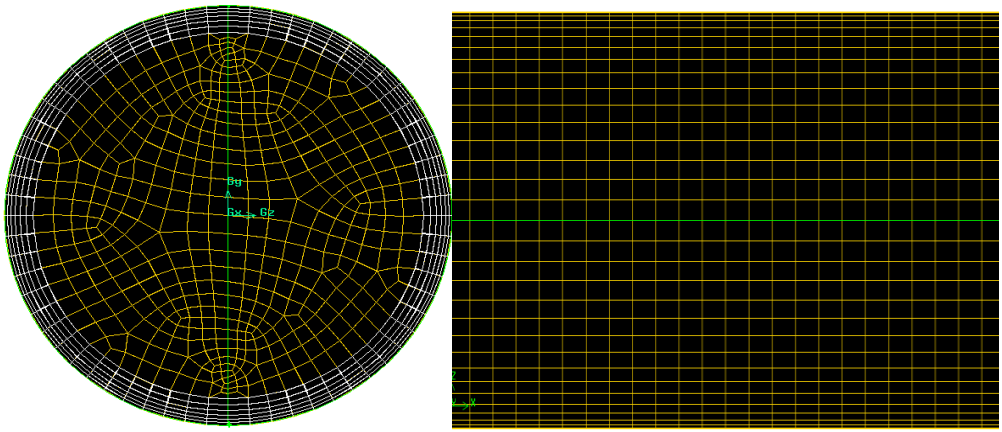

Figure 4.4: Cross section and longitudinal meshing for E32/48/500

E40/55/550-meshing: total element, skew and aspect ratio: 661100 / 69% / 14.2

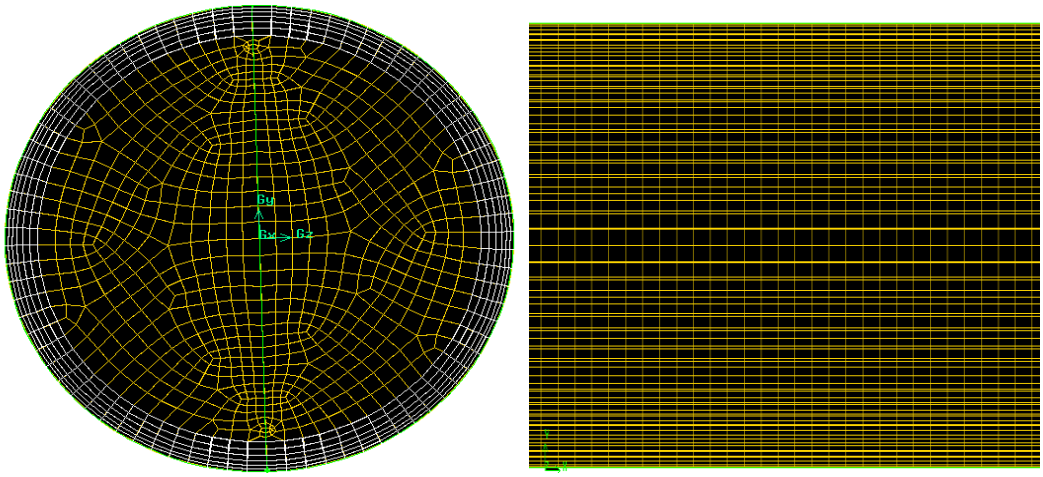

Figure 4.5: Cross section and longitudinal meshing for E40/55/550

The pipe is configured with defining different planes in cross-sections at certain distances along the pipe as shown in Figure 4.6. The planes are named: X0, X1, X2, X3, X4, X5 and X6. The comparisons of contours for water phase contents for different meshing work per base case operation conditions are shown in Table 4.4 and Figure 4.5. Water phase velocity contour is shown in Table 4.5 and Figure 4.8. Oil phase velocity contour is shown in Figure 4.9.The result is that the differences in the patterns and water holdup (local contents) disappear as the mesh densities increases from E20 to E40.

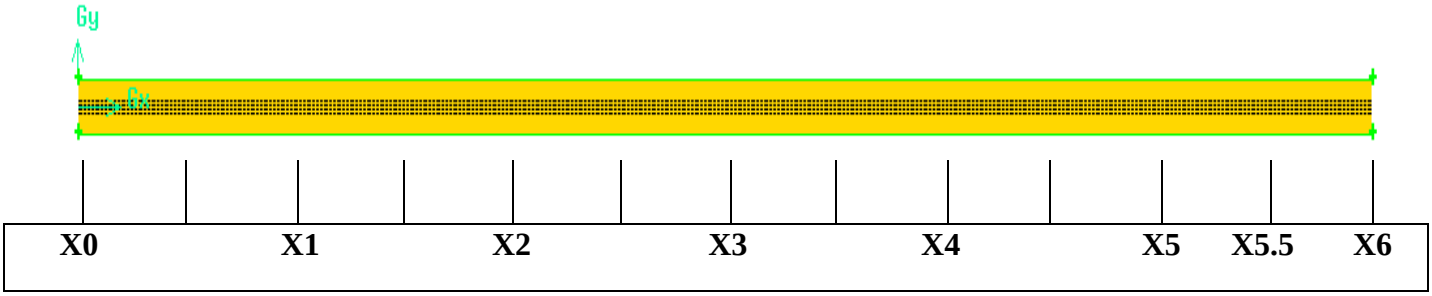

Figure 4.6: Planes along the pipe

Contours comparison

Water phase contours comparison for cross sections of the pipe for the four (4) stages of meshing is shown in Table 4.4. It shows that at same cross sections for different stages of meshing the flow patterns get closer until they get so similar for the last two levels of meshing. Water velocity contours comparison for cross sections at the pipe for the four (4) stages of meshing is shown in Table 4.5. It shows that at same cross sections for all levels the flow patterns get closer until they get so similar for the last two levels of meshing.

a) Y-X – cross-plane for water phase/velocity contours (plane Z = 0)

Table 4.4: Water phase contour along meshing dependency test levels

	E20/32/300	E24/38/400	E32/48/500	E40/56/550
X0	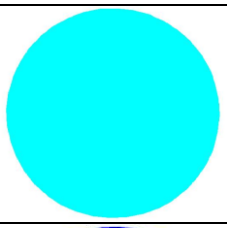	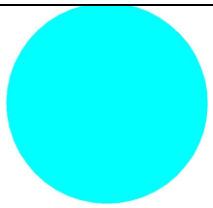	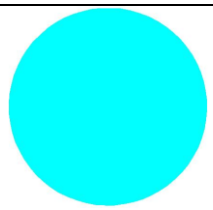	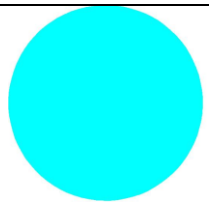
X1	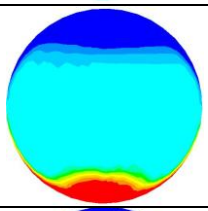	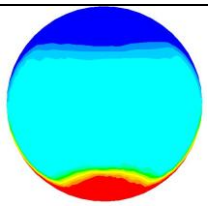	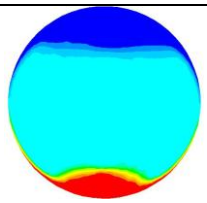	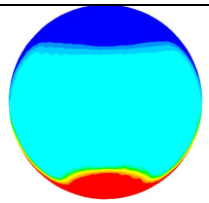
X2	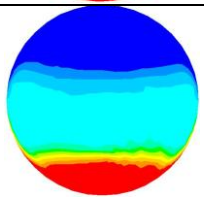	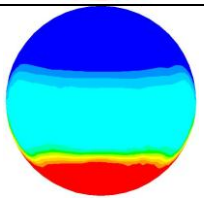	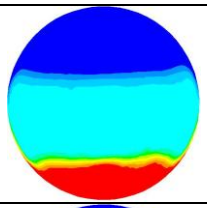	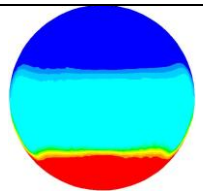
X3	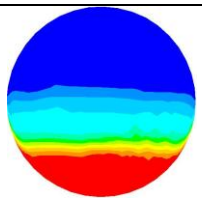	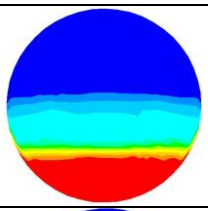	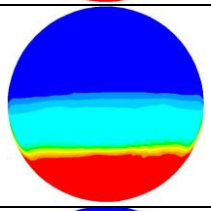	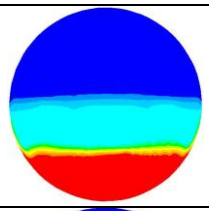
X4	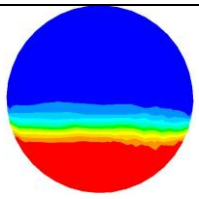	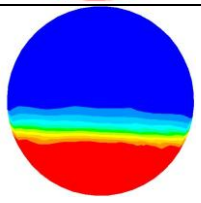	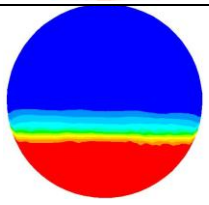	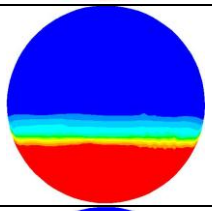
X5	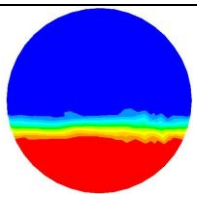	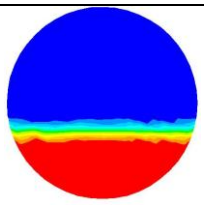	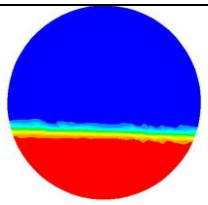	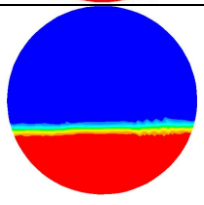
X6	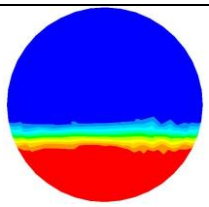	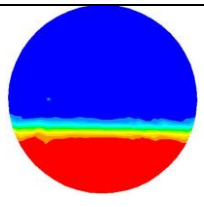	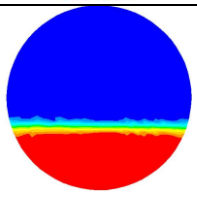	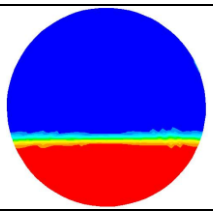

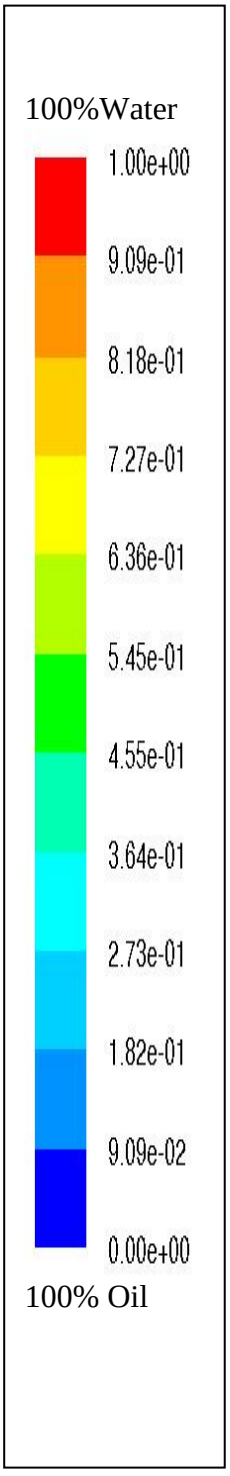

Table 4.5: Water velocity contour along meshing dependency test levels

	E20/32/300	E24/38/400	E32/48/500	E40/56/550
X0	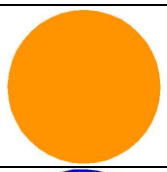	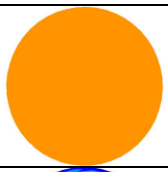	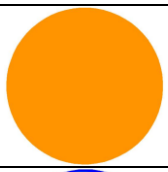	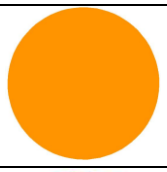
X1	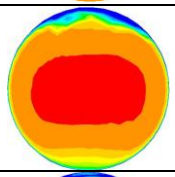	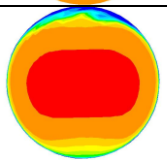	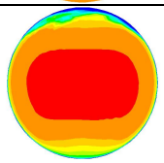	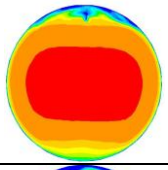
X2	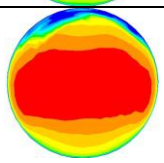	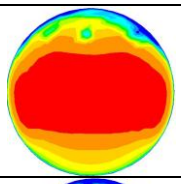	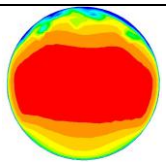	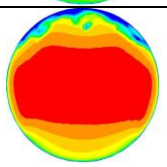
X3	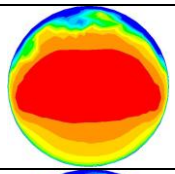	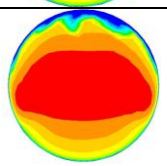	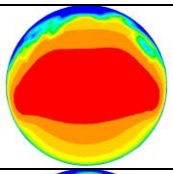	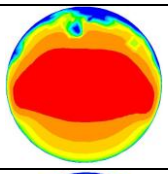
X4	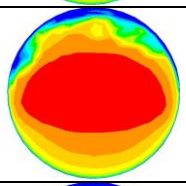	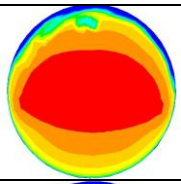	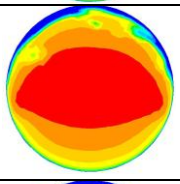	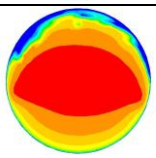
X5	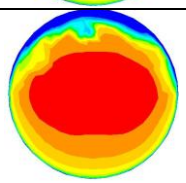	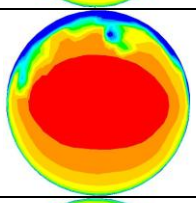	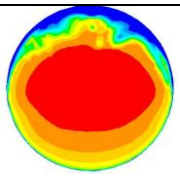	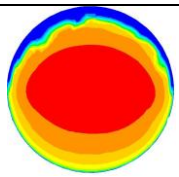
X6	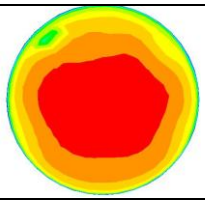	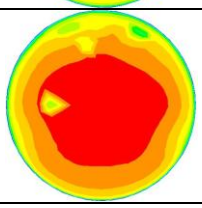	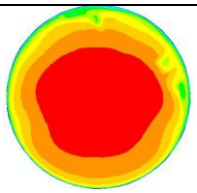	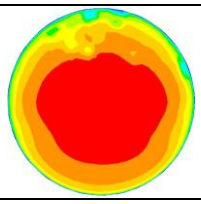

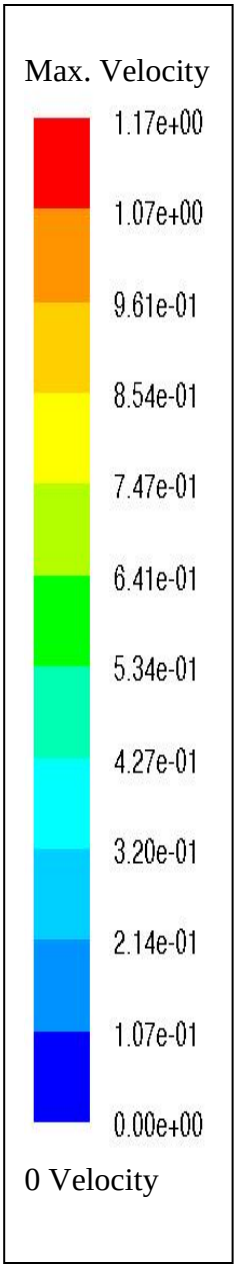

b) Y-Z- longitudinal–plane for phase/velocity contours (plane X = 0)

The contours comparison for flow at the vertical center plane along the pipe is shown in Figure 4.7, 4.8 and 4.9 for water phase contours, water velocity contours and oil velocity contours respectively. The last two stages of all different counters for E32 and E40 are identical.

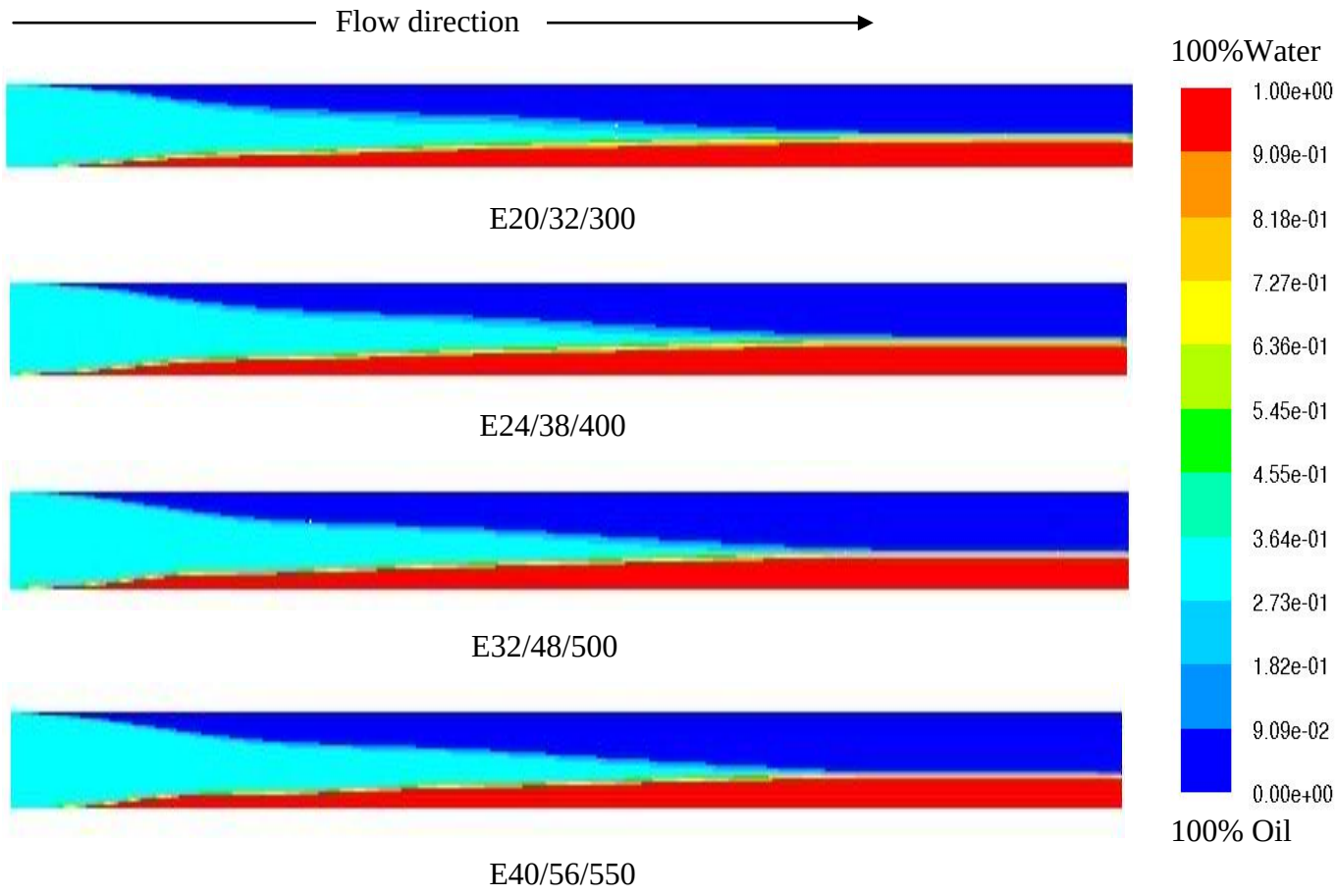

Figure 4.7: Water content contour along longitudinal central-vertical planes for each stage of mesh dependency test

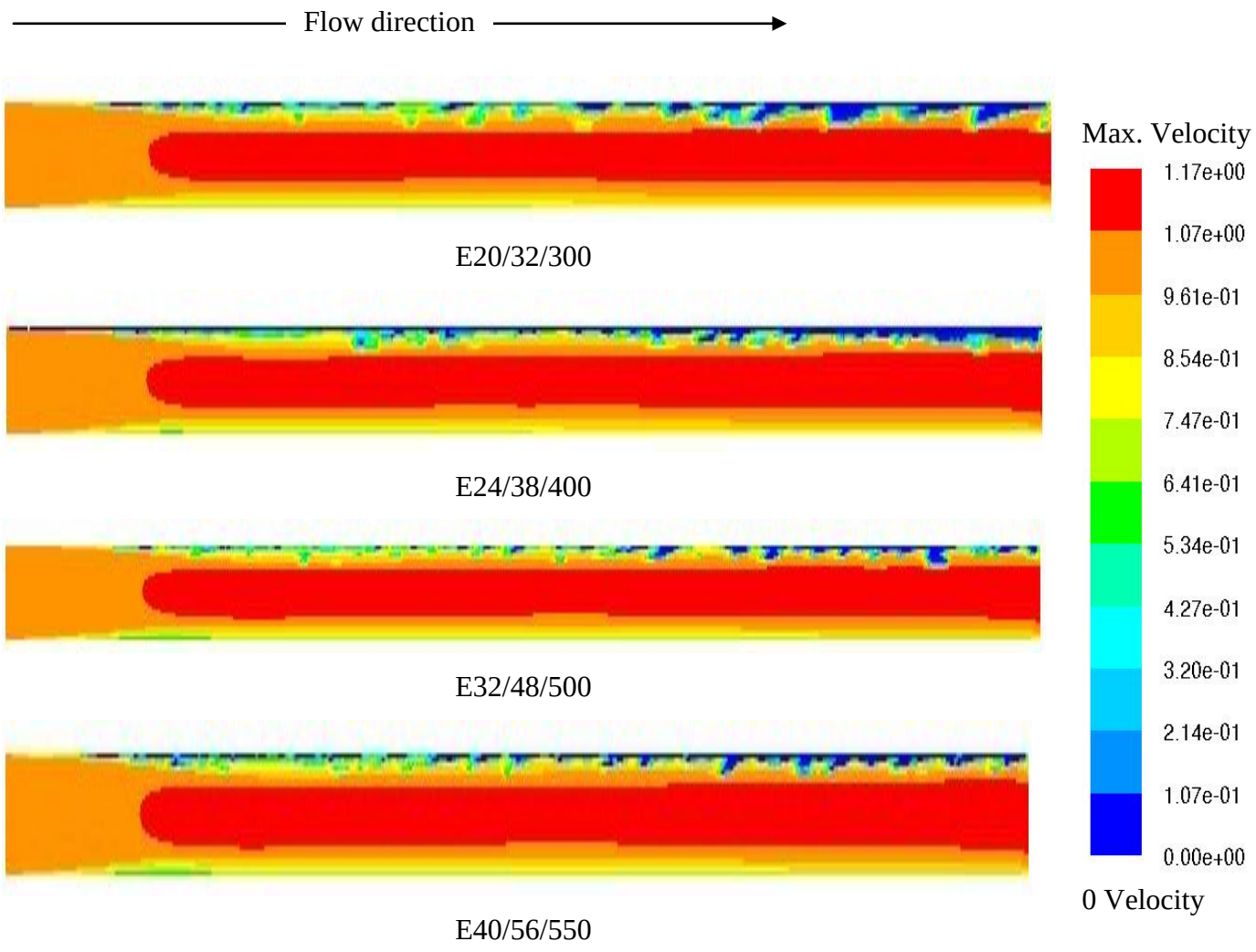

Figure 4.8: Water velocity contour along longitudinal central-vertical planes for each stage of mesh dependency test

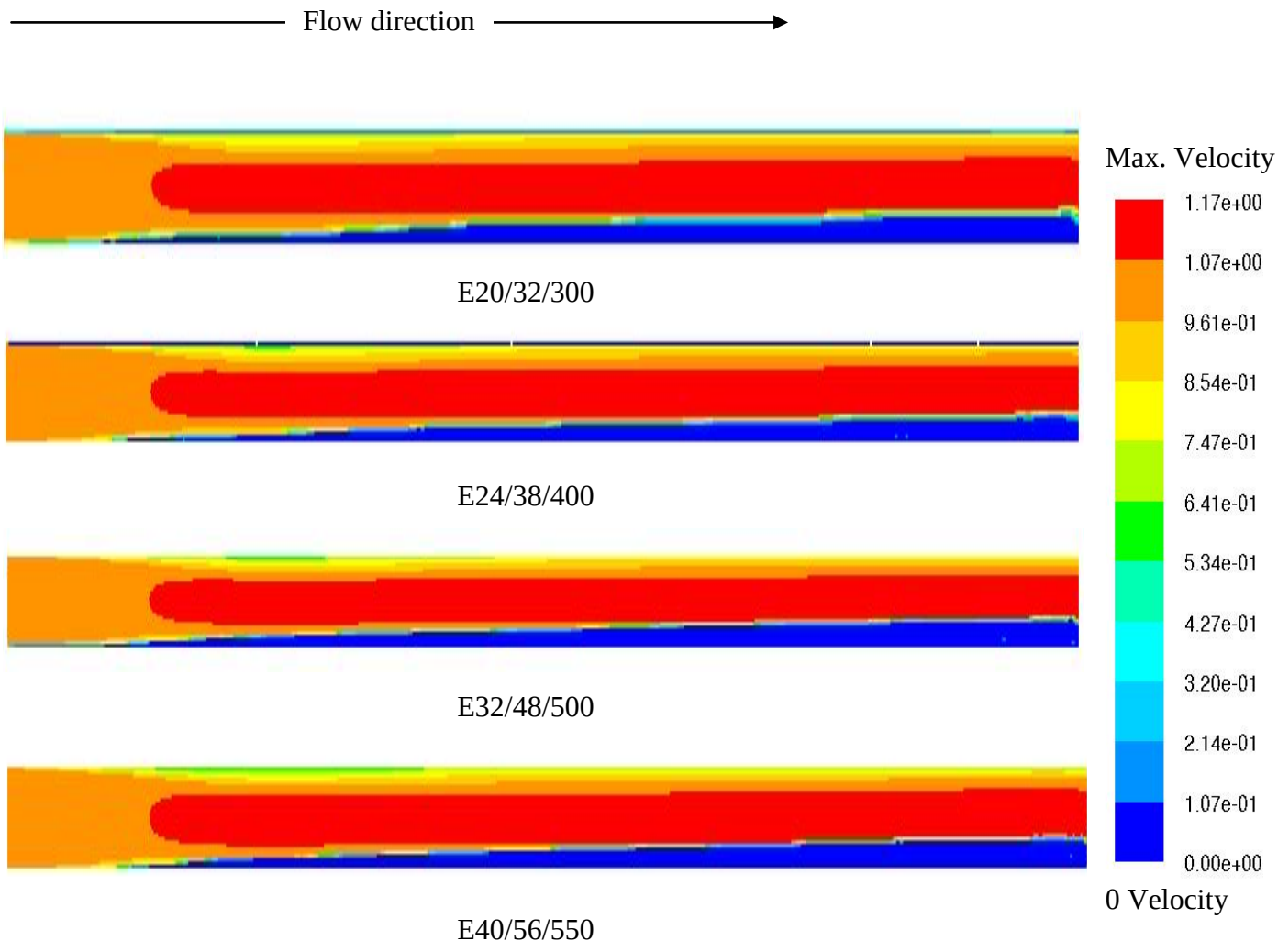

Figure 4.9: Oil velocity contour along longitudinal central-vertical planes for each stage of mesh dependency test

Radial plots

As a continuation to meshing dependency test, radial water height concentrations along vertical-central lines are monitored at different locations along the pipe for the four (4) stages. The lines are a normalized of height from pipe bottom to the diameter as shown in Figure 4.10. These lines are located at 1000, 2000, 3000, 4000, 5000 and 6000 mm distances downstream the inlet as shown in Figure 4.6

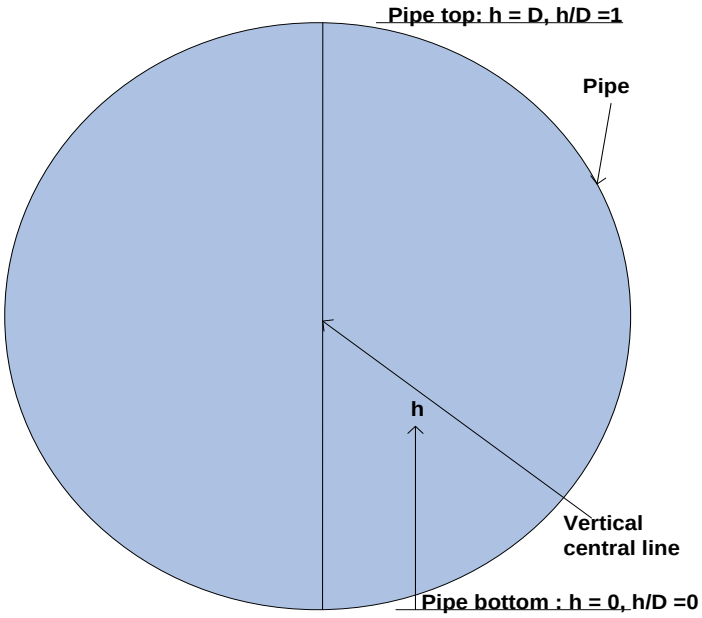

Figure 4.10: Radial vertical line at the center of the pipe for water concentration height measurement

Concentration error comparisons of water in vertical height are presented at X2 and X5 which are 2000 and 5000 mm from inlet, respectively, as presented in the Figures 4.11 and 4.12. The figures have the water concentration on the x-axis and the

ratio height of the pipe on the y-axis. The figures show very negligible differences referring to E32 that is considered not affecting the flow patterns behavior. Accordingly, the meshing of E32 features is selected for conducting the simulation of the present work.

Simulation error based on water concentration calculations

Error of simulation based on water concentration calculation in the radial direction for different meshing density calculated using method below for E20, E24, E32 and E40:

$$\boxed{\text{Error in E20} = \text{E40 - E20}}, \quad \boxed{\text{Error in E24} = \text{E40 - E24}}, \quad \boxed{\text{Error in E32} = \text{E40 - E32}}$$

Per the selected cross-sections at X2 and X5, the error range shows the highest value for E20 that is followed by E24 and the lowest error is shown by E32 as shown in Figure 5.10 and Figure 5.11. The error increase downstream towards the outlet with having more phases' separation. E32 change ranges for all X-planes are shown in Table 4.6.

Table 4.6: Range of errors in water concentrations for E32

Location from inlet	Range of error	
	Min	Max
X1(1000 mm)	- 0.00031	0.00034
X2 (2000 mm)	- 0.0017	0.005
X3 (3000 mm)	- 0.003	0.018
X4 (4000 mm)	- 0.0036	0.02
X5 (5000 mm)	- 0.0032	0.017
X6 (6000 mm)	- 0.0039	0.017

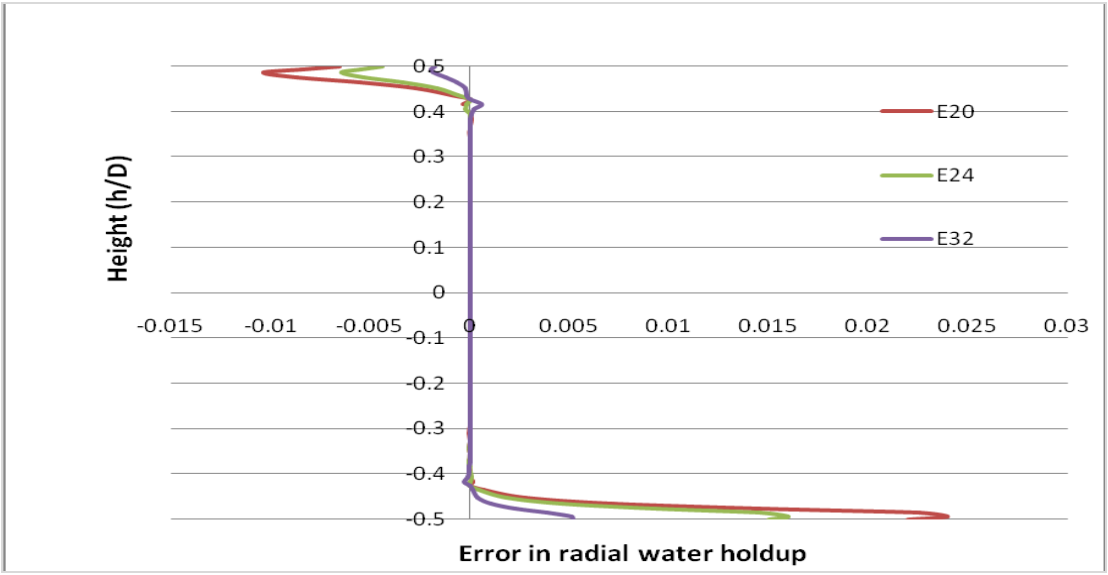

Figure 4.11: Error range changes for meshing dependency test at X2, L/D = 13.0

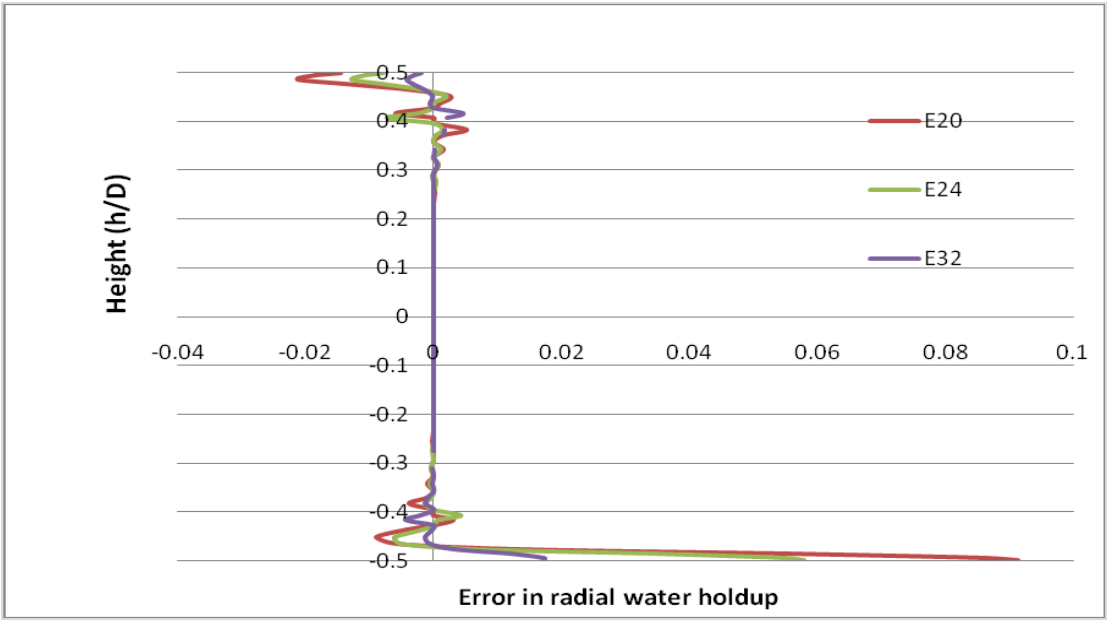

Figure 4.12: Error range changes for meshing dependency test at X5, L/D = 32.5

4.3 Model Validation

The present work is validated against available experimental work in the field of oil-water flow in horizontal and slightly inclined pipes with similar operation conditions. The validations were conducted with comparisons with the work of Shi (2001), Vedapuri et al. (1997), Kumara et al. (2010) and Cai et al. (2004). The details of these experimental results are described in the following:

Shi (2001)

The first reference is the experimental work done by Shi (2001). Shi (2001) conducted an experiments work for the dissertation to study many parameters influencing oil-water flow characteristics including oil-water distributions, velocity profile, droplet size, etc. All experimental work was performed in horizontal Plexi-glass pipe of 101 mm inner diameter.

All of experimental work was performed using a Conoco LVT200 oil and ASTM seawater. The system is equipped with electrical heater and water cooling systems to maintain the test temperature in the system at 25°C. The fluids properties at 25°C are shown in Table 4.7. The oil-water mixture from an agitate oil-water mixture tank to ensure well-mixed flow is used.

Table 4.7: Properties of oil and water at 25°C (Shi, 2001)

Property	Viscosity (cP)	Density (Kg/m^3)	Water Cut %	Mixture Velocity (m/s)	Pressure (MPa)
Oil (LVT 200)	3.0	820	0 -100%	0.4 – 3.0	13
ASTM Seawater	1.0	1024			

Shi (2001) investigated water holdup of oil-water two-phase flow in detail for input water cut of 5, 10, 15, 20, 30, 40, 50, 60 and 80% at different inlet mixture velocities in the range from 0.4 to 3.0 m/s in the 101 mm ID pipe. The liquid was withdrawn at different heights along the vertical diameter of the pipeline by a sampling tube inserted into the test section. The experimental error reported is within 5%. The work shows that as inlet mixture velocity increases, mixing increases. From velocity profiles, it shows that velocities are the highest at the pipe center. Moreover, the velocity at the pipe top is faster than the bottom because of more oil layer at the top compared to more water at the pipe bottom.

For corrosion test purposes, the test section acrylic pipe of 2.0 m long, and 101 mm in diameter is used. The system was purged with oxygen to get it mixed in the fluid, then carbon dioxide was injected into the system to keep a pressure of 0.13 MPa and temperature of 25°C. Electrical Resistance (ER) probes are installed to measure the corrosion rate by using a metal samples ER.

Vedapuri et al. (1997)

The second reference is the experimental work done by Vedapuri et al. (1997). They studied experimentally oil-water flow in horizontal and slightly inclined (+/-2 degree) plexiglas pipes of 10 cm diameter with oil viscosity of (2 and 90 cP) and ASTM standard water. The study covered the mixture velocity from 0.1 to 2 m/s with water cut 20, 40, 60 and 80%. They used a pitot tube to measure the local velocity along the vertical pipe diameter. The pitot tube has an inherent disadvantage by disturbing the flow field and affect the local velocity. The flow patterns observed from the experiments are as follows:

For low viscosity oil:

- In horizontal flow:
  - In the velocity range from 0.4 to 0.6 m/s: a semi-segregated flow pattern.
  - In the velocity range from 0.8 to 1.4 m/s: a semi-mixed flow pattern.
  - Above 1.4 m/s: semi-dispersed flow.
- In 2-degree upward inclined flow: flow mixing enhancement with more oil reaching the bottom of the pipe.

- For high viscosity oil:
  - In the velocity range of 0.4 to 0.8 m/s: semi-segregated flow pattern.

They summarized the cross-section flow patterns of three layers as shown in Figure 2.1 where both semi-segregated and semi-mixed flow patterns are called by other researchers as stratified flow with mixing at the interface ST&MI or three-layers (3L) or dual continuous flows.

Kumara et al. (2010)

Kumara et al. (2010), conducted experimental work of oil (density 790 kg/m^3 and viscosity 1.64 mPas) and water (density 996 kg/m^3 and viscosity 1.00 mPa.s) in a pipe (56 mm ID), horizontal and slightly inclined (5 to -5 degree). The test was conducted at a mixture velocity of 0.50 and 1.00 m/s with 50% water cut. The different flow regimes are determined based on visual observations. Stratified flow with mixing at the interface is observed at mixture velocity of 0.50 m/s. Interfacial waves are observed in upwardly and downwardly inclined flows. At a mixture velocity of 1.00 m/s, interfacial mixing is increased and dual continuous flows are observed.

They studied the effect of velocity and pipe inclination on the flow patterns and water holdup. The cross-sectional phase distribution is measured with a single-beam gamma densitometer. The different flow regimes are determined by visual observations and camera. The results are summarized as follows:

a) For horizontal pipe : The water holdup at 0.5 m/s is almost 0% above h/d of 0.1 and 100% below h/d of (-0.05) while between (-0.05) and 0.1 h/d ratio the flow is dual. The water holdup at 1.0 m/s is almost 0% above h/d of 0.2 and 100% below h/d of (-0.35) while between (-0.35) and 0.2 of h/d ratio the flow is dual.

b) For 5-degree inclined up pipe: The water holdup at 0.5 m/s is almost 0% above h/d of 0.5 and 100% below h/d of (-0.05) while between (-0.05) and 0.5 h/d ratio the flow is dual. The water holdup at 1.0 m/s is almost 0% above h/d of 0.38 and 100%

below h/d of (-0.2) while between (-0.2) and 0.38 of h/d ratio the flow is dual. Higher mixture inlet velocity reduces the local water concentration.

c) For 5-degree inclined down pipe: The water holdup at 0.5 m/s is almost 0% above h/d of 0.18 and 100% below h/d of (-0.5) while between (-0.5) and 0.18 h/d ratio the flow is dual. The water holdup at 1.0 m/s is almost 0% above h/d of 0.10 and 100% below h/d of (-0.2) while between (-0.2) and 0.10 of h/d ratio the flow is dual. From previous comparisons, local water concentration decreases for inclined down pipes and higher mixture inlet velocity.

Cai et al. (2004)

Cai et al. (2004) numerically investigated the parameters that affect water holdup by calculating the required critical velocity for water entrainment. They used LVT200 oil at 25°C (ρ_o = 820 kg/m^3, μ_o = 2 cP). The water is ASTM seawater (ρ_w=1024 kg/m^3, μ_W =1 cP) up to 40% water cut. The oil-water mixture velocity flow rate was in the range of 0.4 to 3.0 m/s. The study covered the parameters including: pipe diameter, oil viscosity and density. Accordingly, they produced a model that predicts the thickness of the water film, the local film velocity and wetted area in order to estimate corrosion rate. They reached to that: (1) Increasing water cut requires higher critical velocity to entrain water, (2) increasing pipe diameter increases the required critical velocity for water entrainment, (3) Increasing oil density decreases the critical velocity required to entrain water, and (4) Increasing oil viscosity forms stable water-in-oil dispersion that lowers critical velocity.

By showing the main experimental reference work to validate the present work, following paragraphs are the validation results.

4.4 Validation Results

Influence of inlet conditions:

The present work is validated against available experimental work in the field of oil-water flow in horizontal and slightly inclined pipes with similar operation conditions as the present work [Shi (2001), Vedapuri et al. (1997), Cai et al. (2004) and Kumara et al. (2010)].

The validation here referred to Shi (2001) work, the inlet water cut is 30% at 1.0 m/s inlet mixture velocity. Figure 4.13 reflects the flow patterns per the cross section of the present work compared to the flow patterns map of the reference of identical operating conditions (30% WC and 1.0 m/s). The pipe diameter is 101 mm and 102 mm for Shi (2001) and present work, respectively. The comparison is done by taking a print of the cross-section of the present work (1) and places it over the pattern map of the reference work (2). The print is centered by a vertical line (3) passing by the input mixture velocity on the reference map. The flow pattern of the reference crossed by the vertical line is compared to the present work for expected flow patterns. The flow pattern of the present work is defined as shown in Figure 2.1 as defined by Vedapuri et al. (1997). The comparison as shown in Figure 4.13 depicts good agreement of segregated flow pattern with the reference Shi (2001).

Figure 4.14 depicts the radial water local content changes across the pipe diameter for the reference Shi (2001) compared to the present flow in 102 mm pipe diameter. The water local contents comparison has good matching for the two works. The validation in Figure 4.15 is referred to Kumara

et al. (2010), of 56 mm pipe diameter with inlet water content of 50% WC at 1.0 m/s inlet mixture velocity. Figure 4.15 depicts the radial water local content changes across the pipe diameter for the reference compared to the present work in 154 mm pipe diameter. The water local contents comparison shows small difference in local water contents that might be due to large difference in diameters between the two cases.

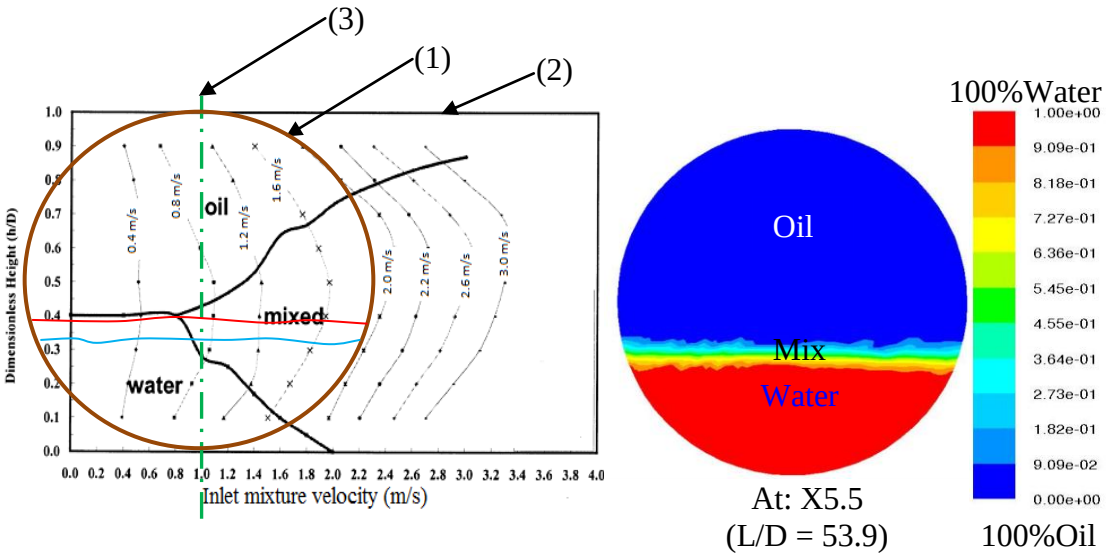

Figure 4.13: Flow pattern validation in straight pipe at 1.0 m/s and 30% WC% for present work and the reference (Shi, 2001)

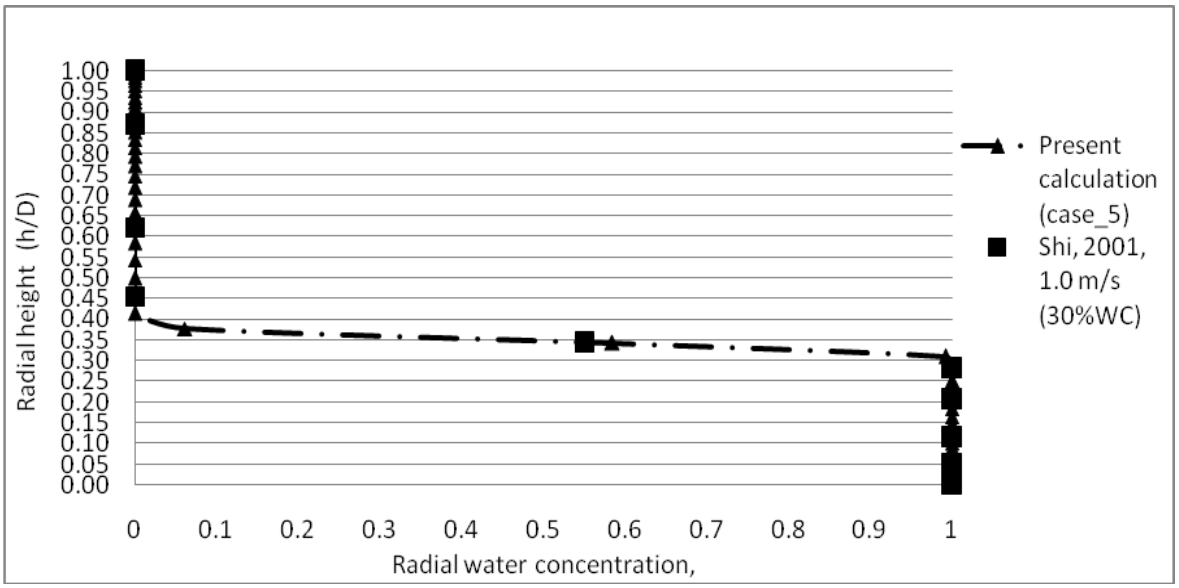

Figure 4.14: Local water contents at 1.0 m/s and 30% WC% for both present work and the reference (Shi, 2001)

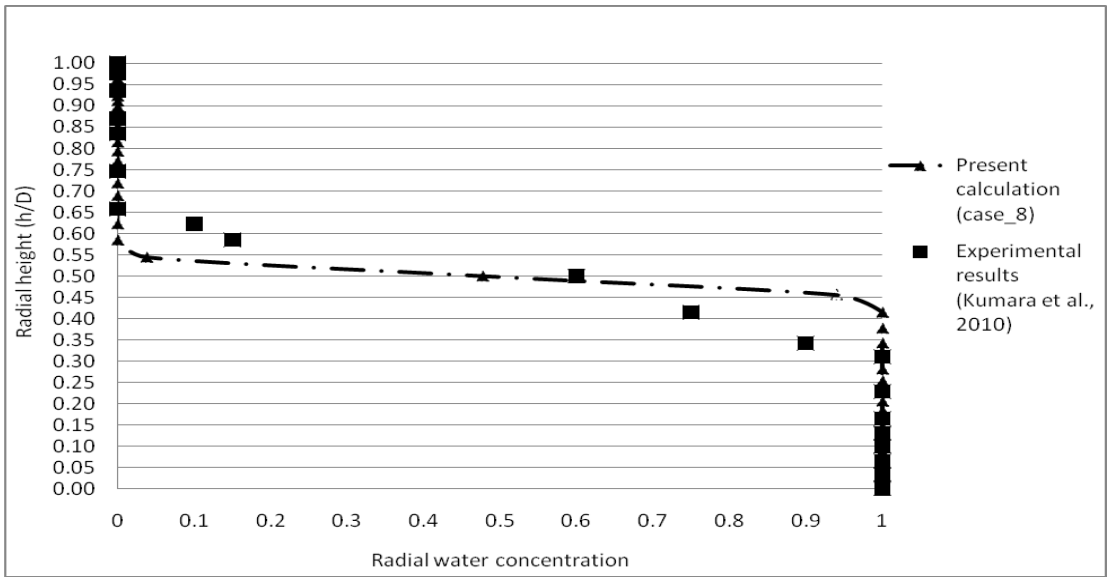

Figure 4.15: Local water contents at 1.0 m/s and 50% WC% for both present work and the reference (Kumara et al., 2010)

Influence of oil physical properties:

Up to the best of the author knowledge, there are no experimental works investigating the effect of the oil properties alone with fixing all the other variables. All available work changes other variables with changing the oil physical properties. The only available work that can be utilized to validate the present work is a numerical work. The available numerical work shows the concept of the effect of the oil properties on the water holdup and flow patterns. The other support validations are general comments received from some work in this field. The validations here are referring to Arirachakaran et al. (1989), Yeo et al. (2000) and Cai et al. (2004).

Per the study of Arirachakaran et al. (1989) in the field of oil-water, it is reported that the flow patterns depend on oil viscosity when oil is the continuous phase. Yeo et al. (2000) showed that large density differences between the aqueous and continuous phases make dispersion more difficult to achieve. That means reducing density difference between oil and water, increase oil-water mixing zone.

By referring to the above observations, all can be observed in the present work where it shows clear impact of density and viscosity on oil-water separation. Figure 4.16 and Figure 4.17 show that as viscosity increases, the mixing zone increases leading to low water separation. It seems that the water droplet get stabilized and suspended in the oil phase because of decreasing the coalescence of droplets with increasing the oil viscosity. In this case, higher oil viscosity leads to low water content (holdup) downstream the two phase flow of oil-and-water. That means the required critical velocity to entrain water phase decreases and that matches the concept of Cai et

al. (2004) work. The densities impact is shown in Figure 4.18 and 4.19 for the present work. These figures indicate that as oil to water density ratio increases, the separation decreases. By another definition, as the term $|\rho_w - \rho_o|$ approaches zero, the mixing improves. Accordingly, the local water content (holdup) decreases. These findings are in parallel with Cai et al. (2004) work , which shows that increasing oil density decreases the critical velocity and water can be much easier entrained by the oil phase.

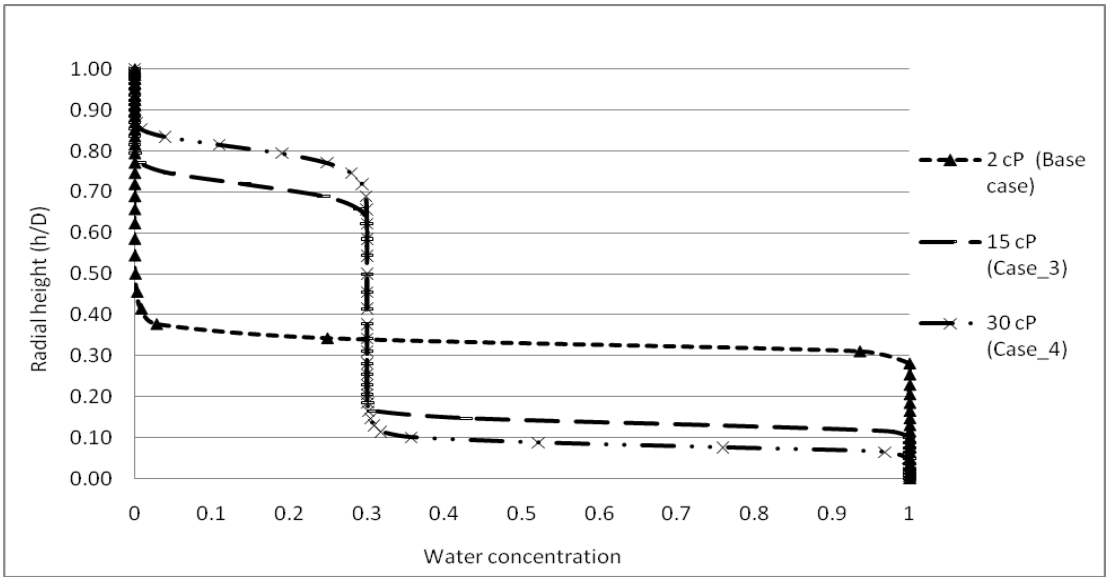

Figure 4.16: Variation of water concentration in vertical position of different oil viscosities at plane X5.5 (L/D = 35.7)

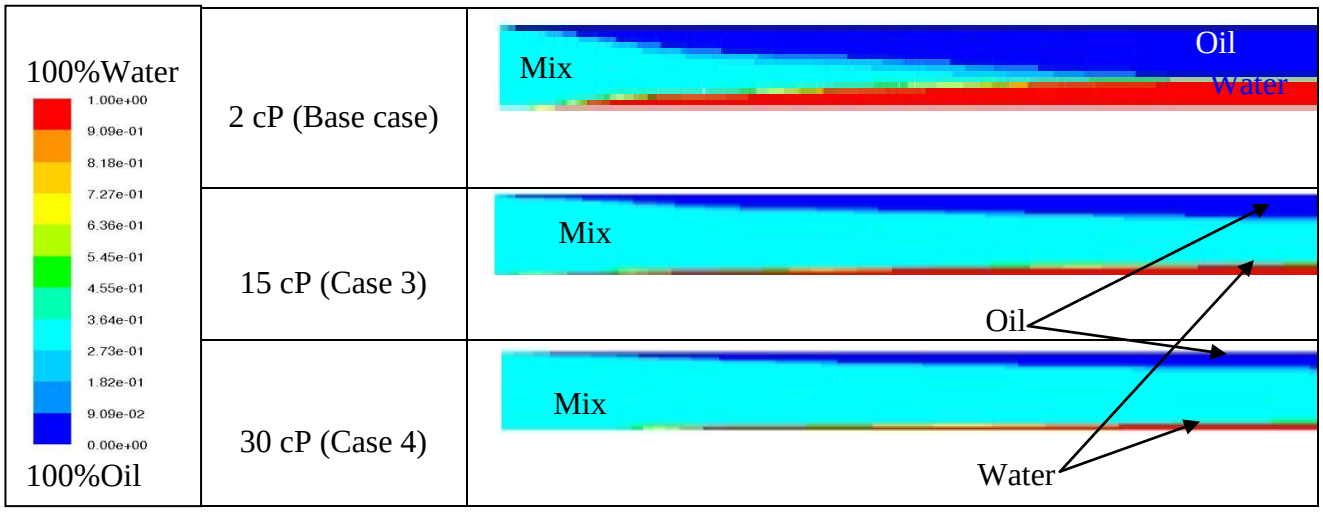

Figure 4.17: Water contours at different oil dynamic viscosities for longitudinal vertical contour, X-Y-plane

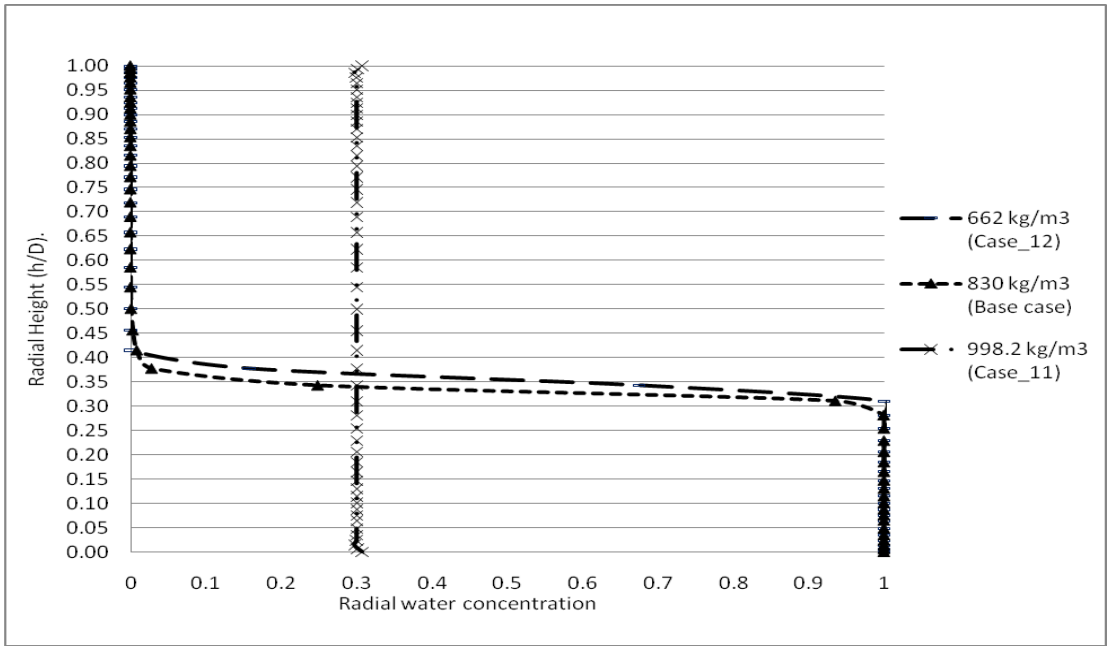

Figure 4.18: Comparison of water concentration in vertical position of different oil densities at plane X5.5 (L/D =35.7)

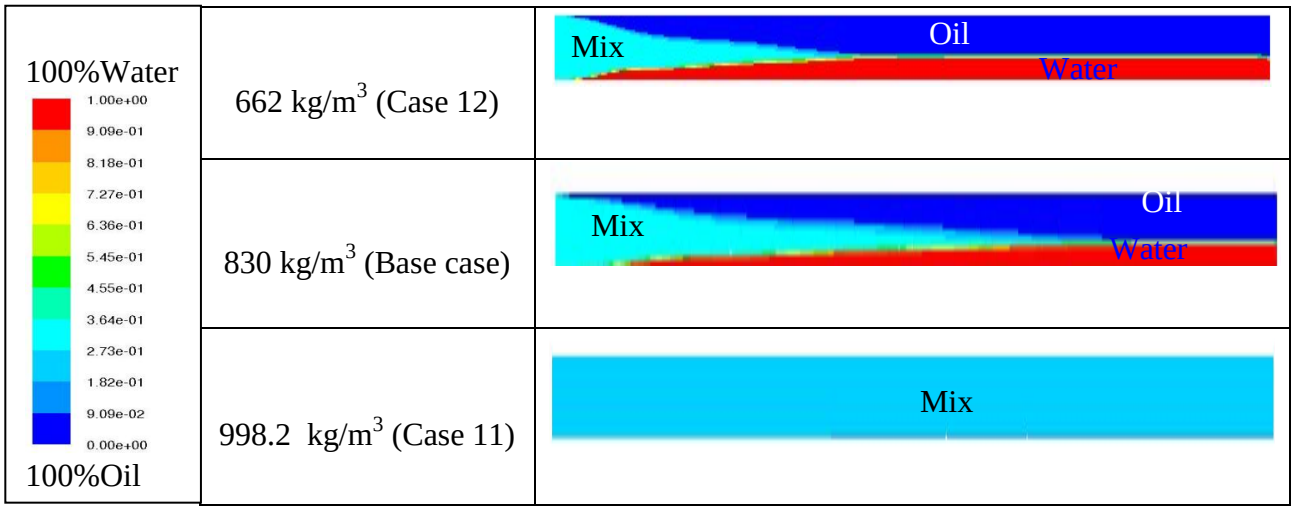

Figure 4.19: Water contours at different oil densities for longitudinal vertical contour, X-Y-plane

Influence of piping geometry:

The flow patterns of the two-phase flow are very sensitive to the pipe diameter size, pipe inclination and water cut. Up to the knowledge of the present work author, there are no available works matching the present work for all these variables. So the validation here will be based on the concept of the flow patterns change based on the change of these variables. The validations here are referring to Kumara et al. (2010) and Cai et al. (2004).

Figure 4.20 compares water content for the present work to Kumara et al. (2010) for different pipes inclinations and design conditions. Both works have horizontal cases. However, the present work calculates water separation in 15 degree Up & Down inclined pipe and Kumara et al. (2010) experiment was done in 5 degree

Up & Down inclined pipe. The present calculation is for 30% WC in 154 mm pipe while Kumara et al. (2010) work is for 50% WC in 56 mm pipe. Both cases have same inlet mixture velocity of 1.0 m/s. Referring to Kumara et al. (2010) in Figure 4.19, the degree of mixing largely depends on the pipe inclination. Water holdup values increase for upwardly inclined flow and decreases for downwardly inclined flow compared to the flow in the horizontal pipe. Similar work is presented in Figure 4.19 from the present work. Although the degrees of inclinations in the present work (-15, 0 and 15 degree) are different from Kumara et al (2010) work, the local water contents behave in the same manner. The difference between both results shown in Figure 4.20 is probably due to the difference in inlet water cut, pipe size and inclinations.

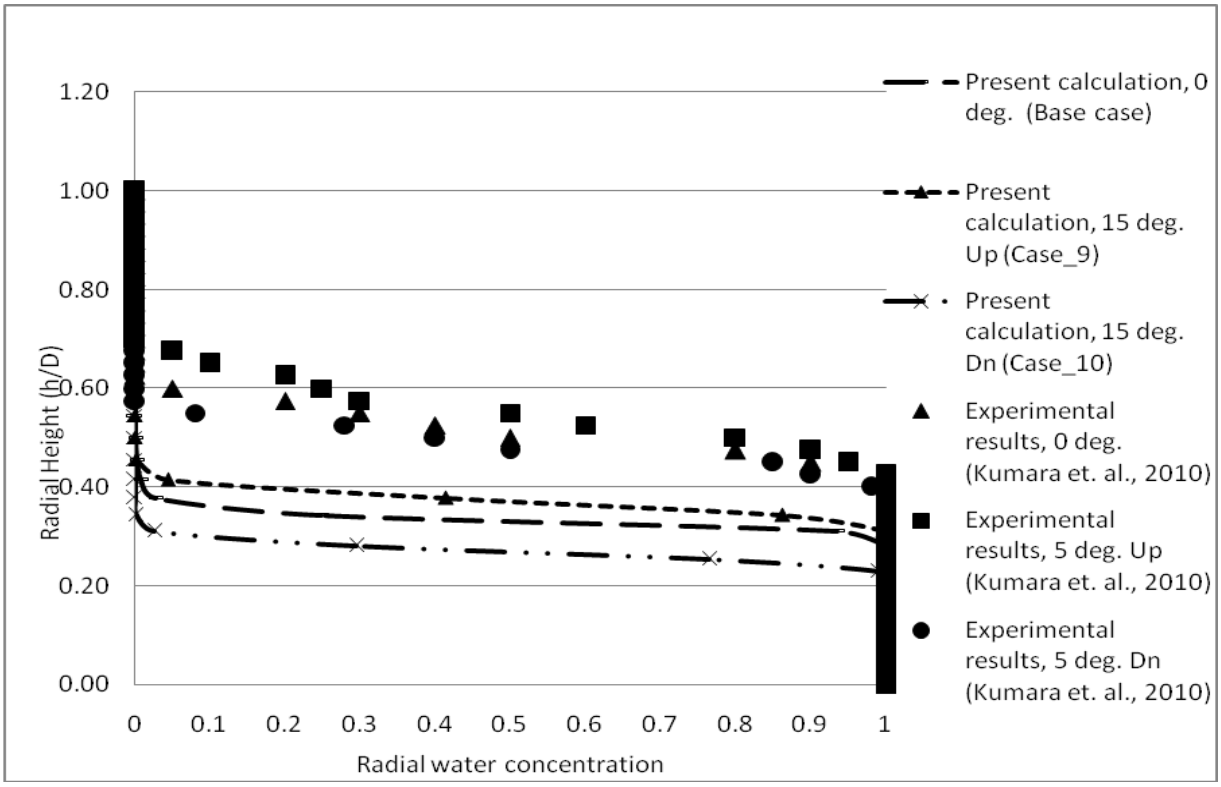

Figure 4.20: Comparison of water concentration for the present work (horizontal and inclined 15 deg. Up & Down and 30% WC in 154 mm pipe) and Kumara et al. (2010)'s work (horizontal and inclined 5 deg. Up & Down and 50% WC% in 56 mm pipe) both at 1.0 m/s inlet mixture velocity

At upward inclination from the horizontal, water accumulating at the pipe bottom slows down. On the other hand, water velocity increases at pipe bottom in case of downward inclinations as shown in Figure 4.21. Figure 4.21 compares radial average velocities of oil and water for the present work and Kumara et al. (2010) for different pipes inclinations and operation conditions. As both cases have same inlet mixture velocity of 1.0 m/s, they are different in other parameters that cause the different in the velocity profiles shown in Figure 4.21. Referring to the average velocity distribution for the present work, the general radial velocity profiles for both works behave in the same

approach. The shown differences might be due to the different tools used for the measurements additional to the differences in geometry and operation conditions highlighted above.

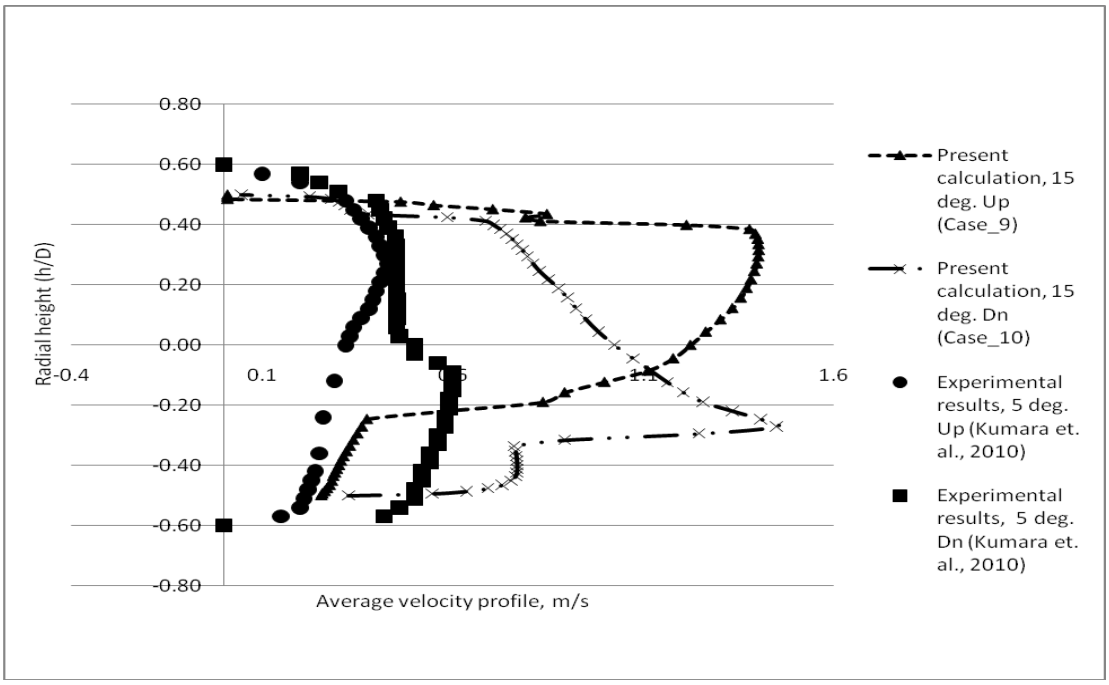

Figure 4.21: Comparison of average velocity distribution for different inclined pipes from present work (15 deg. Up, Down and 30% WC in 154 mm ID) and Kumara et al. (2010) work (5 deg. Up, Down and 50% WC% in 56 mm ID)

For same operation conditions of all pipe sizes, the pipe with larger diameter has higher inlet amount of water that requires more effort to avoid separation. Cai et al. (2004) presented that as the pipe diameter increases, the critical velocity increases required to entrain the free water. They showed that by increasing the pipe diameter from 100 to 200 mm, the required critical velocity increases from almost 0.9 to 1.2 m/s. This is not shown clearly in the present work as shown in Figure 4.22. Figure 4.22

compares three different pipe sizes 102, 154 and 202 mm at X5.5 which is 5500 mm downstream the inlet, where L/D is 53.9, 35.7 and 27.2 respectively. The water separation height for 154 mm pipe seems to be more than 102 mm pipe at this location and that is in agreement with Cai et al. (2004) work. However, comparing the water separation in 202 mm to 102 mm or 154 mm pipes shows that the separation in 202 mm is lower. This observation is opposite to the previous observation. The discrepancy might be justified by that the flow in 202 mm pipe is not yet get enough length to complete separation where the mixing zone in Figure 4.22 is still wide and the separation get delayed as shown clearly in Figure 4.23. Figure 4.23 compares longitudinal contours of water in the three pipe sizes. Moreover, increasing pipe diameter delays water separation. To conclude, both works has high agreement from the concept point of view.

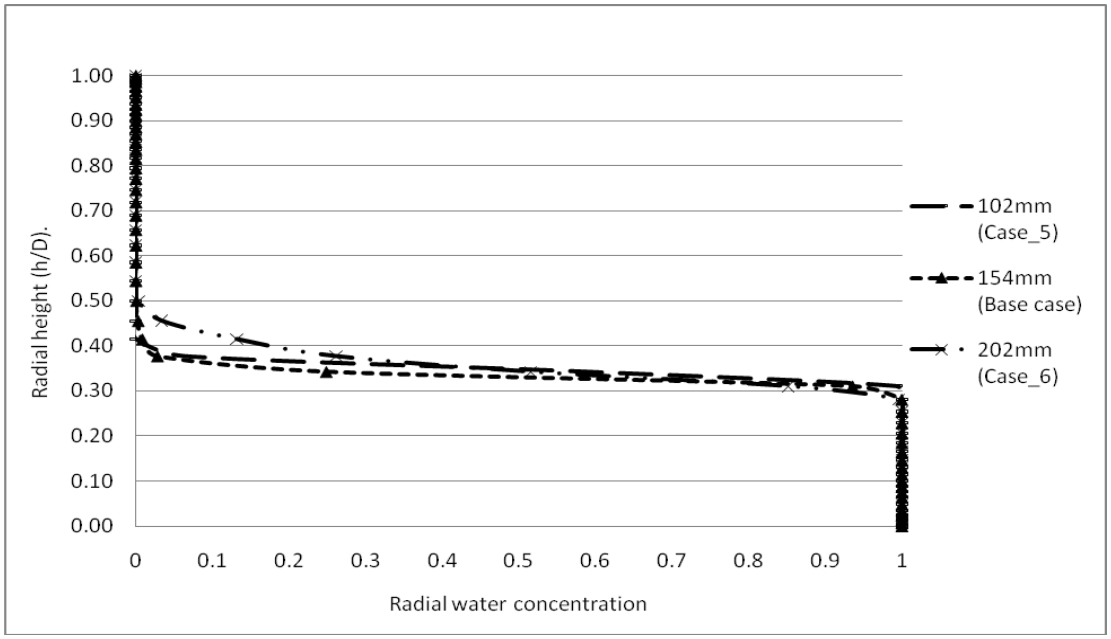

Figure 4.22: Comparison of water concentration in vertical position for different sizes of pipe diameters102, 154, and 202 mm, equivalent to L/D of 53.9, 35.7 and 27.2

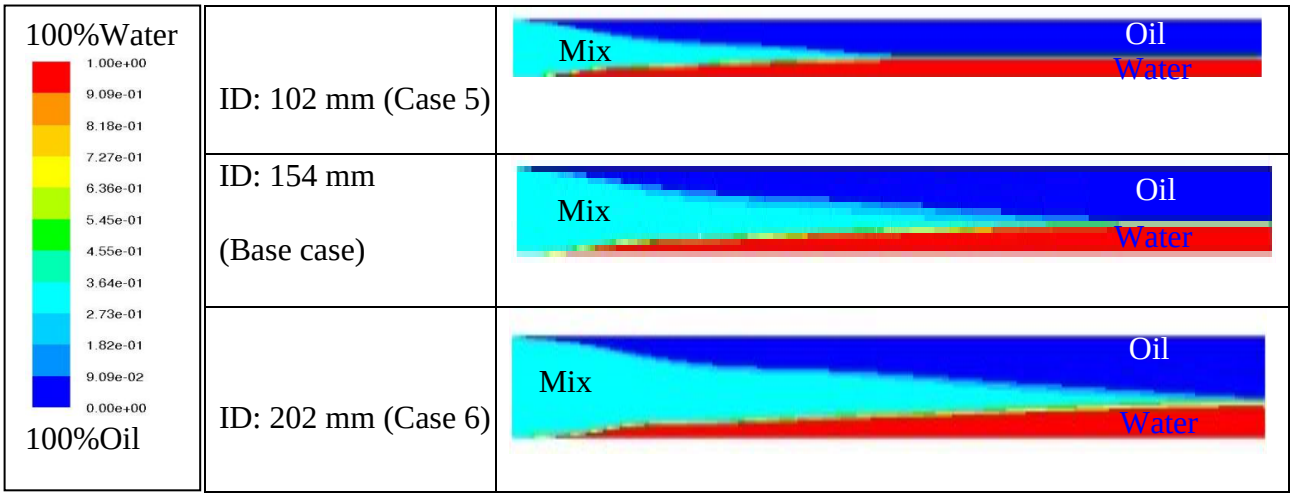

Figure 4.23: Water contours at different pipe inner diameters for longitudinal vertical contour in X-Y-plane

4.5 Result and Analysis

A detailed study of the oil-water distribution characteristics was carried out for the different variable parameters based on Table 4.1 that are related to operation conditions, piping geometry and fluid physical properties for fifteen (15) cases. The outcome of the fifteen (15) cases resulted in seven (7) comparisons of the different variable parameters. The influence of these parameters is evaluated based on their effect on the flow patterns and water local concentration. Comparisons of contours for different cases of water phase and velocity profiles are presented along the pipe and across the vertical diameter. The ratio of the height of the water layer from the bottom of the pipe to the diameter of the pipe, h, is plotted against the water concentration for different cases.

The first type of the contour is presented on a vertical-plane along the pipe. It presents water contours in the X-Y plane. The second type of the contours is to present the water contours in cross-section radial planes at different X-planes located at 0.0, 1000, 2000, 3000, 4000, 5000 and 6000 mm downstream the pipe in the Y-Z plane. Referring to Vedaburi et al. (1997) and shi (2001), the present flow patterns are classified based on the flow pattern definition shown in Figure 2.1, the present work shows six (6) flow patterns as follows:

- Segregated
- Semi-segregate
- Semi-mixed
- Semi-dispersed
- Dispersed flow
- Mixed flow

In some references, the semi-patterns are presented under one name called stratified flow with a mixing at the interface (ST&MI) or three-layer (3L). Based on these definitions, the present work can show only four types of the flow patterns, as defined by Fairuzov et al. (2000):

- Stratified flow
- Dispersed flow
- ST&MI or 3L (dual flow)
- Mixed flow

The following paragraphs present the different parameters of each condition: inlet operation (inlet mixture velocity and inlet water cut), oil properties (density and viscosity) and pipe geometries (diameter and inclinations) as coming.

4.5.1 Effect of Inlet Operation Conditions

Two factors are selected to present the inlet operation conditions: inlet mixture velocity and inlet water cut percentage. These two variables are investigated for two features: flow pattern types and water holdup.

Effect of inlet mixture velocity

The effect of the inlet mixture velocities of 0.5, 1.0 and 2.0 m/s at 30% WC on flow patterns and local water contents (holdup) is investigated. The summary of water contours and velocity profiles at different planes are shown in Figure 4.24 and 4.25.

Figure 4.24 compares water contours at the cross-sectional planes, X5.5, that is 35.7 of L/D downstream the inlet and longitudinal planes at the different inlet mixture velocities. The contours of the cross-sections show that as the velocity increases, the mixing zone increases. The longitudinal planes show that as the velocity increases, the separation is delayed.

Figure 4.25 presents velocity profiles for both water and oil along the pipes for the three velocity changes. As flow moves forward, water velocity disappeared at the top of the pipe. On the other hand, the radial oil velocity distributions on the same figures have different profiles. The velocities distributions for oil are parabolic at the pipe inlet between both bottom and top sides and they disappear at the pipe bottom as the flow moves downstream. However, the upper half of the pipe shows parabolic velocity profiles distribution for the oil phase along the pipe length. The velocity profile for water slows down at the top of the pipe but not as low as the oil velocity at the pipe bottom. The two phases have different velocity at the top and the bottom of the pipe that results in a slip velocity. It shows that increasing inlet mixture velocity increases overlap (mixing zone) between oil and water velocity profiles. That agrees with the contours result above where it shows that water separation decreases with increasing inlet mixture velocity. Accordingly, water holdup reduces with increasing the mixture inlet velocities.

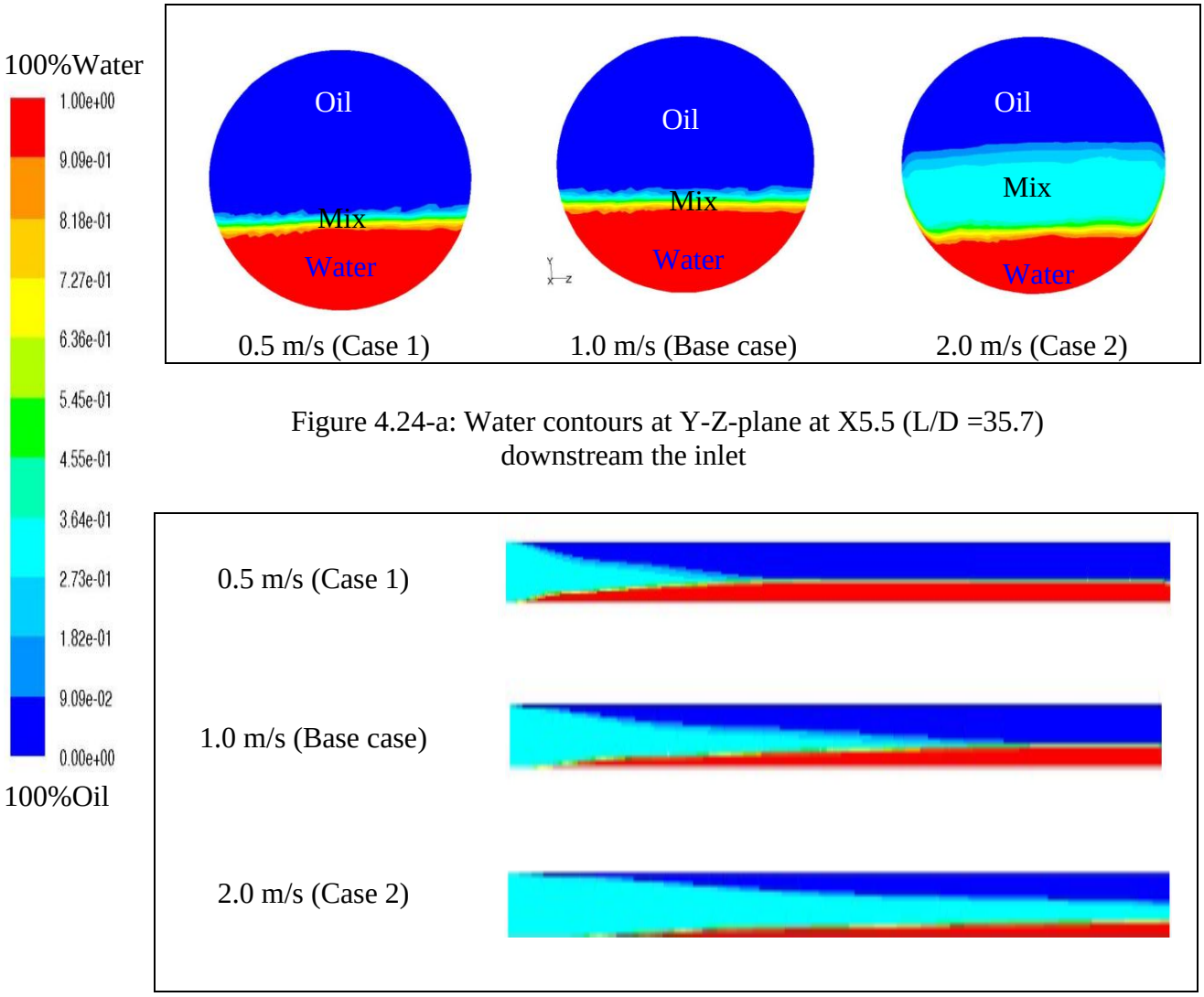

Figure 4.24-a: Water contours at Y-Z-plane at X5.5 (L/D =35.7) downstream the inlet

Figure 4.24-b: Water contours along X-Y-plane

Figure 4.24: Water contours at different planes for different inlet mixture velocities

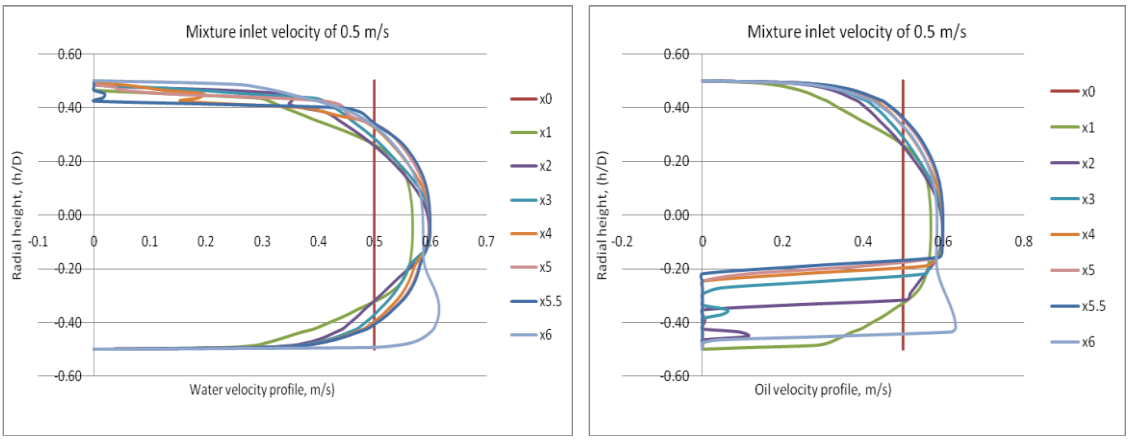

a) Water and oil radial velocity profiles at 0.5 m/s

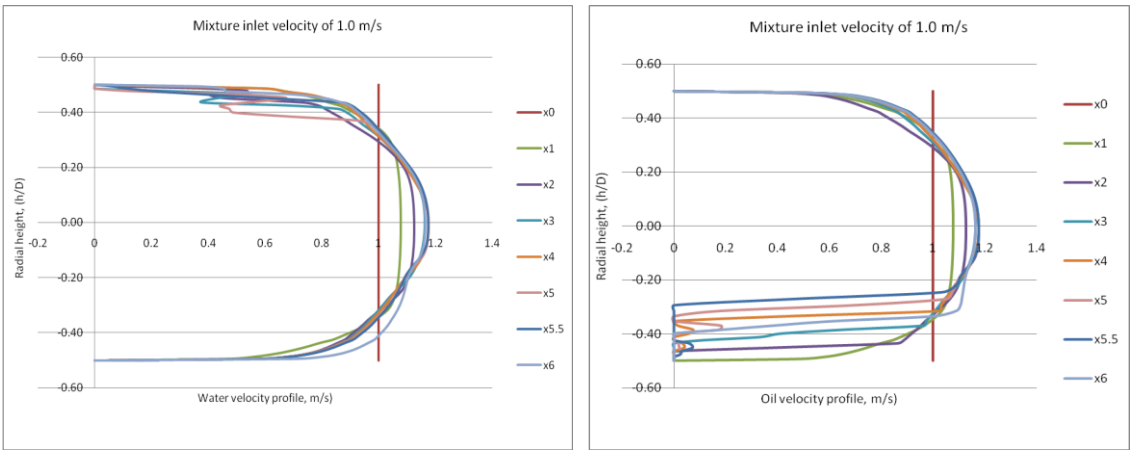

b) Water and oil radial velocity profile at 1.0 m/s

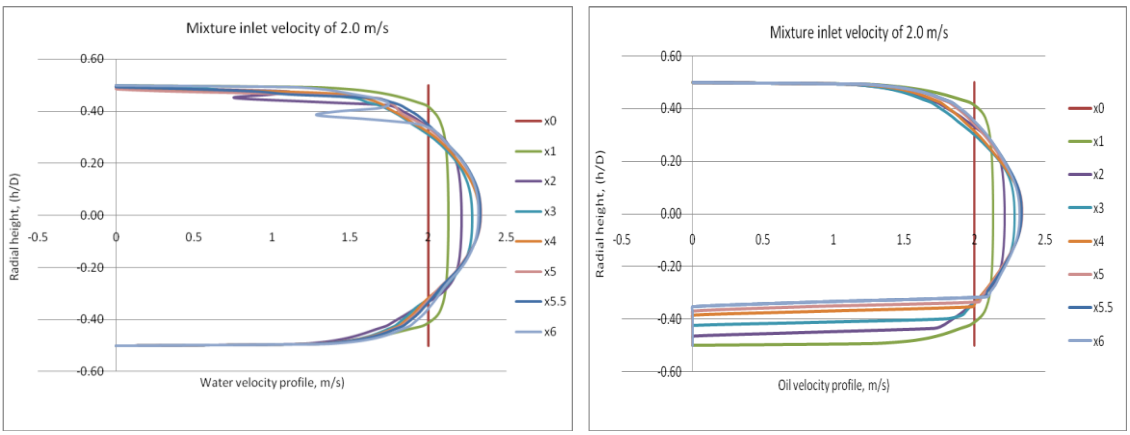

c) Water and oil radial velocity profile at 2.0 m/s

Figure 4.25: Velocity profiles for water and oil at radial planes along the pipes at different inlet mixture velocities

The following figures, Figure 4.26, 4.27 and 4.28 compare water contours at the cross-sectional plane, X5.5, that is 35.7 of L/D downstream the pipe inlet of each inlet mixture velocity at the present work to the Shi (2001) work. The comparison is done as per procedure provided for Figure 4.13. The difference in flow patterns between the present work and the reference work for Shi (2001) might be due to the difference in pipe diameters between the two woks.

Figure 4.24 shows that it requires doubling the pipe length for 1.0 m/s inlet mixture velocity in order to have complete separation compared to 0.5 m/s inlet mixture velocity. It is not achievable at this pipe length limitation to know if a complete separation at 2.0 m/s compared to the previous cases can occur or not. However, at same plane of X5.5, the flow patterns for 2.0 m/s inlet mixture velocity has large area of cross-section mixing.

As mixture inlet velocity increases, more mixing occurs and that appears clearly at 2.0 m/s. The inlet mixture velocity greatly influences the oil-water distribution. Comparisons of water contours shown in Figure 4.24 and water level change shown in Figure 4.31, the flow pattern can be identified as follows:

1. Figure 4.26: at 0.5 m/s and 30% WC: The flow pattern is segregated flow compared to segregated flow at Shi (2001) based on the following decision:
   - The vertical line matches the present work just below the sketch of Shi (2001) with segregated flow.
   - While the present work contour shows very thin mixing at the interface (ST&MI) which per Vedaburi et al. (1997) is defined as a segregated flow, Figure 4.32 shows

a mixing area increasing from 0 and 100% water contents over small height drop that varies from 0.36 to 0.30 of h/D. On the same figure, Figure 4.32, it shows a good agreement to Shi (2001) work for water concentration changing across the pipe diameter.

2. Figure 4.27: at 1.0 m/s and 30% WC: semi-segregated flow pattern compared to semi-mixed flow at Shi (2001) based on the following decision:
   - The vertical line matches the present work mixing zone within the mixing zone of Shi (2001) work.
   - The present work shape shows mixing at the interface and Figure 4.33 shows a high mixing area increasing from 0 and 100% water contents over a height that varies from 0.37 to 0.28 of h/D. On the same figure, Figure 4.33, it shows a good agreement to Shi (2001) work of water concentration changing across the pipe diameter.
3. Figure 4.28: at 2.0 m/s and 30% WC: semi-mixed flow pattern compared to mixed at Shi (2001) based on the following decision:
   - The vertical line matches the present work mixing zone within the mixing zone of Shi (2001) work.
   - The present work shape shows mixing at the interface and Figure 4.34 shows a mixing area increasing between 0 and 100% water contents over a large height that varies from 0.65 to 0.2 of h/D. On the same figure, Figure 4.34, it shows acceptable matching result to Shi (2001) work of water concentration changing across the pipe diameter.

The flow patterns based on the effect of the inlet mixture velocity of 0.5, 1.0 and 2.0 m/s at 30% is summarized as follows:

- **Segregated flow** versus segregated flow pattern at Shi (2001)
- **Semi-segregated flow** pattern versus semi-mixed flow pattern at Shi (2001)
- **Semi-mixed flow** pattern versus mixed flow pattern at Shi (2001)

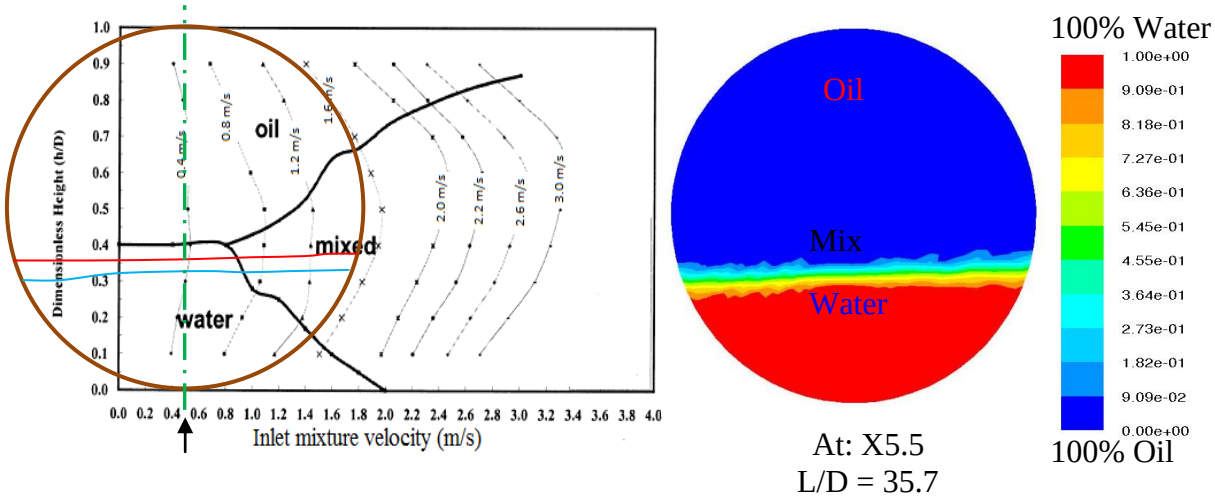

Figure 4.26: Flow pattern of the present work compared to Shi (2001)'s work based on mixture inlet velocity of 0.5 m/s and 30% WC

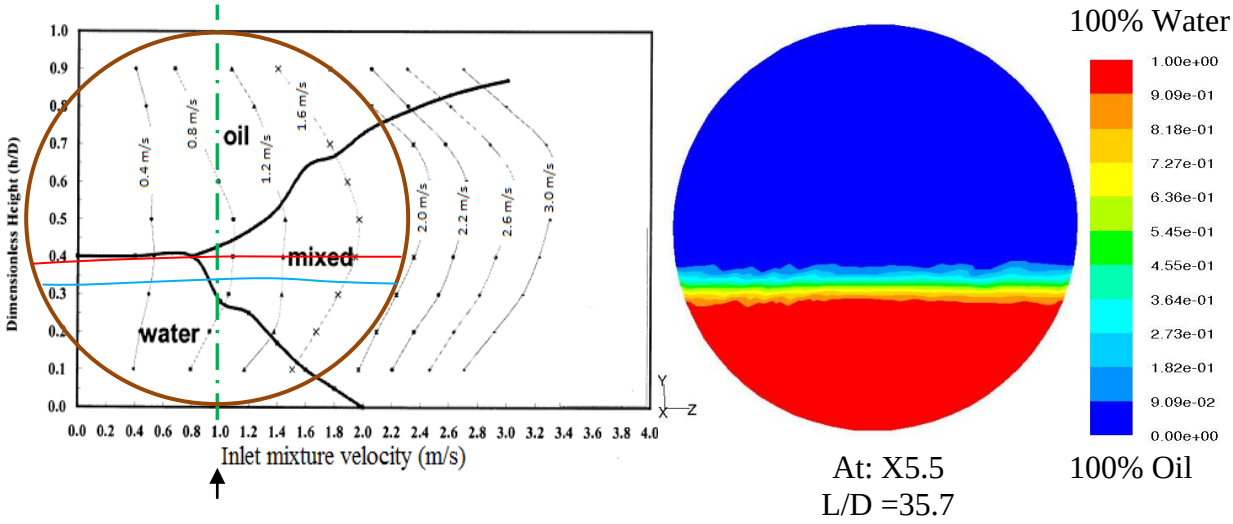

Figure 4.27: Flow pattern of the present work compared to Shi (2001) work based on mixture inlet velocity of 1.0 m/s and 30% WC

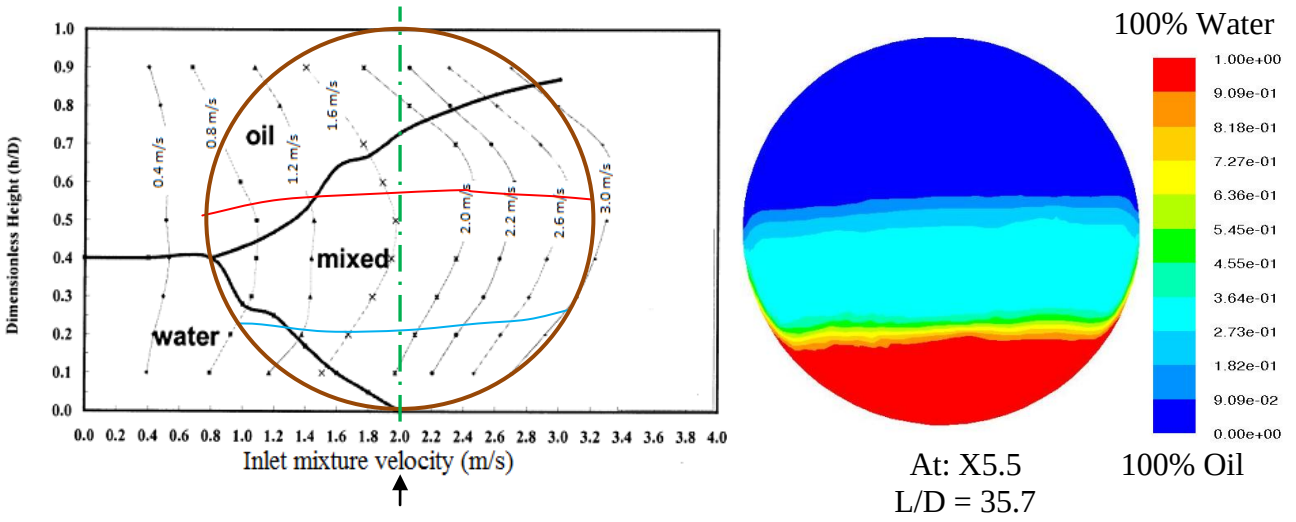

Figure 4.28: Flow pattern of the present work compared to Shi (2001) work based on mixture inlet velocity of 2.0 m/s and 30% WC

Focusing to the plane X5.5 where L/D = 35.7, as shown in Figure 4.29, the radial water velocity distributions for the three velocities show almost axial parabolic velocity across the pipe diameter. For low inlet mixture velocity of 0.5 m/s, while water velocities profile almost the same, the oil velocity profile appears almost above 28% the height from the pipe bottom. Moreover, as the velocity input increases, the oil mixing or water entrainment in oil increases. Accordingly, the oil velocity appears below this value where it is approaching the pipe bottom. The oil velocity profiles appear at 20% and 12% of the height respectively for 1.0 and 2.0 m/s. It is important to highlight that the two phases have different velocities at the top and bottom of the pipe ant that is due to velocity slip between the two phases. However, the slip velocity is more at the pipe bottom. The reason is that, the oil phase bounces up to the pipe top and the water phase settles down at the pipe bottom. That is expected because the flow is under different forces; turbulent force and the gravity

force. At high velocity, water tries to settle down. However; the water phase is entrained by the oil due to high turbulent velocity. At certain forces balance, more water appears at the pipe bottom and mixing with oil on most of the pipe cross-sections. Water holdup changes according to the velocity change. The drift velocity as a result of velocities different between the two-phase is shown in Figure 4.30. In general, the slip velocity is more at the pipe bottom and the mixed layer flows faster than both oil and water layers.

Figure 4.31 compares water concentration at different velocities. The curves of the different velocities are analyzed as follows based on the inlet mixture velocity:

- At 1 m/s: 100% water concentration appears at pipe bottom for a height ratio of almost 0.33 of h/D. Above 0.39 of h/D, the concentration of water is almost zero. Between 0.33 and 0.39 of h/D, the flow is mixed of oil and water.
- At 0.5 m/s: 100% water concentration appears at pipe bottom for a height ratio of almost 0.33 of h/D. Above 0.39 of h/D, the concentration of water is almost zero. Between 0.33 and 0.39 of h/D, the flow is mixed of oil and water.
- At 2.0 m/s: 100% water concentration appears at pipe bottom for a height ratio of almost 0.2. The concentration of water is then drops gradually to 30% water local contents at 0.32 ratio of the h/D as a mixing area of oil and water. The mixing area is then increases to 0.5 of h/D at same water concentration. The water concentration gradually drops to 0 at 0.65 of h/D.

Figure 4.32 compares the present work to different references where it shows good agreements. In Figures 4.32 and 4.33, the water concentrations across the plane X5.5 at this work is compared to water contents change across the pipe in Shi (2001) work for the mixture velocities of 0.5 and 2.0 m/s respectively additional to the Figure 4.34 comparing

water concentration at the inlet mixture velocity of 1.0 m/s to Shi (2001) work. The water contents change for the different inlet mixture velocities are matching.

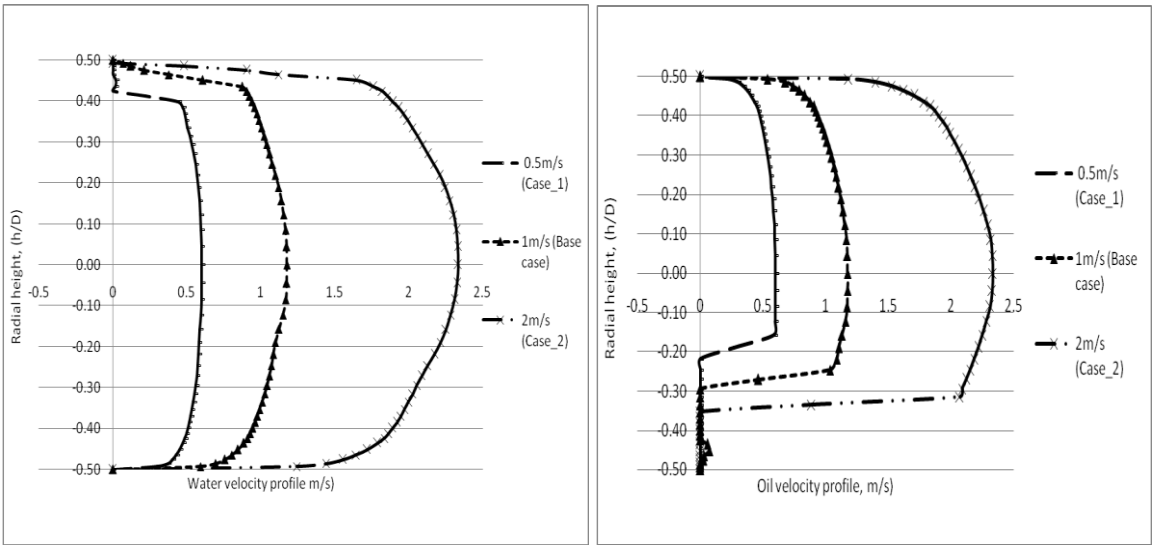

Figure 4.29: Velocity profile for water and oil at plane X5.5 of 154 mm ID pipe at three velocities of 0.5 m/s, 1.0 m/s and 2.0 m/s

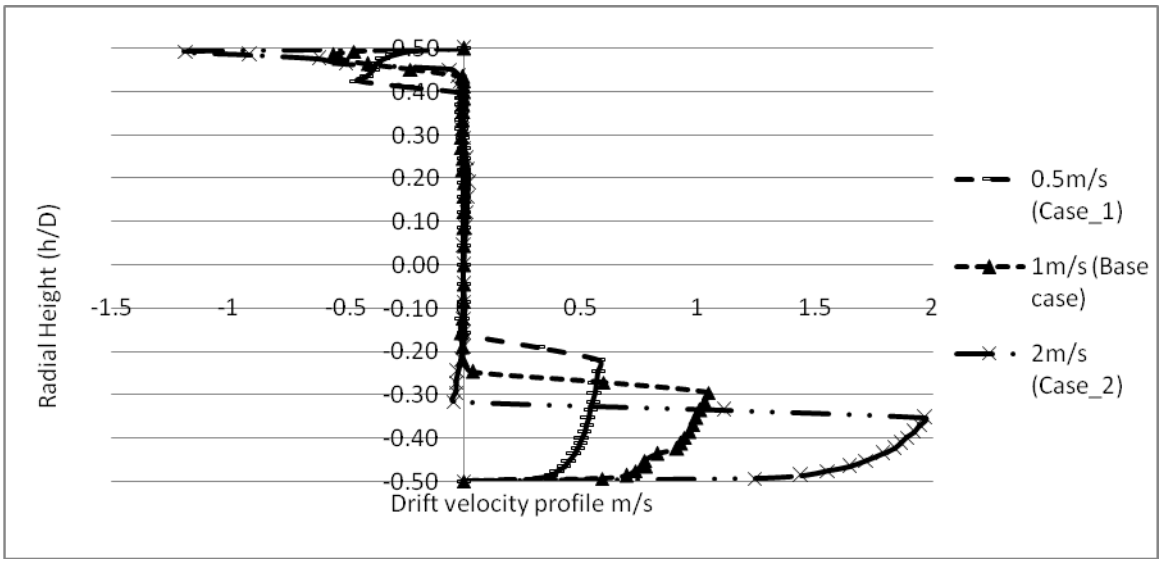

Figure 4.30: Comparison of radial drift velocity for different inlet mixture velocities of 0.5, 1.0, and 2.0 m/s

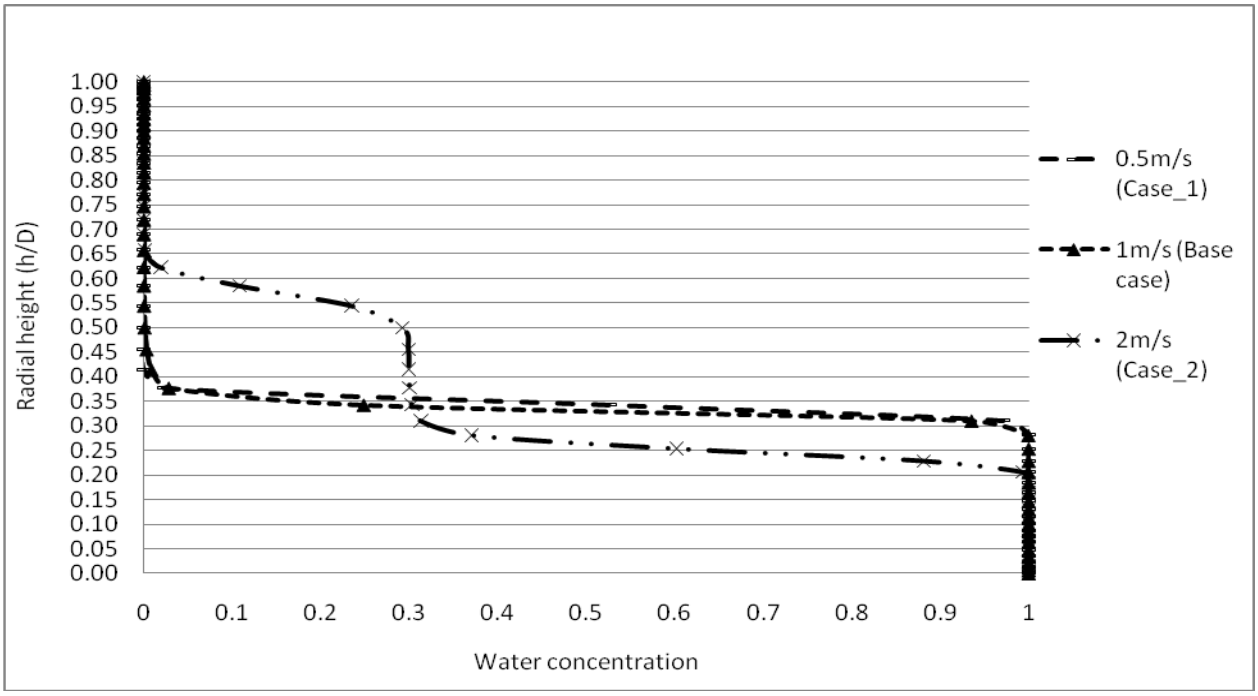

Figure 4.31: Variation of water concentration in vertical position of different inlet mixture velocity for present work

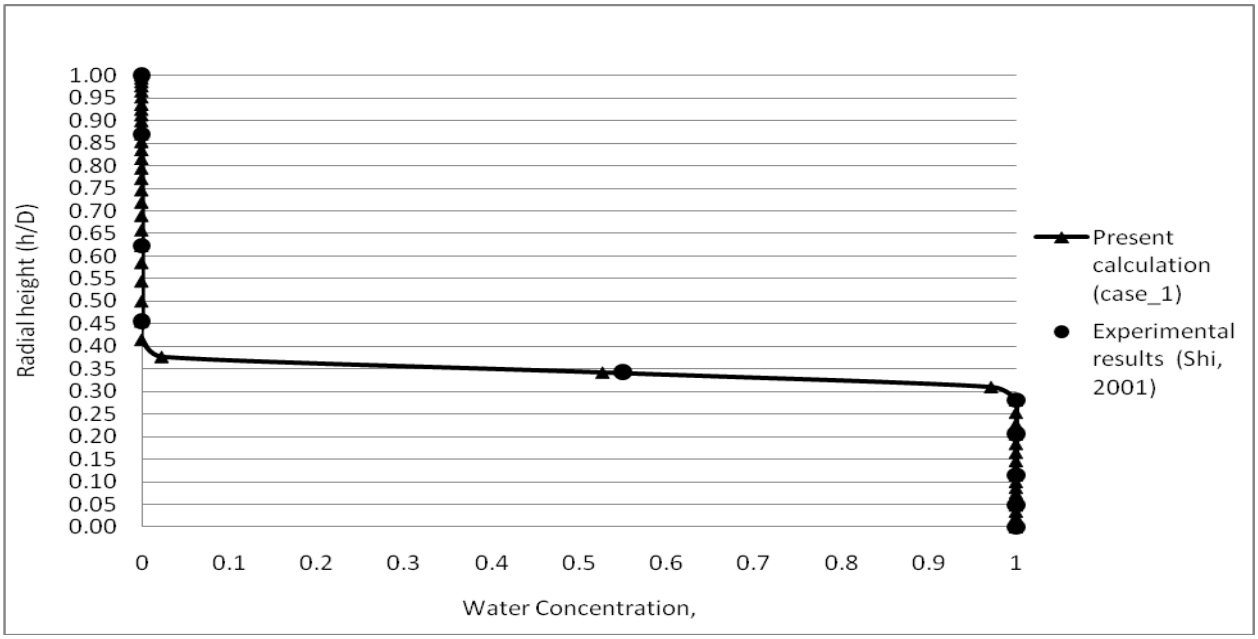

Figure 4.32: Comparison of present work to experimental work of Shi (2001) for water concentration in vertical position for 0.5 m/s inlet mixture velocity

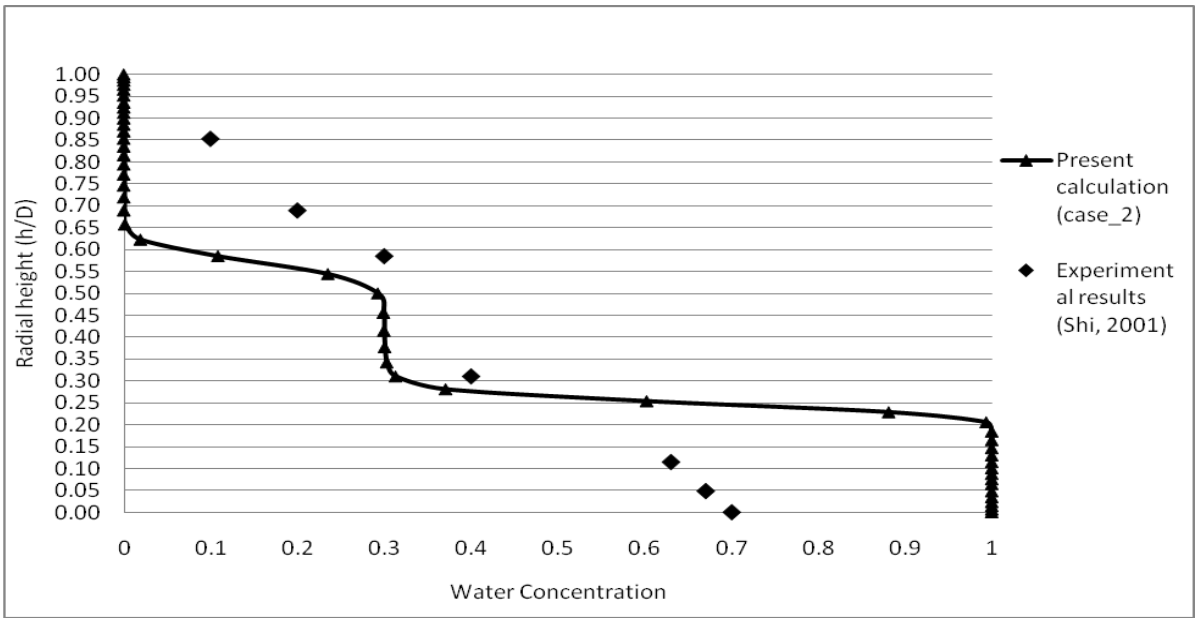

Figure 4.33: Comparison of present work to experimental work of Shi (2001) for water concentration in vertical position for 2.0 m/s inlet mixture velocity

Effect of inlet water cut (WC)

The effect of the inlet water cut of 20%, 30% and 50% WC at 1.0 m/s on flow patterns and local water contents (holdup) is investigated. The summary of water contours and velocity profiles at different planes are shown in Figure 4.34 and 4.36.

Figure 4.34 compares water contours at the cross-sectional planes, X5.5, that is 35.7 of L/D downstream the inlet and longitudinal planes at the different inlet water cuts. As water content increases, the local water contents increases and there is no delay to the phase separation. The figures show that as the inlet water cut increases, the mixing contents of water increases from 0.2, 0.3 to 0.5 for each case respectively. However, the mixing zone range is the same for the three cases with no acceleration or deceleration in the separation that appears clearly in Figure 4.34.

Figure 4.35 shows comparison of local water velocity distribution for the three inlet water contents across the radial pipe diameter. As the inlet water cut increases, there is no change in water velocity profiles. Figure 4.35 shows that increasing inlet water cut increases the water holdup. As flow moves forward, water velocity disappeared at the top of the pipe. On the other hand, the radial oil velocity distributions on the same figures have different profiles. The velocities distributions for oil are parabolic at the first portion of the pipe and they disappear at the pipe bottom as the flow moves downstream. The velocity profile for water slows down at the top of the pipe but not as low as the oil velocity at the pipe bottom. For low water content of 20% WC, while water velocity profile almost the same, the oil velocity profile appears at almost above 10% of h/D from the pipe bottom. Moreover, as the

water cut input increases, the water separation height at the pipe bottom increases so oil velocities shifts up based on the level of the oil layers. The oil velocity profiles for high input cuts of 30 and 50% appear at 20% and 32% of the height h/D respectively. The mixed layer flows faster than both oil and water layers for all planes.

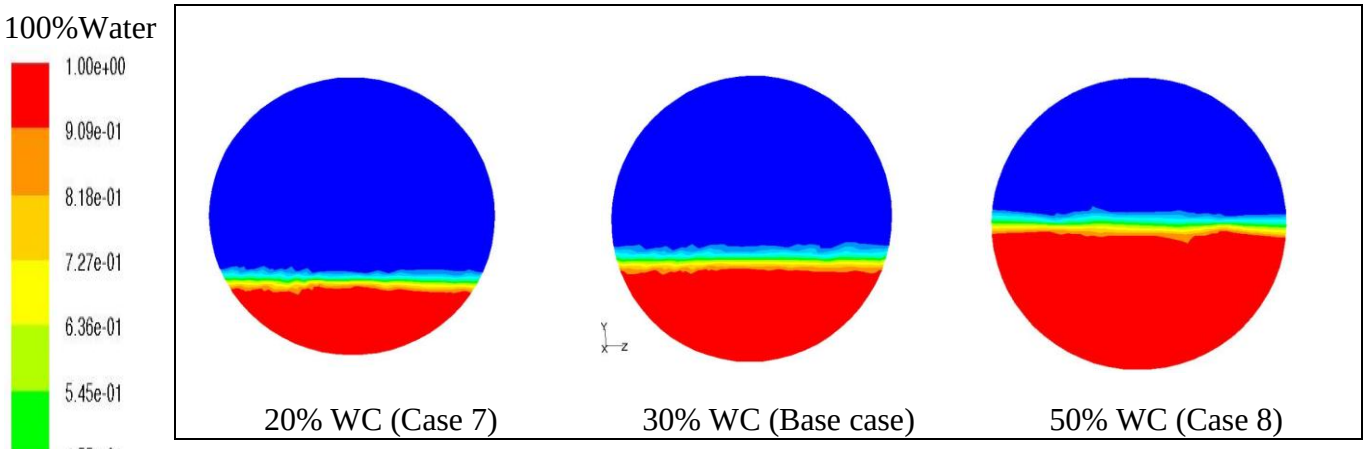

Figure 4.34-a: Water contours at Y-Z-plane at X5.5 (L/D =35.7) downstream the inlet

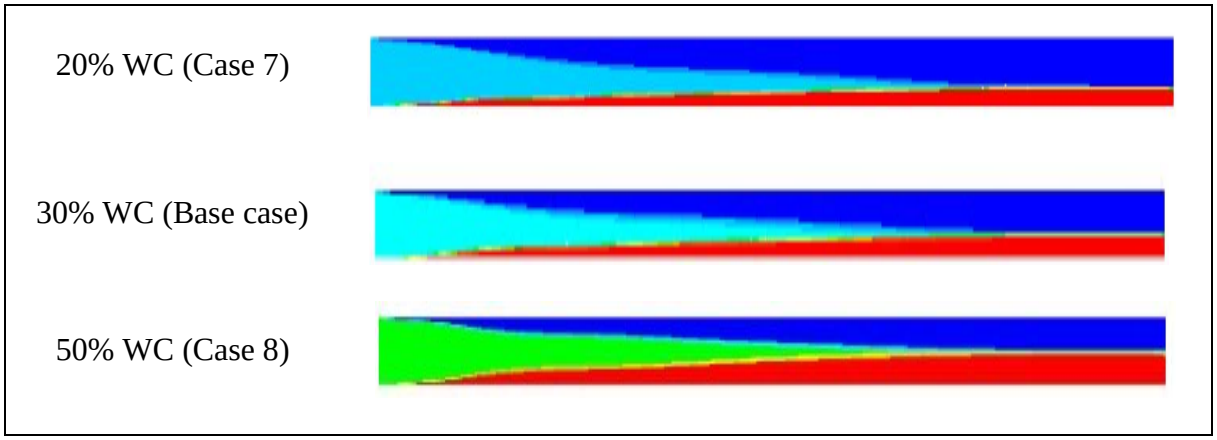

Figure 4.34-b: Water contours along X-Y-plane

Figure 4.34: Water contours at different planes for different inlet water cuts

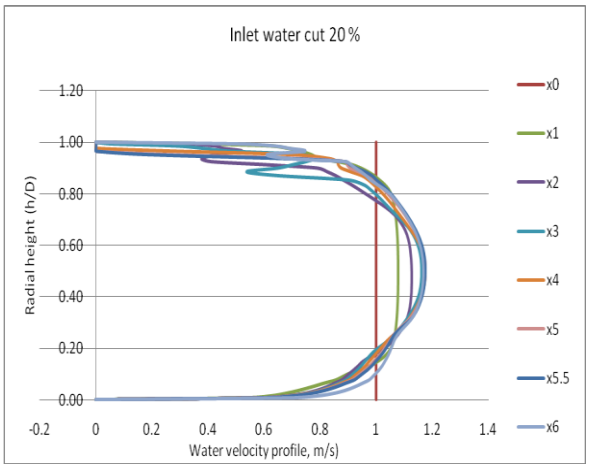

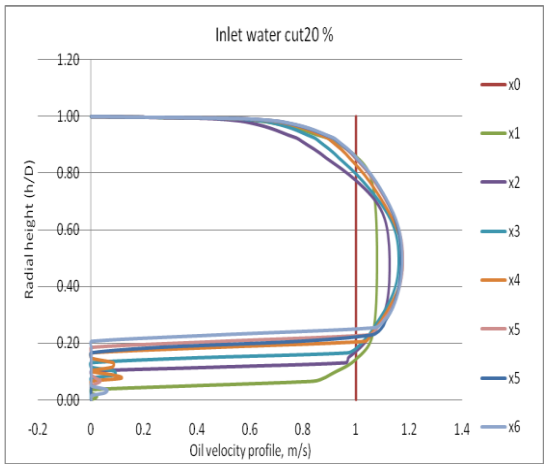

a) Water and oil radial velocity profile at 20% WC

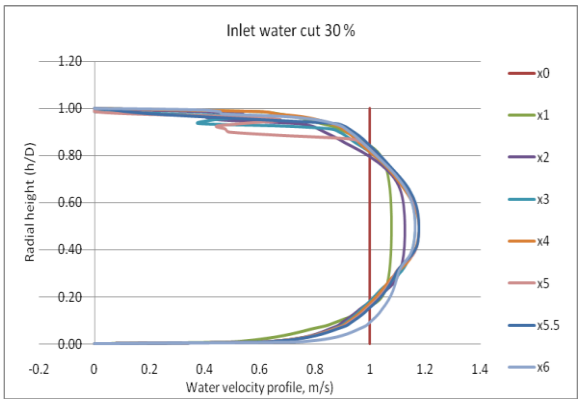

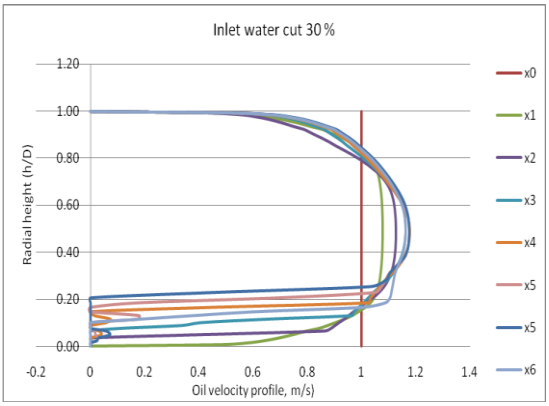

b) Water and oil radial velocity profile at 30% WC

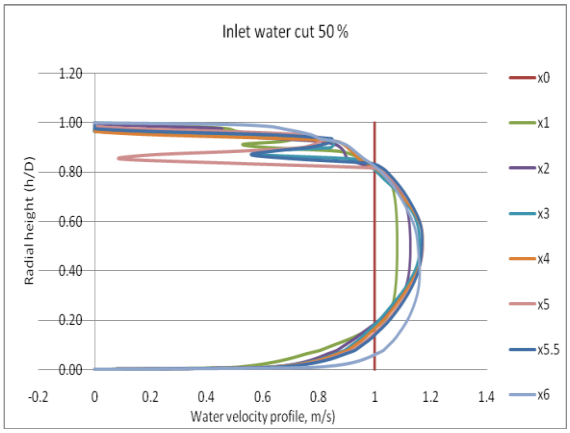

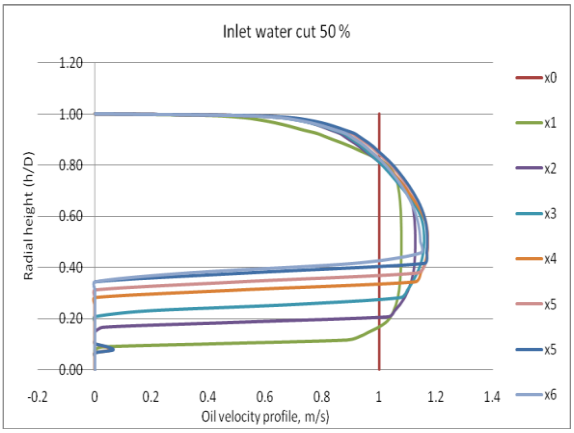

c) Water and oil radial velocity profile at 50% WC

Figure 4.35: Velocity profiles for water and oil at radial planes along the pipes at different percentage of the inlet water cuts (WC)

The following figures, Figure 4.36, 4.37 and 4.38 compare water contours at the cross-sectional plane, X5.5, that is 35.7 of L/D downstream the pipe for different inlet water cuts of 20, 30 and 50% WC to Shi (2001) work for same inlet water content and same mixture inlet velocity of 1.0 m/s. The flow patterns are identified as follows:

4. **Figure 4.36: at 20% WC, and 1.0 m/s**: The flow pattern is **semi-segregated flow** compared to semi-segregated flow at Shi (2001) work based on the following decision:
   - The vertical line matches the present work within a mixing zone at the sketch of Shi (2001).
   - The present work shape shows mixing at the interface and Figure 4.42 shows a mixing area increasing from 0 and 100% water contents over a height that varies from 0.3 to 0.22 of h/D. On the same figure, Figure 4.42, it does not show high agreement to Vedapuri et al. (1997) work of water concentration changing across the pipe diameter.
5. **Figure 4.37: at 30% and WC 1.0 m/s**: **semi-segregated flow** pattern compared to semi-segregated flow at Shi (2001) work based on the following decision:
   - The vertical line matches the present work mixing zone within the mixing zone of Shi (2001) work.
   - The present work shape shows mixing at the interface and Figure 4.43 shows a mixing area increasing from 0 and 100% water contents over a height that varies from 0.37 to 0.27 of h/D. On the same figure, Figure 4.43, it does not show high agreement to Vedapuri et al. (1997) work of water concentration changing across the pipe diameter.

6. **Figure 4.38: at 50% WC and 1.0 m/s: semi-segregated flow** pattern compared to semi-mixed at Shi (2001) based on the following decision:
   - The vertical line matches the present work mixing zone within the mixing zone of Shi (2001) work.
   - The present work shape shows mixing at the interface and Figure 4.44 shows a mixing area increasing between 0 and 100% water contents over a height that varies from 0.57 to 0.42 of h/D. On the same figure 4.44, it does not show high matching to Kumara et al. (2010) work of water concentration changing across the pipe diameter.

The flow patterns resulted from changing inlet water cuts present the flow patterns of the present work based on the change of the inlet water cuts of 20, 30, and 50% WC compared to Shi (2001) work for same inlet water cuts and inlet mixture velocity of 1.0 m/s. The flow patterns for this variable are:

- **Semi segregated flow** pattern compared to semi-segregated flow pattern at Shi (2001)
- **Semi-segregated flow** pattern compared to semi-segregated flow pattern at Shi (2001)
- **Semi-segregated flow** pattern compared to semi-mixed flow pattern at Shi (2001)

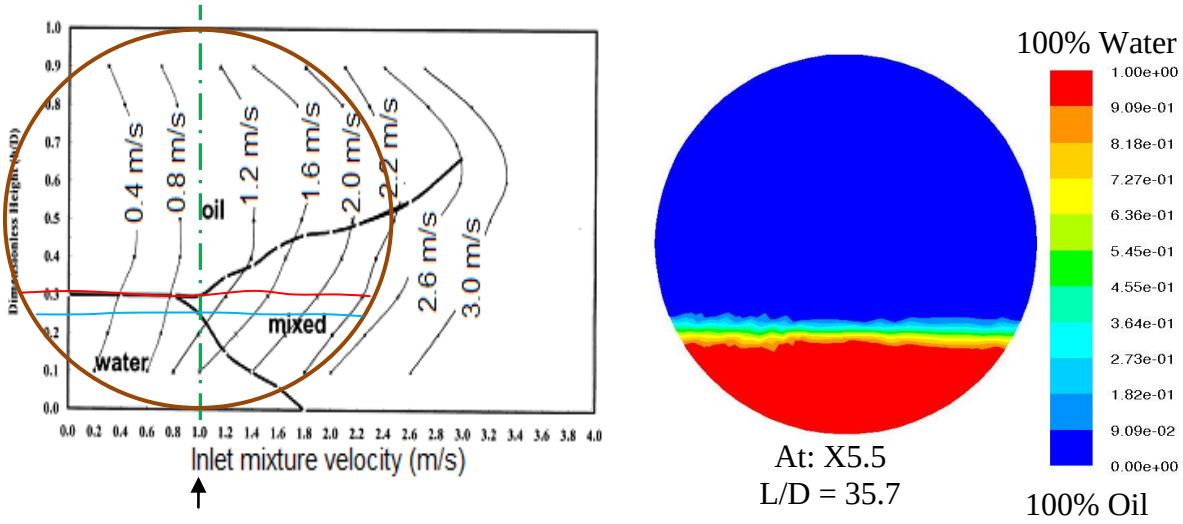

Figure 4.36: Flow pattern map comparison based on 1.0 m/s mixture velocity and inlet water cut of 20% WC

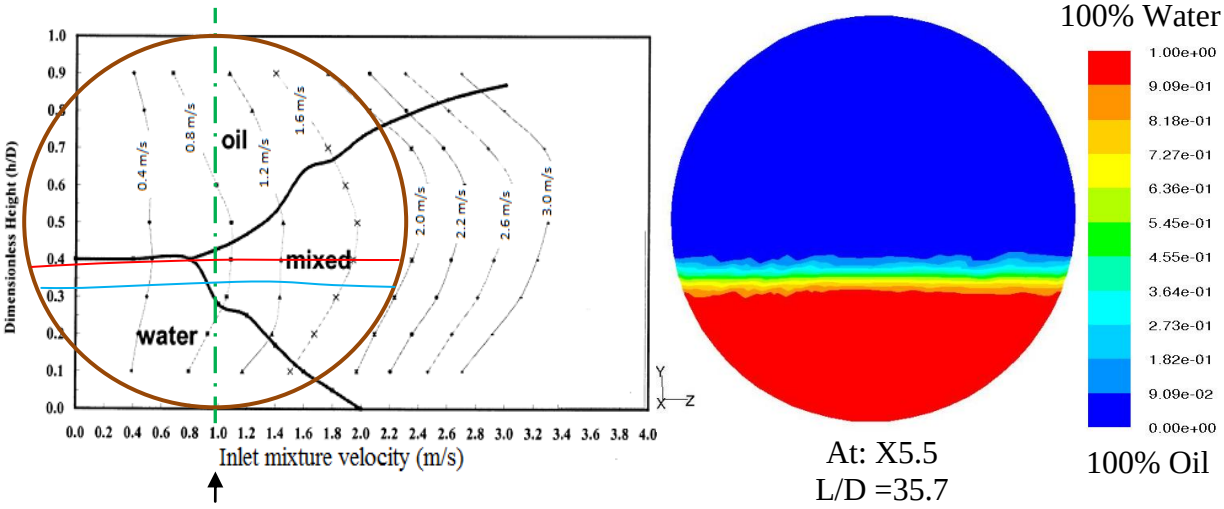

Figure 4.37: Flow pattern of the present work compared to Shi (2001) work based on mixture inlet velocity of 1.0 m/s and 30% WC

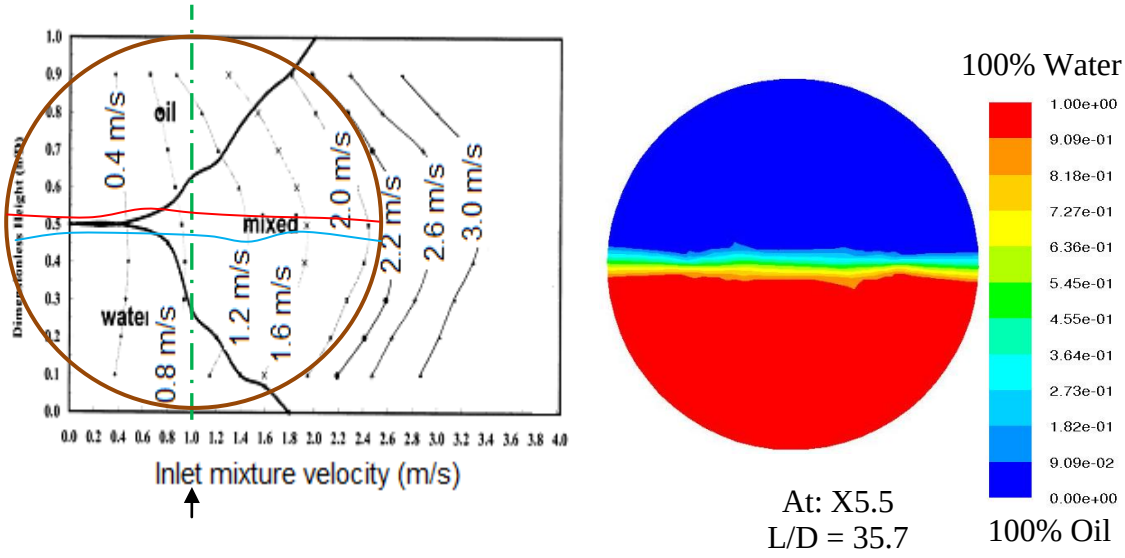

Figure 4.38: Flow pattern of the present work compared to Shi (2001) work based on mixture inlet velocity of 1.0 m/s and 50% WC

More focusing to the plane X5.5, per Figure 4.39, it shows that the water velocity disappears but at the pipe top for all cases. So there is intent movement for both phases but with different percentage. The oil phase bounces and the water phase settles down at the pipe bottom. That is expected as the flow is under different forces; turbulent force and the gravity force. At high water contents, water tries to settle down. There is a change in the entrainment rate compared to velocity increases; however, the water level increases as inlet water content increases. So increasing inlet water contents result into more water separation and less entrainment. The separation of oil-water two-phase flows result in a difference velocities and slippage between the two velocities. Figure 4.40 show velocity drift as a result of different inlet water cuts. The drift is high at the pipe bottom and increases as the inlet water cut increases.

Figure 4.41 is analyzed as follows based on the inlet water contents:

- At WC of 20%: 100% water concentration appears at pipe bottom for a height ratio of almost 0.22 of h/D. Above 0.30 of h/D height, the concentration of water is almost zero. So below a height of 0.22, there is no oil presents. Between 0.22 and 0.30 of h/D height, the flow is mixed of oil and water.
- At WC of 30%: 100% water concentration appears at pipe bottom for a height ratio of almost 0.27. Above 0.37 of h/D height, the concentration of water is almost zero. So below a height of 0.27, there is no oil presents. Between 0.27 and 0.37 of h/D height, the flow is mixed of oil and water.
- At WC of 50%: 100% water concentration appears at pipe bottom for a height ratio of almost 0.42. Above 0.57 of h/D height, the concentration of water is almost zero. So below a height of 0.42, there is no oil presents. Between 0.42 and 0.57 of h/D height, the flow is mixed of oil and water.

Figure 4.42 and Figure 4.43 show a comparison of the present work to the experimental measurements carried out by Vedapuri et al (1997) for water concentration of 20 and 30. For 50 WC, it is compared to Kumara et al. (2010) work as shown in Figure 4.43. All the cases are conducted for same inlet mixture velocities of 1.0 m/s. The present work has acceptable agreement with references for water holdup range. In Figure 4.42, the present work at 20% WC is compared to Vedapuri et al (1997) work for water cut of 20%. Figure 4.43 compares the present work at 30% WC to Vedapuri et al (1997) work for water cut of 30% and 40%. The present work has acceptable agreement with references for water height.

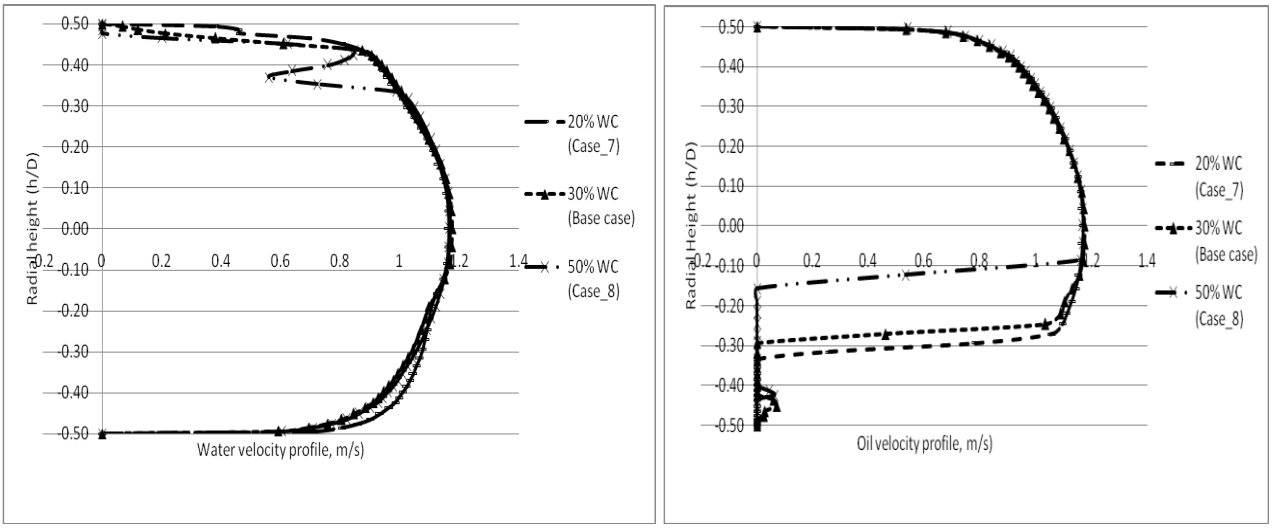

Figure 4.39: Variation of radial (a)- water and (b)- oil velocity for different inlet water contents 20, 30, and 50% WC

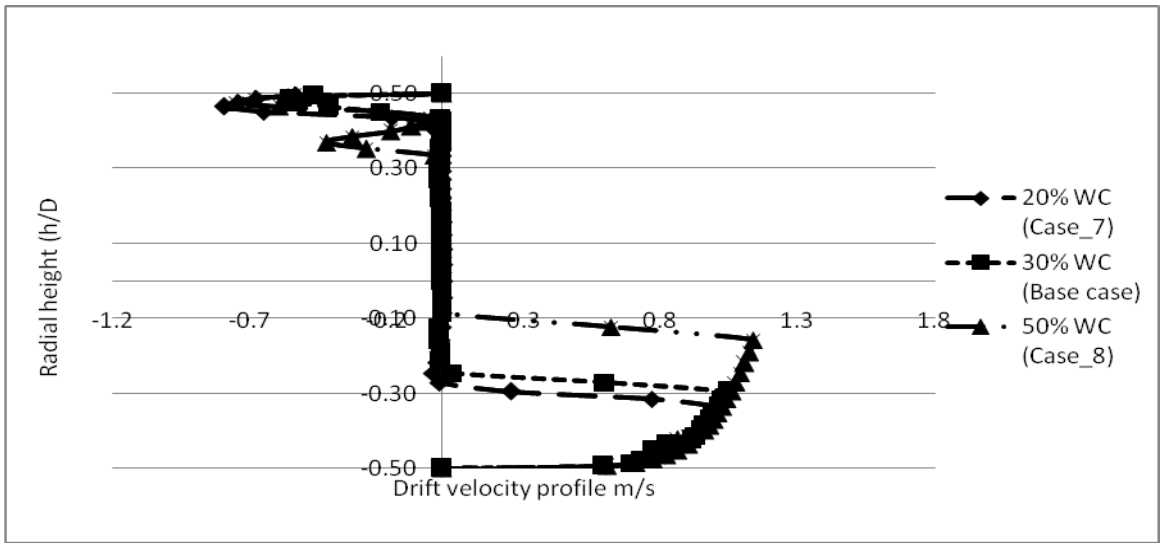

Figure 4.40: Comparison of radial oil/water drift velocity for different inlet mixture contents (20, 30, and 50% WC)

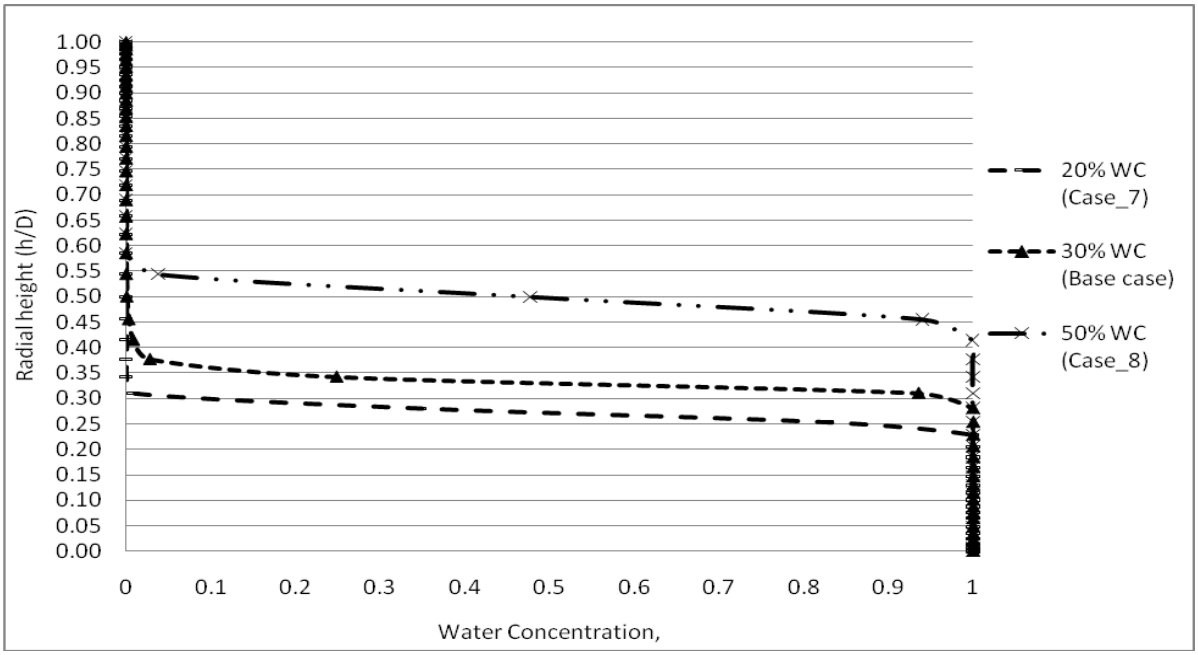

Figure 4.41: Variation of water concentration in vertical position of different inlet water cut for present work

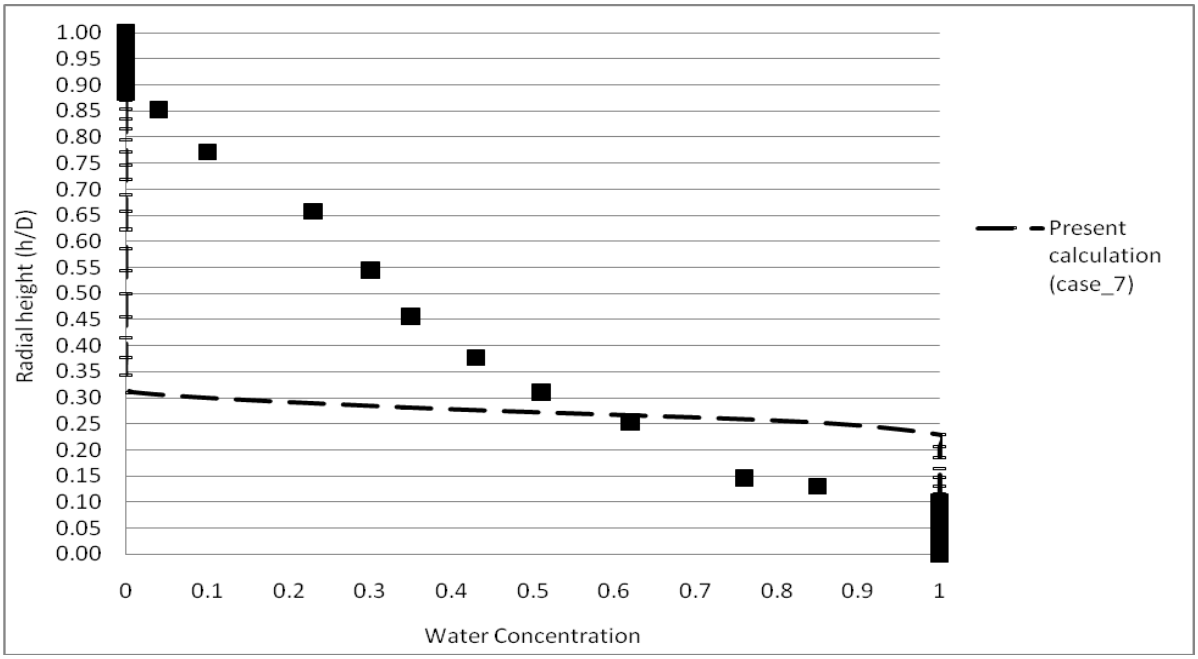

Figure 4.42: Present work comparison of water concentration in radial position for inlet 20% WC to experimental work of Vedapuri et. al (1997)

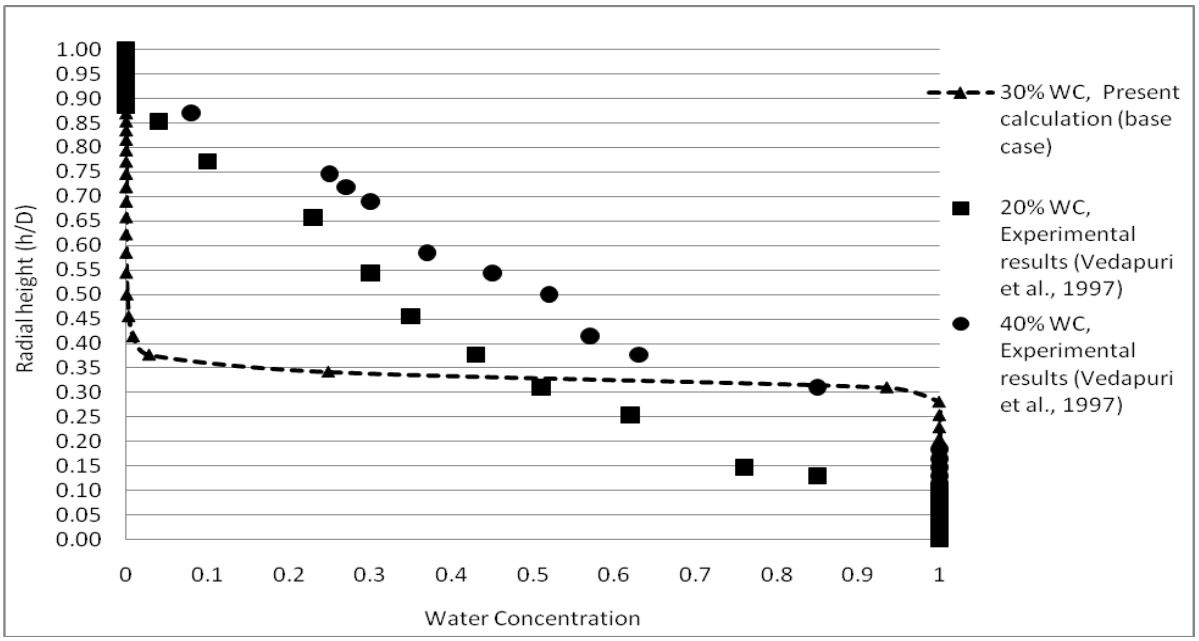

Figure 4.43: Present work comparison of water concentration in radial position for 30% inlet WC to experimental work of Vedapuri et al (1997)

The flow pattern outcome from inlet operating conditions of different inlet mixture velocity or water contents can be summarized as follows and presented in Figure 4.44:

- Increasing inlet mixture velocity increases water entrainment to oil, increases mixing range and result in lower water holdup or *in situ* water contents.
- Increasing inlet water contents (WC) increases water separation height.

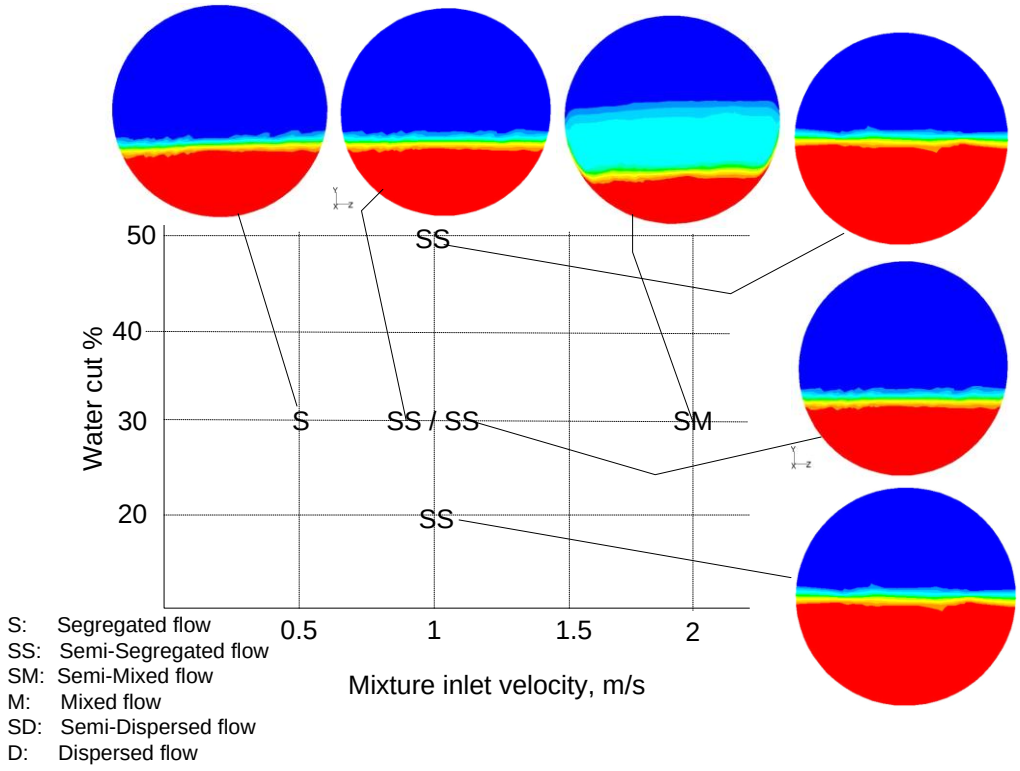

Figure 4.44: Observed flow patterns at different input mixture velocity and water cut

4.5.2 Effect of Oil Physical Properties

Two factors are selected to present the oil physical properties: oil viscosity and oil density. These two variables are investigated for two features: flow pattern types and water holdup.

Effect of oil viscosity

The effect of the oil viscosity on local water contents (holdup) and flow patterns is investigated at oil density of 830 kg/m^3 and oil viscosity of 2.0, 15.0 and 30.0 cP. Figure

4.45 shows the radial and longitudinal contours of the water phase. Figure 4.46 shows the radial velocity profiles along the pipe.

Figure 4.45 compares the radial and longitudinal planes of water contours. The radial plane is located at X5.5 which is 35.7 of L/D downstream the inlet. They show that as the viscosity increases, the mixing zone increases. The figures show also that increasing oil viscosity reduces the separation rate. Figure 4.46 compares the radial velocities for oil and water along the pipe. In general, as oil viscosity increases, the oil velocity profiles have more distribution across the pipe diameter that expands to the pipe surface from top to bottom which reflects more mixing between oil and water. The figure shows also that as oil viscosity increases, the fluid layer at the bottom accelerates more than the layer at the top due to oil layer holds up in the pipe top occupying a great cross section area. The oil layer holding up moves slowly at the top and compresses water layer at the bottom to move at higher velocity than upper part. Accordingly, water entrainment to the flowing oil increases, which decreases water local contents at pipe bottom and increases mixing zone.

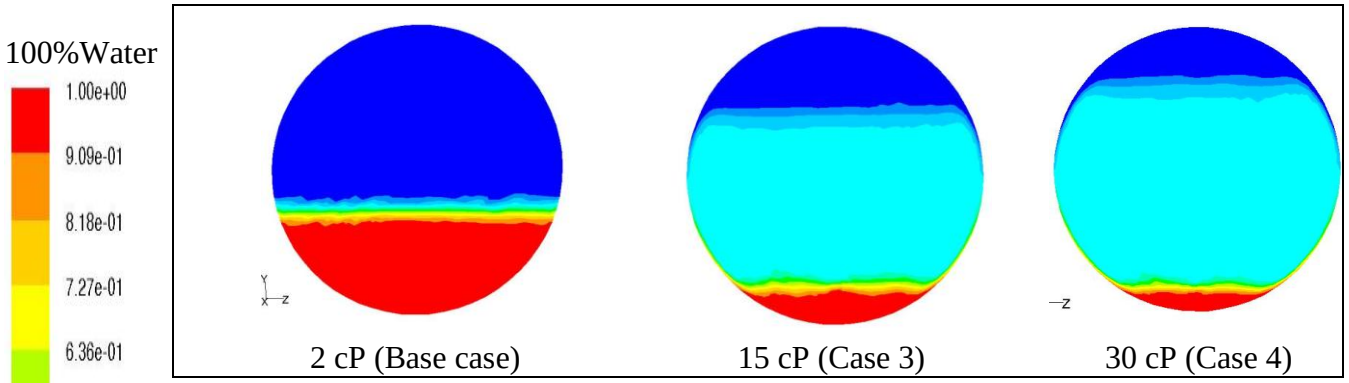

Figure 4.45-a: Water contours at Y-Z-plane at X5.5 (L/D =35.7)

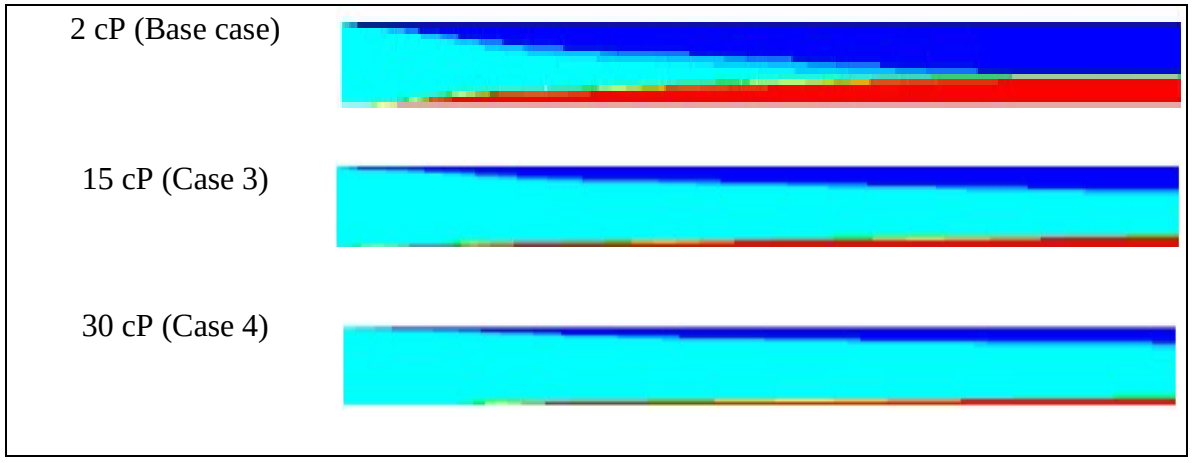

Figure 4.45-b: Water contours along X-Y-plane for longitudinal vertical plane

Figure 4.45: Water contours at different planes for different oil physical properties

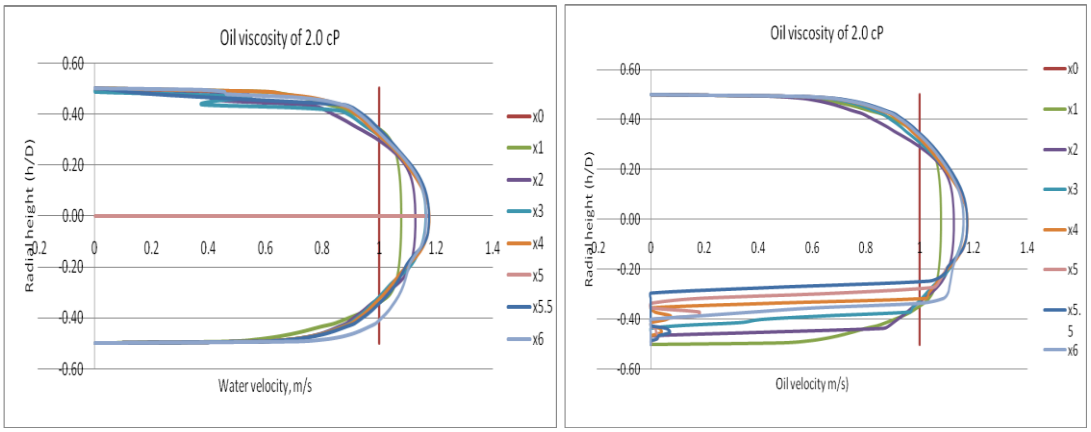

a) Water and oil radial velocity profile at 2.0 cP

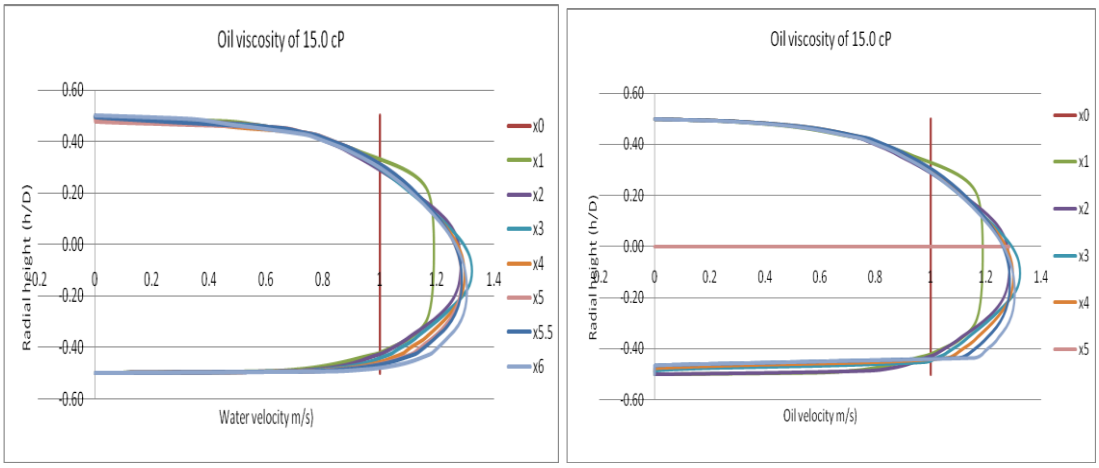

b) Water and oil radial velocity profile at 15.0 cP

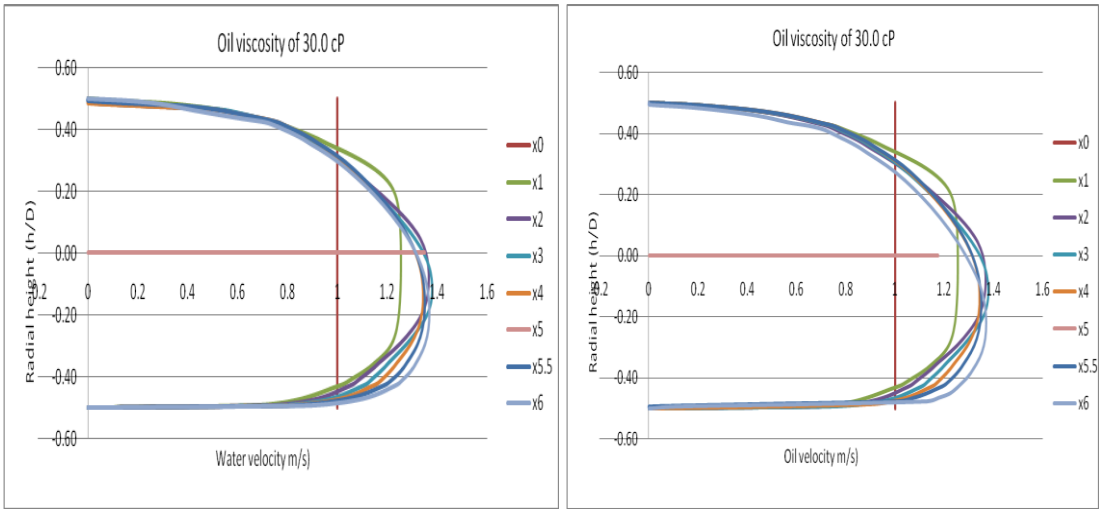

c) Water and oil radial velocity profile at 30.0 cP

Figure 4.46: Velocity profile for water and oil at radial planes along the pipes at a) 2.0 cP, b) 15.0 cP, c) 30.0 cP

By referring to Figure 4.45 and 4.46, it shows that as oil viscosity increases, flow pattern changes to more mixing. As the oil viscosity increases, the mixing zone of oil-water increases that gives an indicating of more tendency of forming stable oil-water mixing flow. The expected flow patterns map based on Figure 2.1 [Vedapuri et al. (1997)] are summarized as follows:

- At 2 cP: segregated flow prevails as the flow pattern.
- At 15 cP: semi-mixed flow prevails as the flow pattern.
- At 30 cP: semi-dispersed flow prevails as the flow pattern.

Figure 4.47 concentrates on the velocities profile at plane X5.5 which is equivalent to 35.7 of L/D. It represents a comparison of velocities profile for oil and water. It shows the influence of increasing oil viscosity on the phase's distribution. Increasing oil viscosity increases overlap between oil and water phases and reduces water height at the pipe bottom by increasing the mixing zone. Figure 4.48 shows the drift velocity as the difference of water velocity and oil velocity at the plane X5.5. The slip velocity is an indication of water holdup per the definition of the drift velocity. The lower the drift at the bottom, the higher the water holdup is. In this case, it shows that the expected water holdup is low at the bottom while oil holdup at the top is high. The water holdup decreases by increasing oil viscosity.

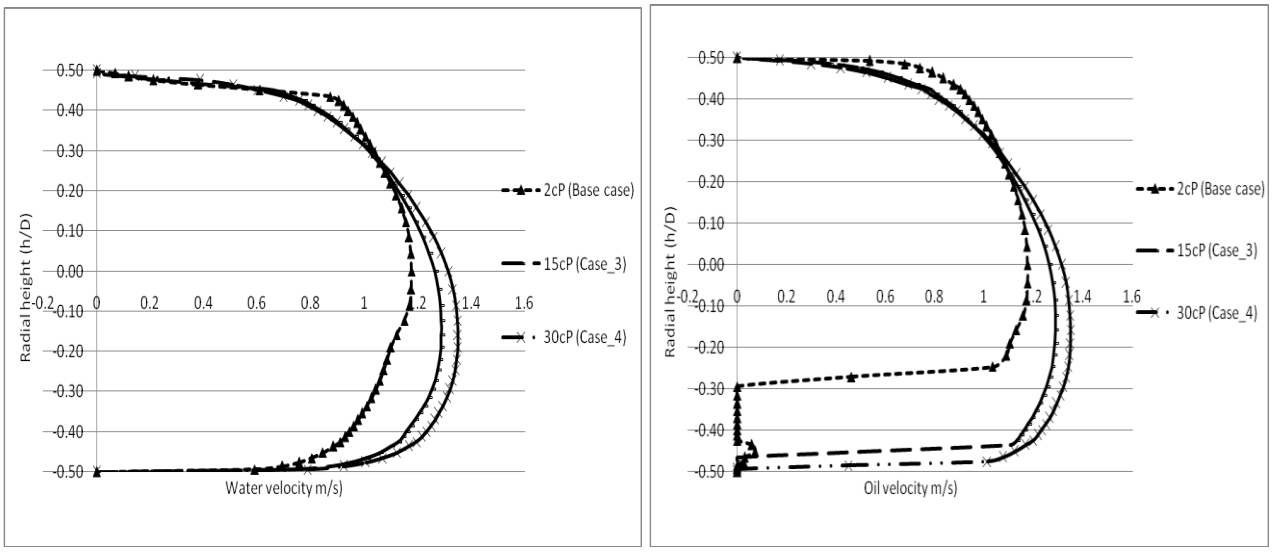

Figure 4.47: Water and oil radial velocity profile comparison for different oil viscosity at plane X5.5 (L/D = 35.7)

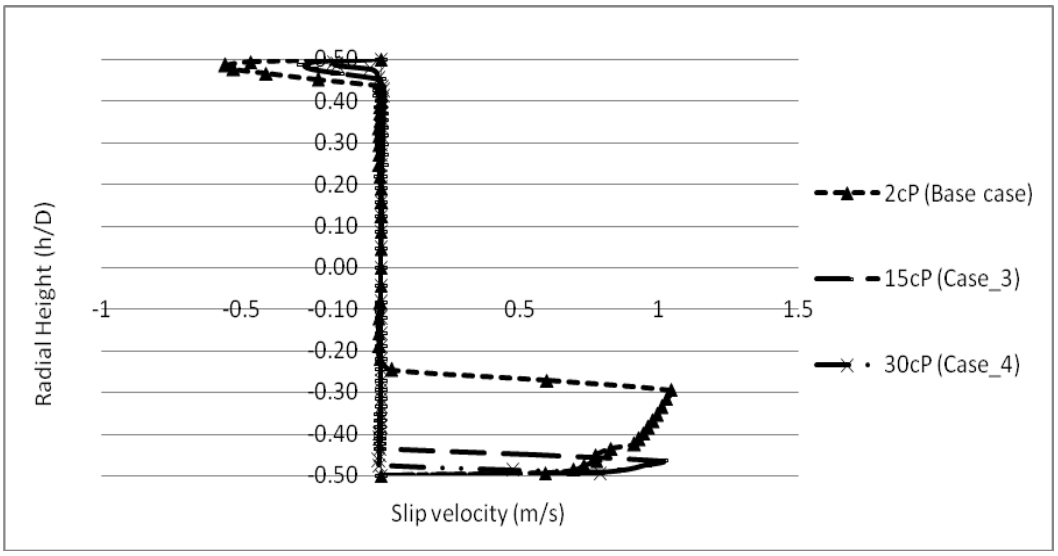

Figure 4.48: Slip velocity in radial velocity profile for different oil viscosity at plane X5.5 (L/D =35.7)

Figure 4.49 monitors the radial concentration changes along the pipe per each viscosity. It compares the effect of oil viscosity on the water concentration for the three cases. As oil viscosity increases, the separation is delayed downstream the pipe. At an oil viscosity of 2.0 cP, the rate of separation is high where it gets almost complete separation 5.0 meter downstream at a height between 0.3 and 0.4 of h/D. Increasing the oil viscosity to 15.0 cP and 30.0 cP reduces the separation rate where the complete separation does not appear in the pipe length 6.0 meter range. At 5.0 meter, the mixing range is between 0.69 to 0.16 of h/D and 0.72 to 0.1 of h/D for 15.0 cP and 30.0 cP respectively. Increasing oil viscosity increases the mixing as was shown in Figure 4.15. The figure compares the influence of the oil viscosity on the mixing zone at X5.5 (L/D = 35.7) for the three cases of 2 cP, 15 cP and 30 cP. It shows that the mixing zone increases by increasing the oil viscosity.

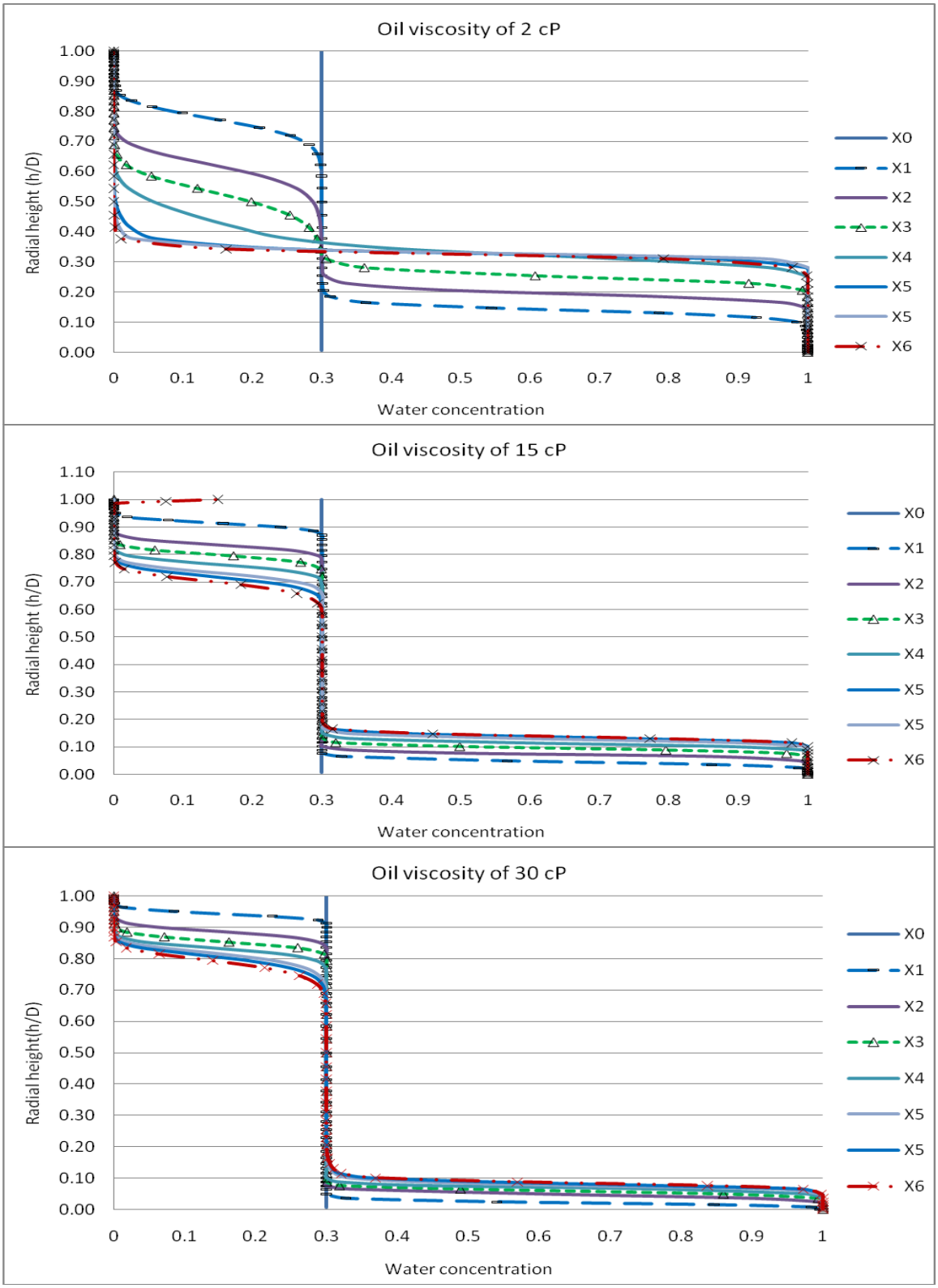

Figure 4.49: Variation of radial water concentration in vertical position of different oil viscosities

Effect of oil density

The effect of the oil density on local water contents (holdup) and flow patterns is investigated at oil viscosity of 2 cP and oil density of 662, 830 and 998.2 kg/m^3. Figure 4.53 shows the radial and longitudinal contours of the water phase. Figure 4.50 shows the radial velocity profiles along the pipe.

Figure 4.50 compares the radial and longitudinal planes of water contours. The radial plane is located at X5.5 which 35.7 of L/D downstream the inlet. They show that as the density increases, the mixing stability increases and the separation rate is delayed. It shows that oil-water mixing is directly proportional to the density difference between oil and water that is dominated by the gravity force. The higher the difference between the two densities, the more separation occurs. Accordingly, heavy fluid accumulates at the pipe bottom and the light fluids moves towards the top. On the other hand, as the oil density approaches water density, the miscibility between oil and water increases. So the closer densities results in easier momentum and mass exchange between oil and water. At equal oil and water densities, the flow is fully mixed and oil shows a more concentrate layer on the inner surface of the pipe.

Figure 4.51 compares the radial velocities for oil and water along the pipe. As the radial velocity profile almost uniform along the pipe for both and water at same densities, it shows differences for other both cases. The velocity difference between oil and water along the pipe is high for oil of 662 kg/m^3 density compared to oil of 830 kg/m^3 density. So it is easier to entrain water by a heavy oil phase.

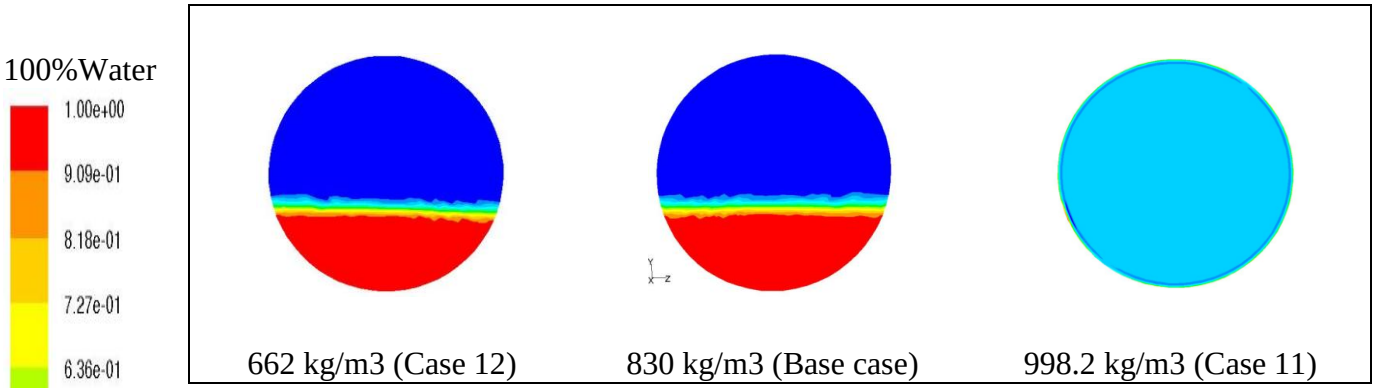

Figure 4.50-a: Water contours at different oil densities for Y-Z-plane at 5.5 m (L/D = 35.7) downstream the inlet

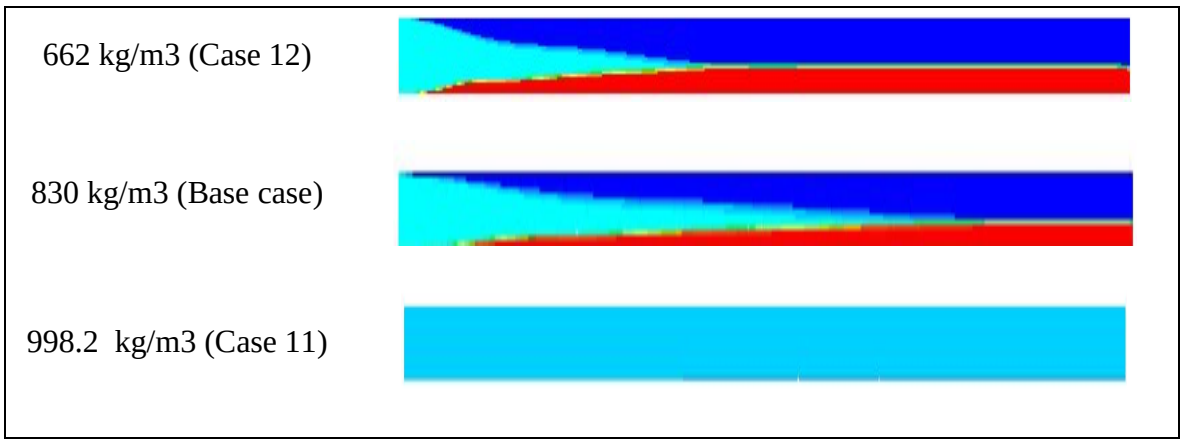

Figure 4.50-b: Water contours at different oil densities for longitudinal vertical contour X-Y planes

Figure 4.50: Water contours at different oil density for cross-sectional and longitudinal planes

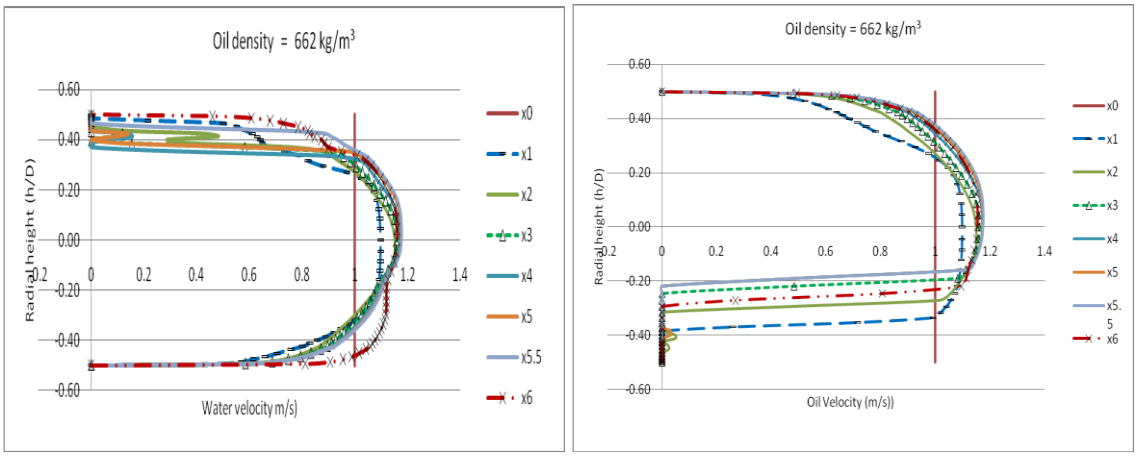

a) Water and oil radial velocity profile at 662 kg.m3

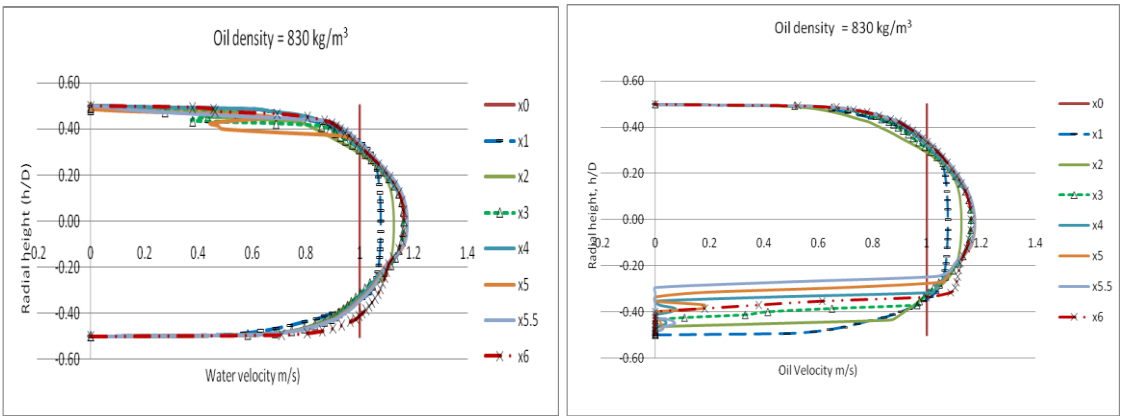

b) Water and oil radial velocity profile at 830 kg.m3

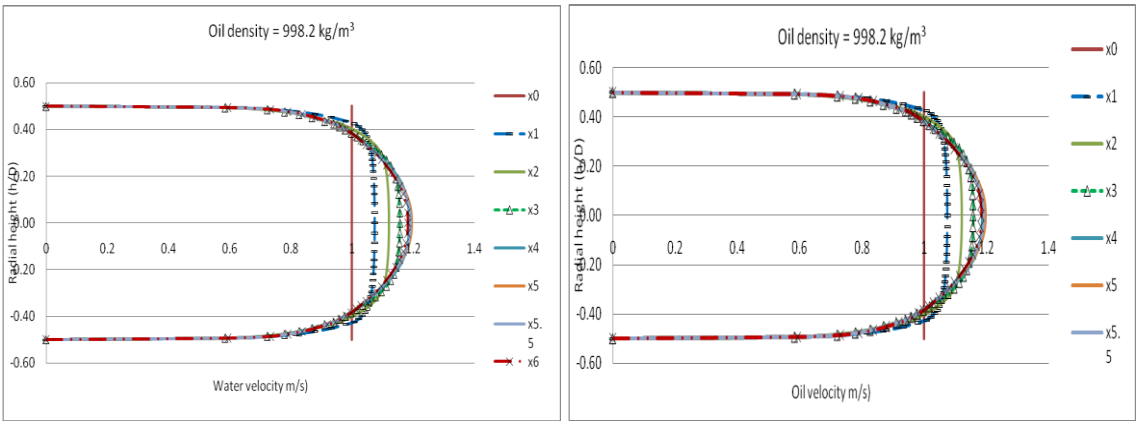

c) Water and oil radial velocity profile at 998.2 kg.m3

Figure 4.51: Velocity profile for water and oil at radial planes along the pipes at a) 662 kg/m3, b) 830 kg/m3 c) 998.2 kg/m3

By referring to Figure 4.50 and 4.51, it shows that as oil density increases, the mixing zone of oil-water increases that gives an indicating of more tendency of forming stable oil-water mixing flow. The expected flow patterns map based on Figure 2.1, Vedapuri et al. (1997), are summarized as follows:

- At 662 kg/m3: segregated flow prevails as the flow pattern.
- At 830 kg/m3: segregated flow prevails as the flow pattern.
- At 998.2 kg/m3: dispersed flow prevails as the flow pattern.

Figure 4.52 concentrates on the velocities profile at plane X5.5 which is equivalent to 35.7 of L/D. It represents a comparison of velocities profile for oil and water. It shows the effect of changing oil density on the phase's distribution. Increasing oil density increases overlap between oil and water phases and reduces water height at the pipe bottom by increasing the mixing zone. For equal oil and water densities, the velocity of both phases is almost the same. Figure 4.53 shows that the drift velocity is affected by oil density change at the plane X5.5. The slip velocity is an indication of water holdup per the definition of the drift velocity. The lower the drift at the bottom, the higher the water holdup is. In this case, it shows that the expected water holdup is low at the bottom while oil holdup at the top is high. In this case, it shows that as oil density increases, the water holdup decreases.

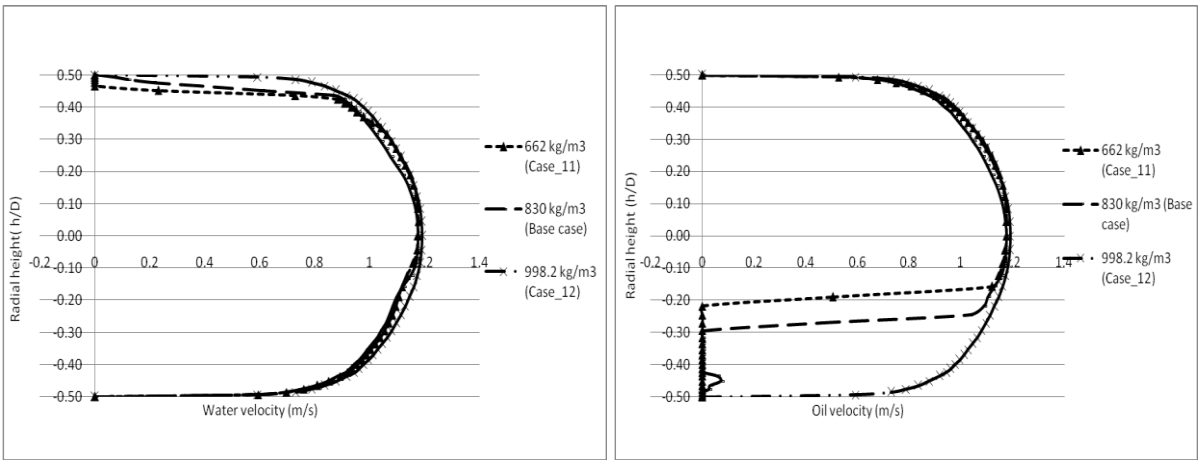

Figure 4.52: Water and oil radial velocity profile comparison for different oil densities at plane X5.5 (L/D =35.7)

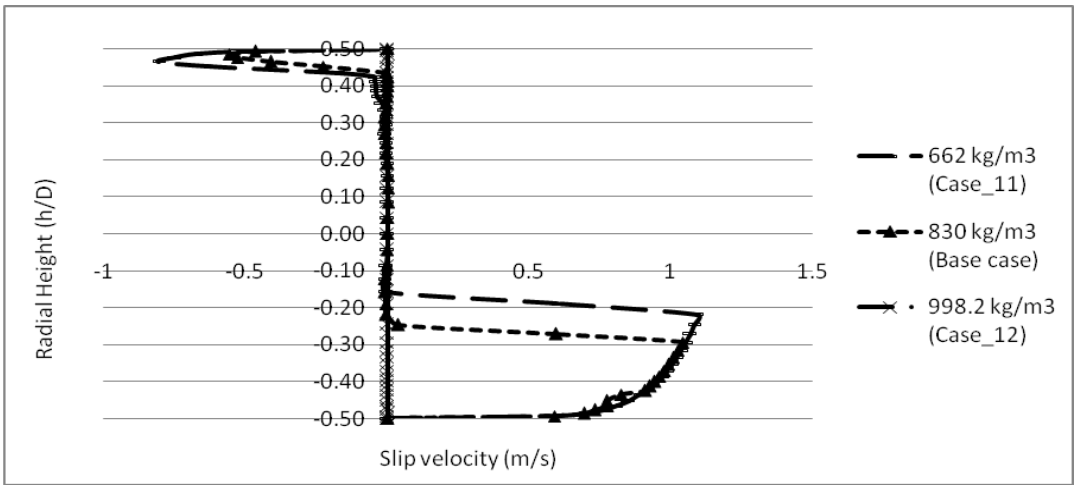

Figure 4.53: Velocity drift (slip) of radial velocity profile for different oil densities at plane X5.5 (L/D =35.7)

Figure 4.54 monitors the radial concentration changes along the pipe per each density change. It compares the effect of oil density on the water concentration for the three cases. As oil density increases, the separation is delayed downstream the pipe. Increasing the oil density from 662 kg/m^3 to 830 kg/m^3 reduce the separation rate gradually. At 998.2 kg/m^3, the two phases are well mixed across the radial height. Figure 4.18, as discussed before, compares the effect of the oil density on the mixing zone at plane X5.5 (L/D = 35.7). It shows that as density of oil approach water density, the mixing zone increases. For equal densities of oil and water, there is no separation and the water phase shows 30% water cut across the pipe radial diameter.

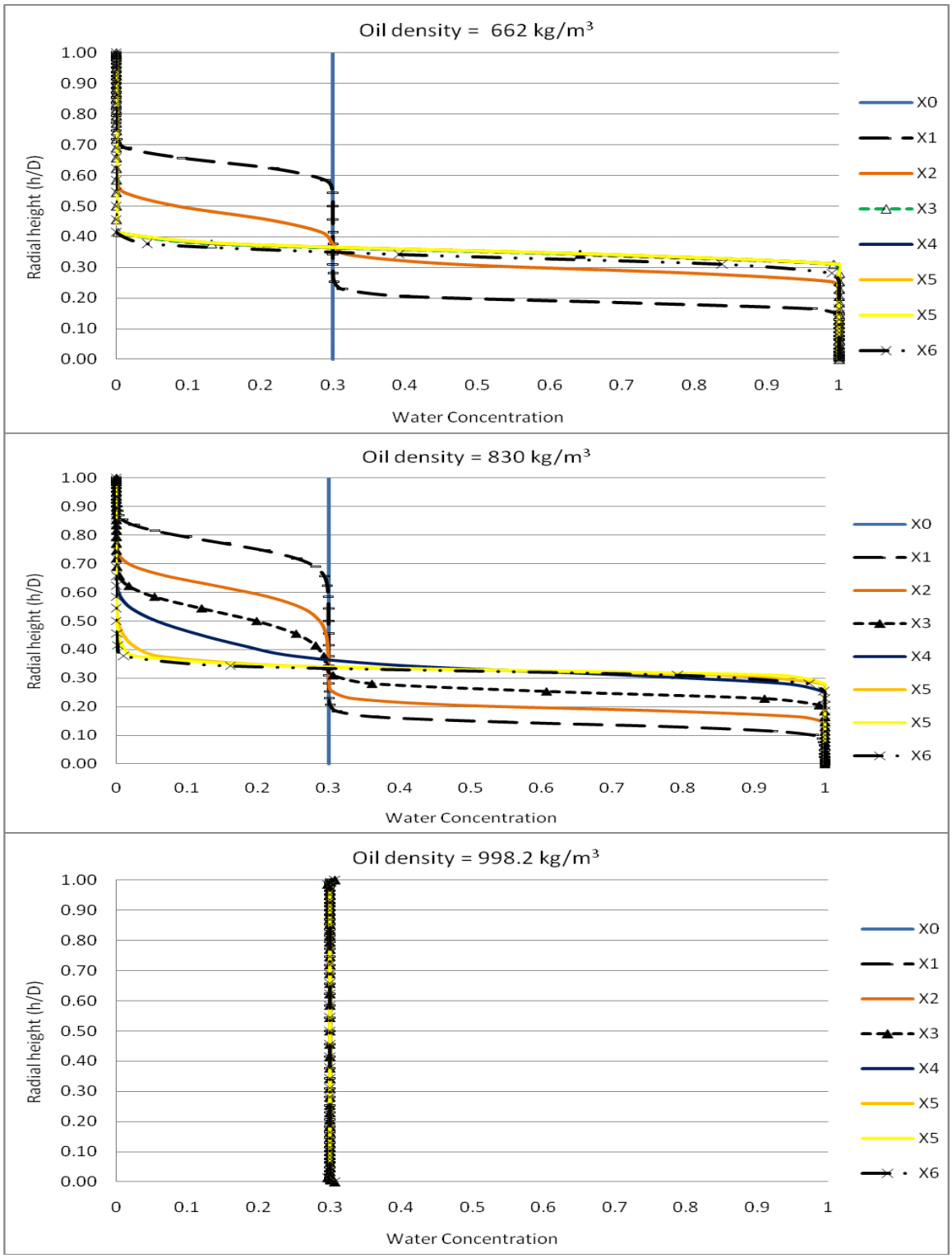

Figure 4.54: Variation of radial water concentration in vertical position of different oil densities at plane X5.5 (L/D = 35.7)

The flow pattern outcome from different oil physical properties can be summarized as follows and presented in Figure 4.55:

- Increasing oil density results in increasing the mixing zone.
- Increasing oil viscosity increases mixing zone and result in lower water holdup or local water contents.

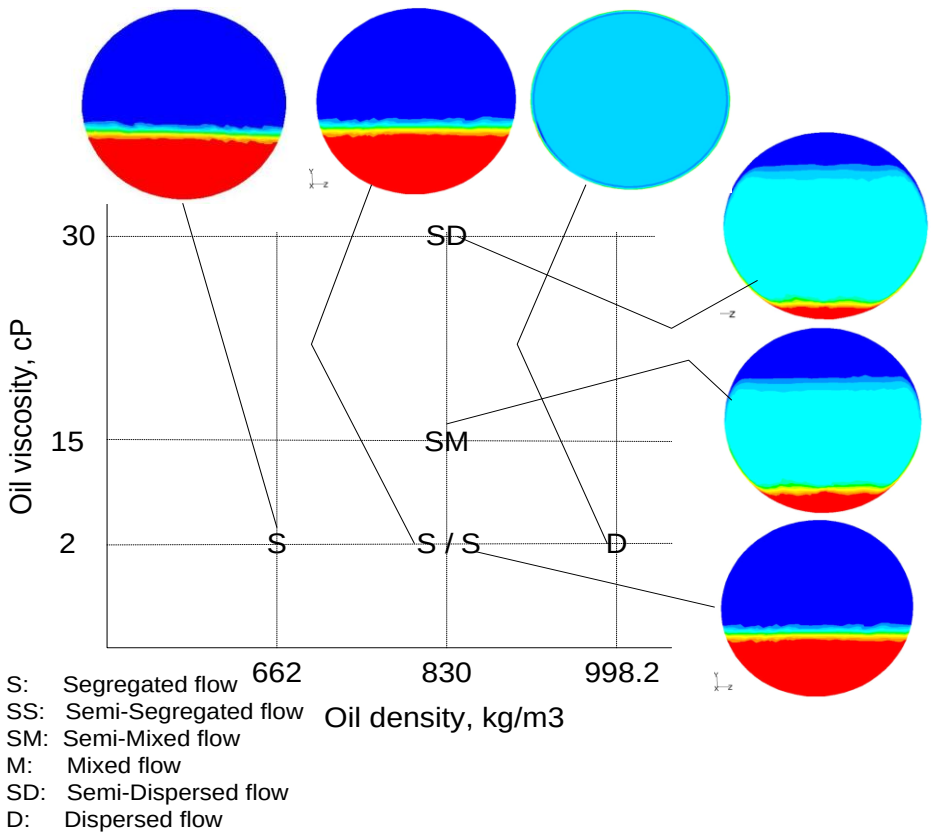

Figure 4.55: Observed flow patterns at different viscosity and density of oil

4.5.3 Effect of Pipe Geometry

With fixing all variables in Table 4.1, three variables are selected as variables to present the piping geometry effect: pipe inner diameter, inclination and internal turbulator device. However, internal turbulator device effect is handled separately in chapter 5. These variables are investigated and compared for two features of two phase flow: flow pattern and water holdup.

Effect of inner diameter

The effect of the inner diameter change on local water contents (holdup) and flow patterns is investigated at pipe diameter of 101, 102 and 202 mm. Figure 4.56 shows the radial and longitudinal contours of the water phase. The radial sections are identified at planes X5.5 (L/D = 35.7). Figure 4.57 shows the effect of the inner diameter change by monitoring the radial velocities along the pipe. Figure 4.56 compares the water contours at both cross section plane and the longitudinal vertical plane. In general, the figures show that as the pipe diameter increases, flow pattern gets more mixing where the mixing zone of oil-water increases. It is clear that the separation is delayed by increasing the pipe diameter. Figure 4.57 compares the radial velocities for oil and water along the pipe. It shows that the influence of the inner diameter on velocity profiles is minor for this range of diameters. As the diameter increases, the reduction in parabolic shape of oil velocity profiles reduces along the pipe downstream as the velocity slows down. That means increasing the pipe diameter increases mixing zone.

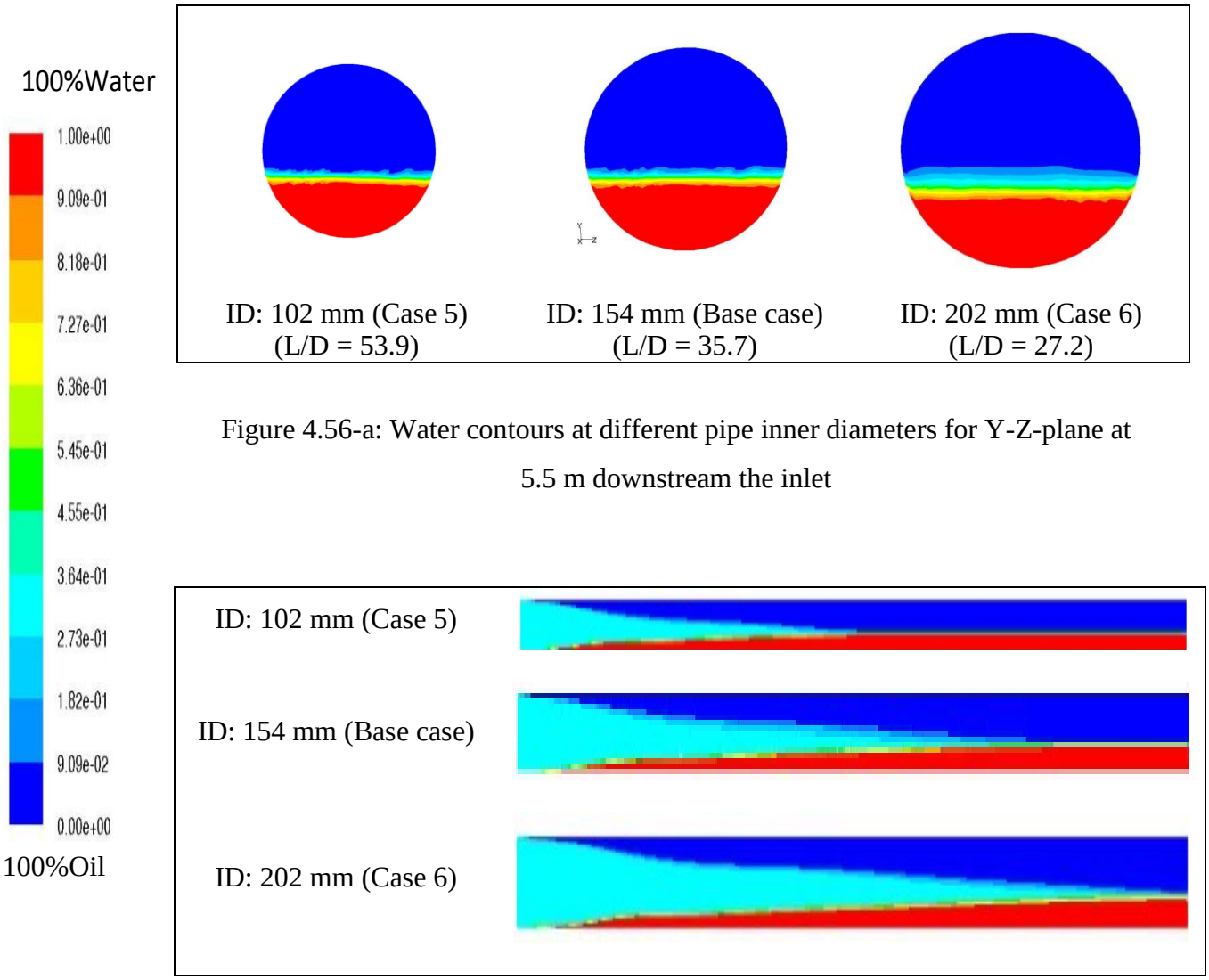

Figure 4.56-a: Water contours at different pipe inner diameters for Y-Z-plane at 5.5 m downstream the inlet

Figure 4.56-b: Water contours at different pipe inner diameters X-Y-plane for longitudinal vertical contour

Figure 4.56: Water contours comparison for different pipe inner diameters at different planes

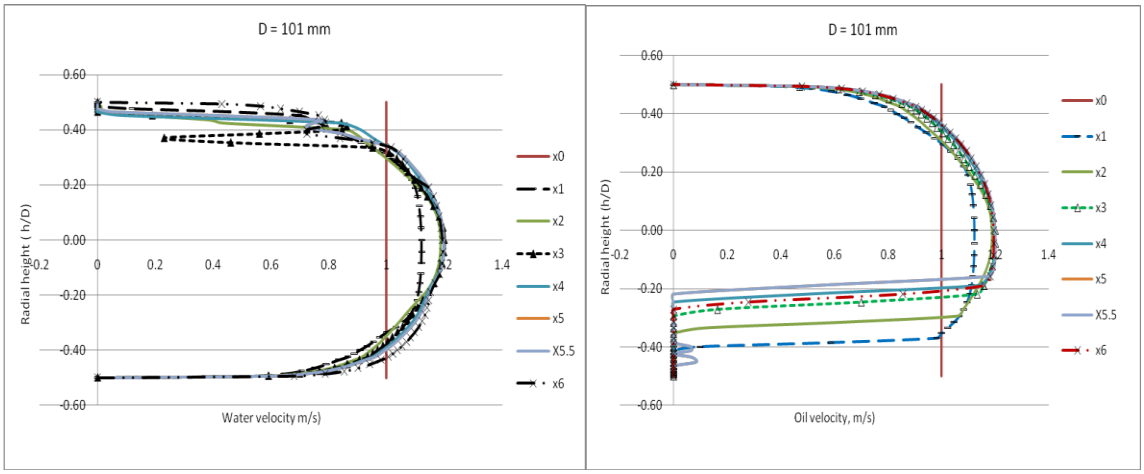

a) Water and oil radial velocity profile at 101 mm

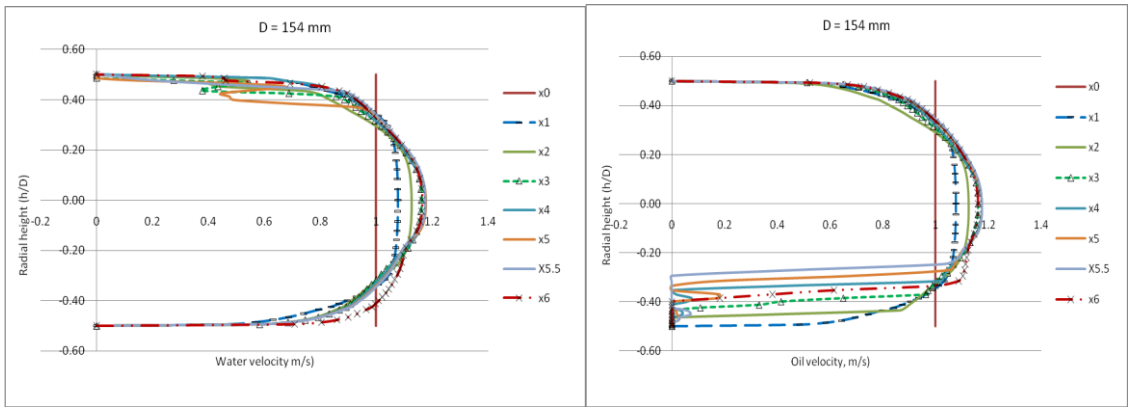

b) Water and oil radial velocity profile at 154 mm

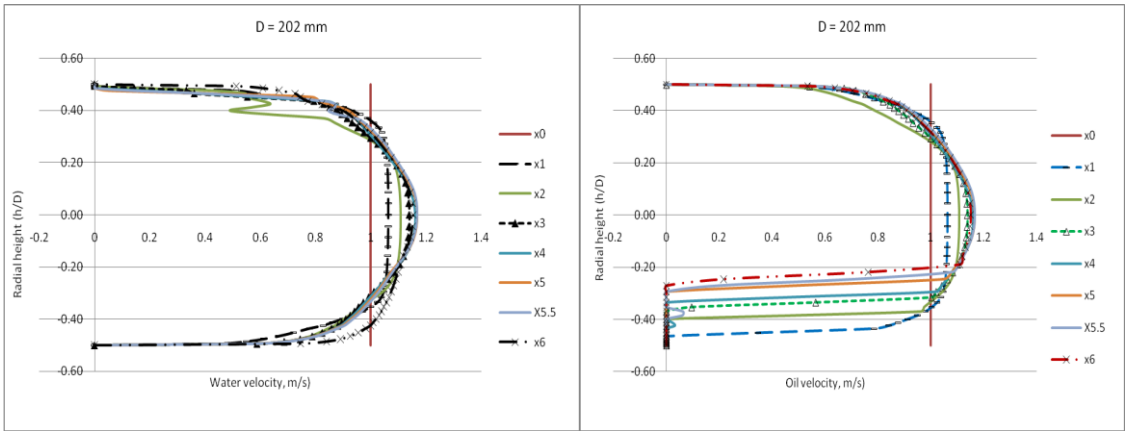

c) Water and oil radial velocity profile at 202 mm

Figure 4.57: Velocity profile for water and oil at radial planes along different inner pipe diameter: a) 101 mm, b) 154 mm c) 202 mm

Referring to Figure 4.56, it compares the water contours at both cross section plane and the longitudinal vertical plane. In general, the figures show that as the pipe diameter increases, flow pattern gets more mixing where the mixing zone of oil-water increases. The expected flow patterns map based on Figure 2.1 [Vedapuri et al. (1997)] is summarized as follows:

- At 102 mm pipe ID: semi-segregated flow prevails as the flow pattern.
- At 154 mm pipe ID: semi-segregated flow prevails as the flow pattern.
- At 202 mm pipe ID: semi-segregated flow prevails as the flow pattern.

Figure 4.58 comparing the three different pipe sizes (102, 154 and 202 mm) at X5.5. It shows that the water separation for 154 mm pipe seems to be more than 102 mm pipe at this location and that is in agreement with Cai et al. (2004). However, comparing the water separation at 202 mm to 102 mm or 154 mm pipes, it shows that the separation at 202 mm is lower. This observation is opposite to previous observation and to the findings of Cai et al. (2004). The discrepancy might be justified by that the flow in 202 mm pipe not yet gets fully developed due to short length. So increasing the pipe diameter delays the separation as shown clearly in the longitudinal contours in Figure 5.60-b. The large pipe diameter carries higher amount of water compared to the smaller pipe diameters operating at same conditions. This higher amount of water requires more effort to avoid separation. The velocity drop between 101 mm and 154 mm is high compared to the difference between 154 mm and 202 mm. Increasing the diameter from 101 mm to 154 shows a more mixing where oil velocity approaches the bottom. Although the oil velocity in the

diameter of 202 mm has more and clear mixing compared to 101 mm, it shows slight shift up by referring to 154 mm which is an indication of drop in the mixing. Oil is shifted up and the heavy flow tries to settle down based on the dominant force. It seems that turbulent dominants the flow for certain sizes then the gravity force takes the lead based on this certain operation condition. Figure 4.59 shows the drift velocity as the difference between water velocity and oil velocity at the plane X5.5. In general, for this case, it shows that the expected water holdup decreases with increasing diameter at the pipe bottom. While increasing the diameter from 101 to 154 mm shows high drift drop, it shows increase in the drift between 154 and 202 mm.

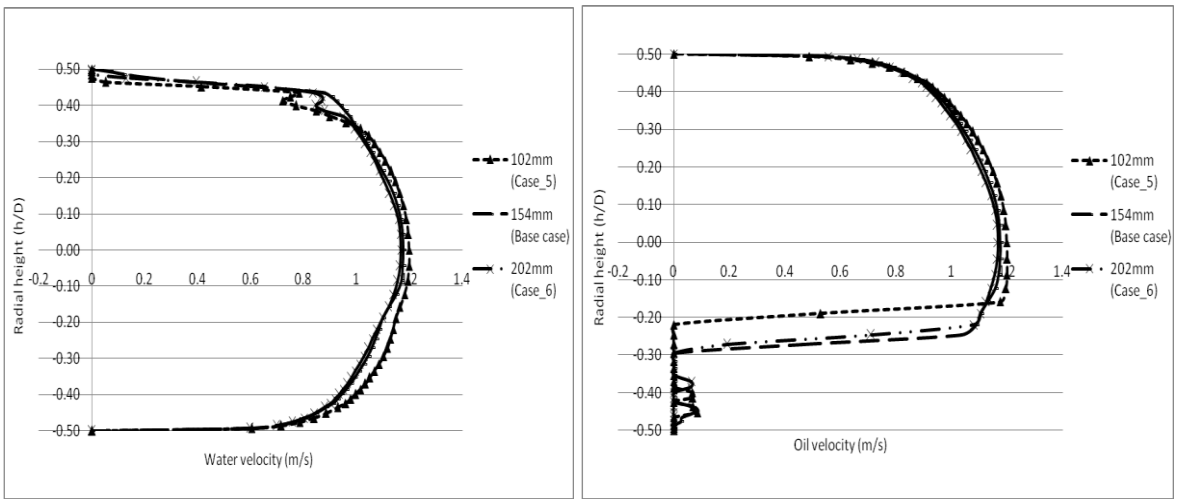

Figure 4.58: Variation of radial (a)- water and (b)- oil velocity for different pipe diameters (102, 154, and 202 mm)

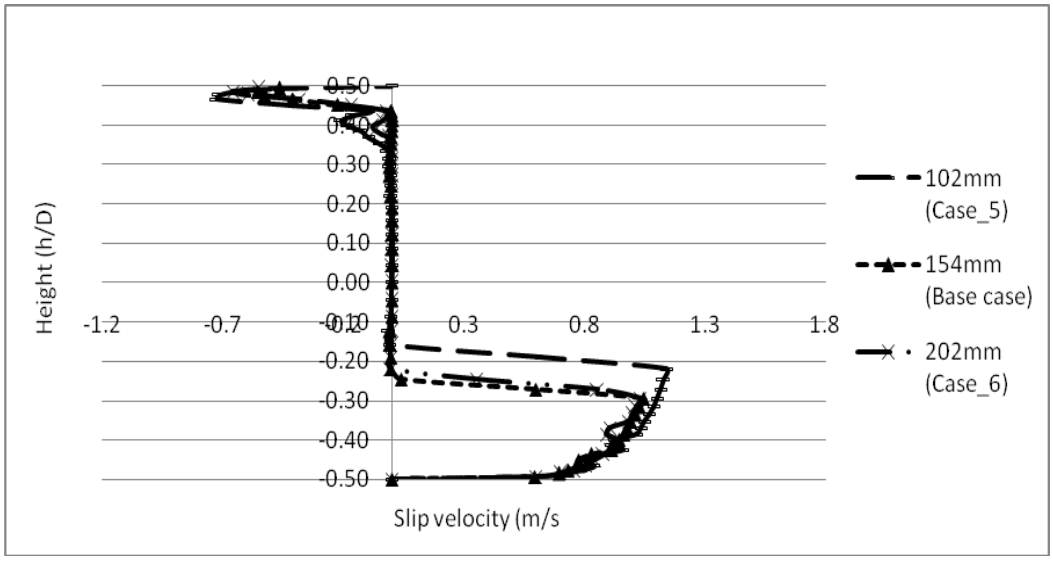

Figure 4.59: Comparison of radial oil/water drift velocity for different pipe diameters (drift: 102, 154, and 202 mm)

Figure 4.60 compares the effect of diameter size on the water concentration. It shows that there is a constant separation rate. As mentioned before in Figure 4.22 that compares the effect of the pipe diameters on the mixing zone at X5.5, increasing the diameter increases the mixing zone. The mixing range height of h/D is between (0.32 to 0.4) for 202 mm, (0.29 to 0.4) for 154 mm and (0.27 to 0.5) for 101 mm. Figure 4.22 shows that as pipe diameter increases, water accumulation at the pipe bottom , water accumulation at the pipe bottom are almost the same. However, the mixing zone is higher at high diameter. The high mixing zone might be due to the high water amount at large diameter. This observation is shown clearly in Figure 4.60. Accordingly, it requires longer pipe to compare water holdup for different operations using different diameters. More water accumulation is expected at the bottom of the large pipe due to more water contents.

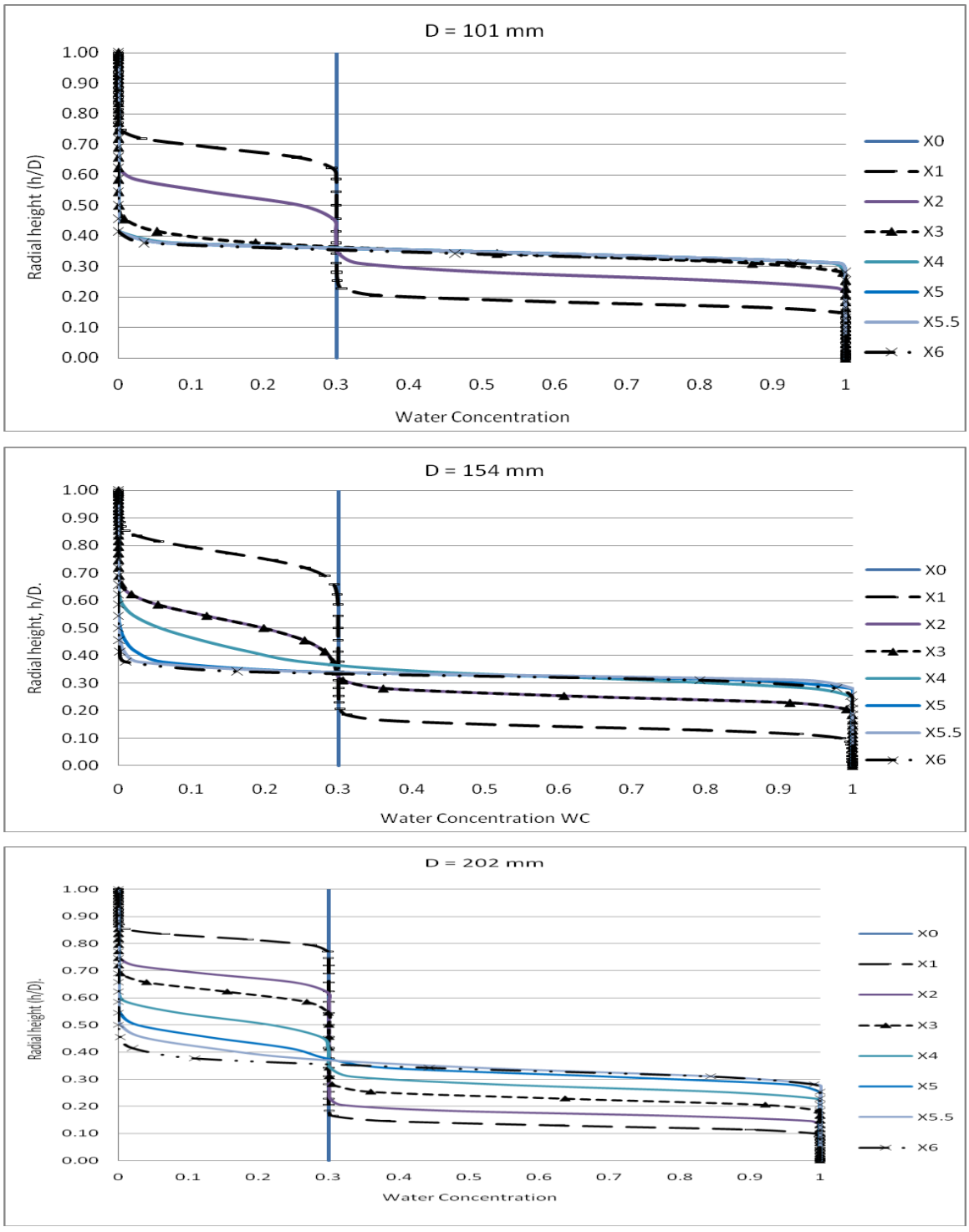

Figure 4.60: Variation of radial water concentration in vertical position of different pipe diameters

Pipes of different diameter size compared at same L/D ratio

The difference in separation start location at different pipe size was noticed as shown in Figure 4.56 comparing the water contours at planes located at same pipe length of X5.5 from inlet. It shows that at both cross section plane and the longitudinal vertical plane that as the pipe diameter increases, flow pattern gets more mixing. It is clear that the separation is delayed by increasing the pipe diameter. Accordingly, the comparison is conducted at planes located at same L/D ration of 27.2 for the three different pipe sizes as shown in Table 4.8. The water contours and content profiles at each plane are compared in Figure 4.61 and 4.62 respectively.

Table 4.8: Change of monitoring planes location based on pipe inner diameter

	Piping geometry		
Variable	102	154	202
Ratio (Lp/D) at 5500 (mm)	53.92	35.71	27.23
Xp (mm) location based on Lp/D of 27.23 ratio	2777.46	4193.42	5500
Pipe length (Lf) (mm)	6000	6000	6000

Figure 4.61 compares water contours at different diameters. The cross-section planes are compared at same L/D ratio of 27.23. At this ratio, the water contours of different pipe size show identical mixing zone.

The comparison of water concentration at along vertical radial line at L/D ratio of 37.23 is shown in Figure 4.62. The water concentrations for the three pipe sizes at same ratio are almost the same.

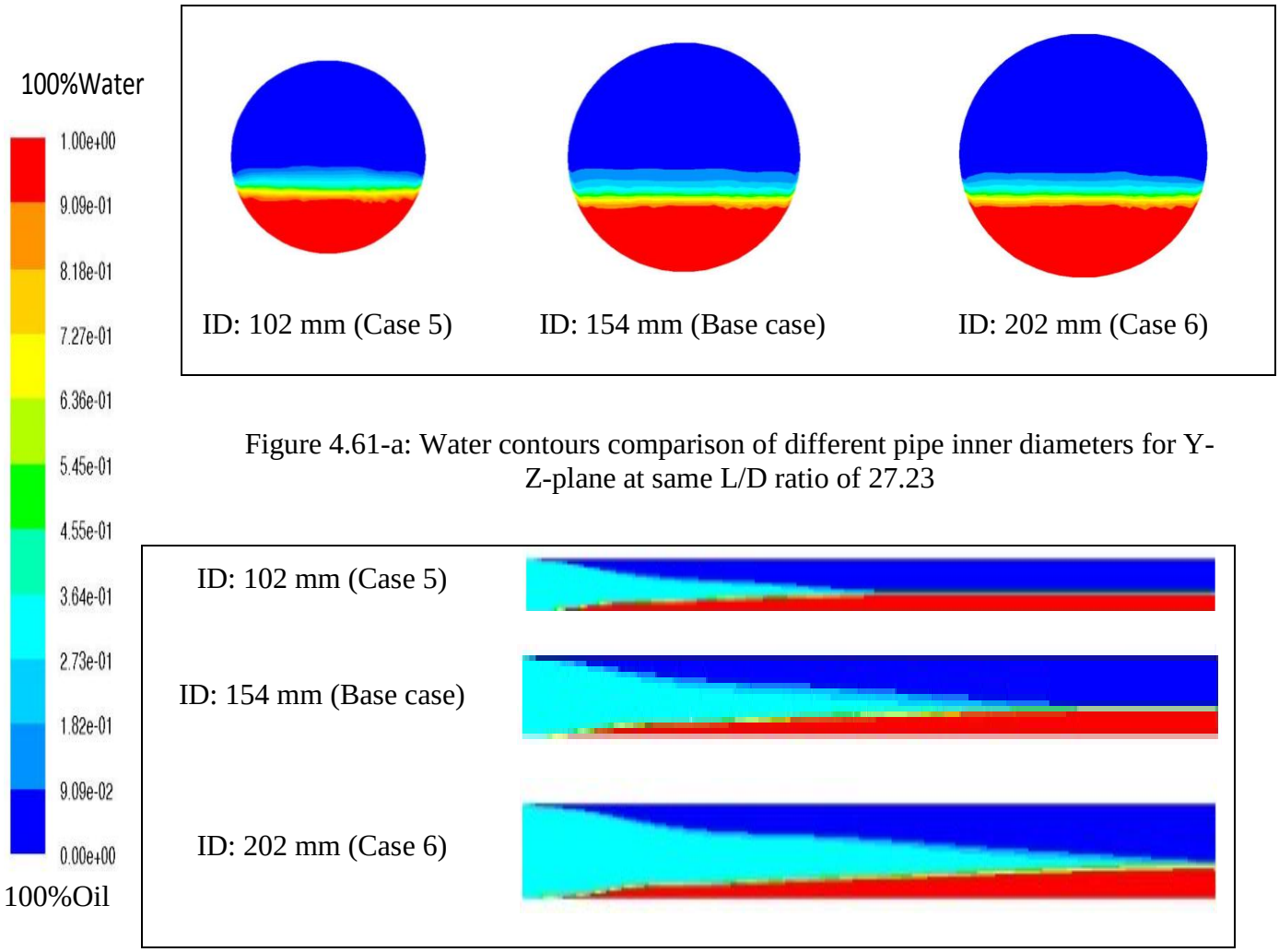

Figure 4.61-a: Water contours comparison of different pipe inner diameters for Y-Z-plane at same L/D ratio of 27.23

Figure 4.61-b: Water contours of different pipe inner diameters X-Y-plane for longitudinal vertical contour

Figure 4.61: Water contours comparison for different pipe inner diameters at different planes

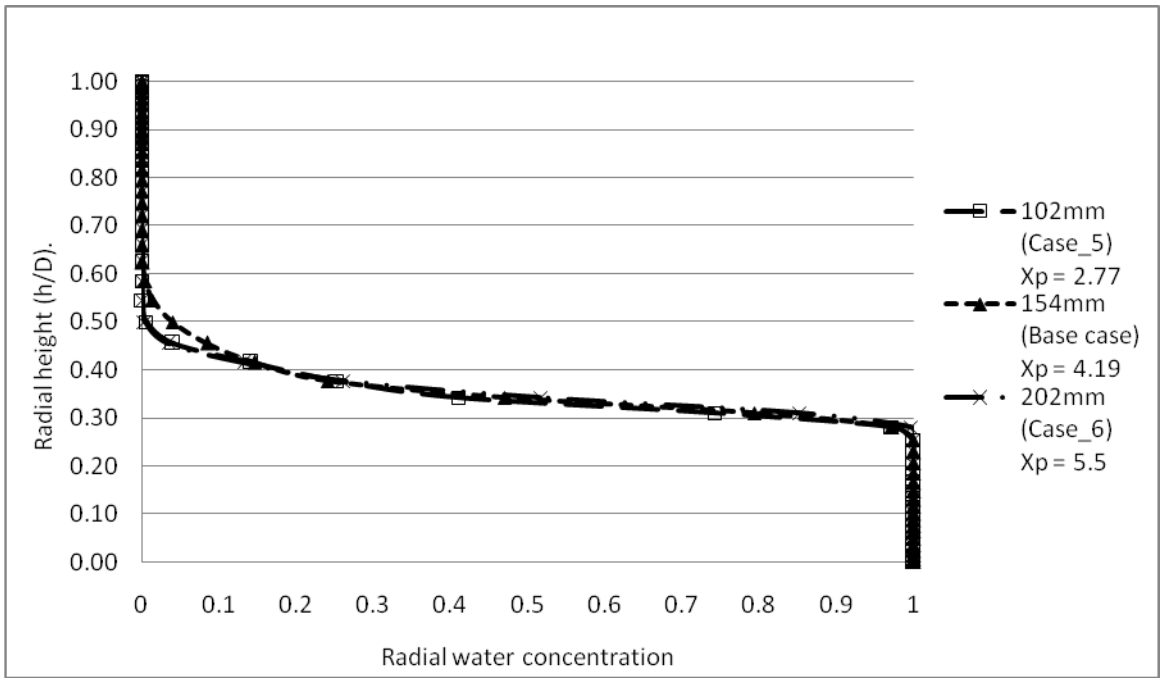

Figure 4.62: Variation of radial water concentration in vertical position of different pipe diameters at L/D = 27.23

Influence of pipes inclination

The influence of the different pipe inclinations on local water contents (holdup) and flow patterns is investigated at pipe inclinations of 0^o (horizontal), -15^o (incline down) and $+15^o$ (inclined up) all at 1.0 m/s and 30% WC. Figure 4.63 shows the radial and longitudinal contours of the water phase. Figure 4.64 shows the influence of different inclination by monitoring the radial velocities along the pipe.

Figure 4.63 compares the water contours at both cross section at plane X5.5 and the longitudinal vertical plane. In general, the figures show that as the pipe inclined up,

flow pattern gets more water holdup and the down inclination reduces water holdup. Figure 4.64 shows that the pipe inclination strongly affects the velocity profiles along the pipe that has an agreement to Kumara et al. (2010) experimental work reporting that inclination affects both holdup and velocity profiles. In general, as pipes incline up, the water velocity profiles are twisted up and slow down downstream the pipe. As the pipes incline down, the water velocity profiles are twisted down and speed up downstream the pipe. On the other hand, as pipe incline up, the oil velocity is shifted away from the pipe bottom. However, as the pipe incline down, the oil velocity approaches the pipe bottom due to reduction of the water layer height. From both cases above, the gravity force dominates oil-water separation in inclined pipes. In case of inclined up, water accumulates at pipe bottom due to gravity causing oil accumulates at the top. In case of inclined down, water accumulates at pipe bottom while oil accumulates at the pipe top accelerating water at the bottom. The mixing at inclined up is higher than the inclined down. The reason is that in inclined up, water rolls back to mix with oil while in inclined down, water moves fast forward.

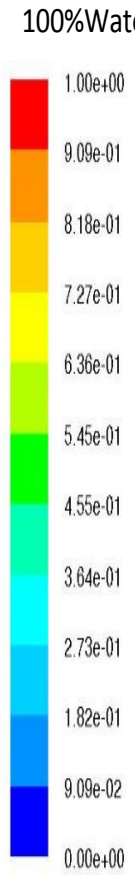

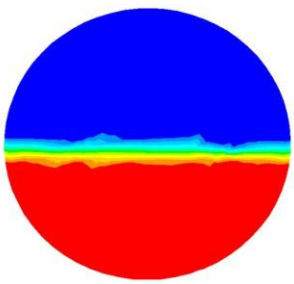	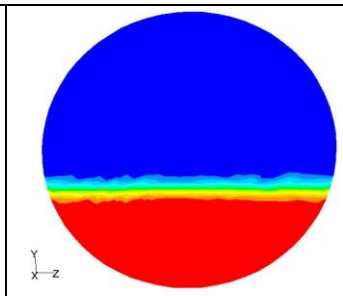	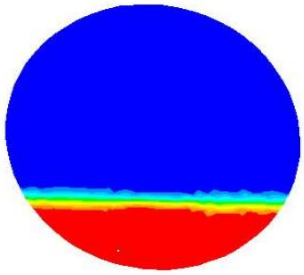
Inclination up (+15^{o}) (Case 9)	Horizontal 0^{o} (Base case)	Inclination down (-15^{o}) (Case 10)

Figure 4.63-a: Water contours at Y-Z-plane at 5.5 m (L/D = 35.7) downstream the inlet

Inclination up +15^{o} (Case 9)	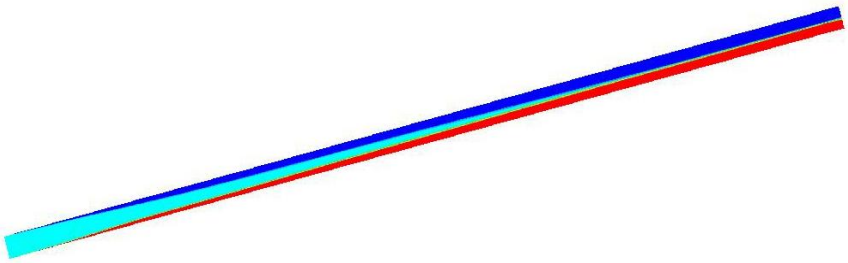
Horizontal 0^{o} (Base case)	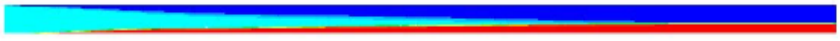
Inclination down (-15^{o}) (Case 10)	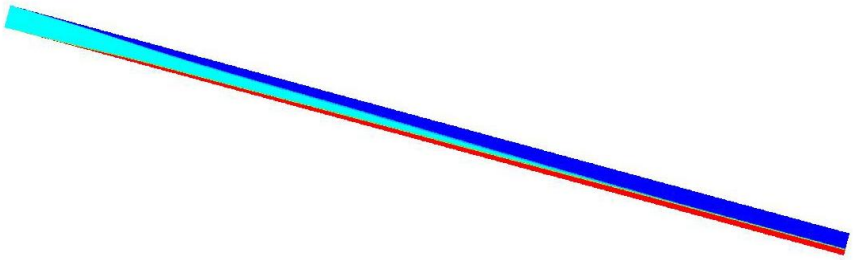

Figure 4.63-b: Water contours for vertical longitudinal Y-X-plane

Figure 4.63: Water contours at different pipe inclinations for cross-section and longitudinal planes

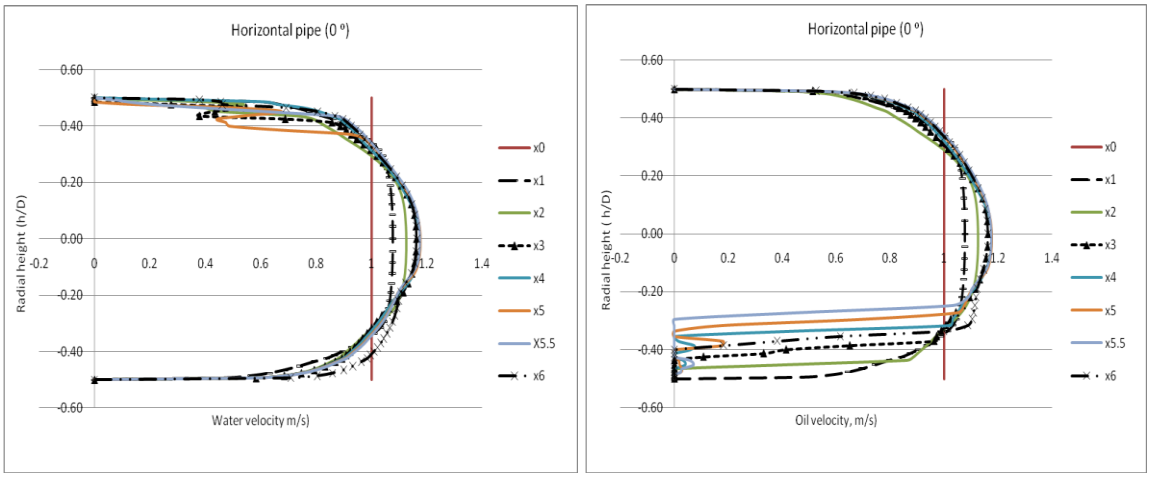

a) Water and oil radial velocity profile at 0^o

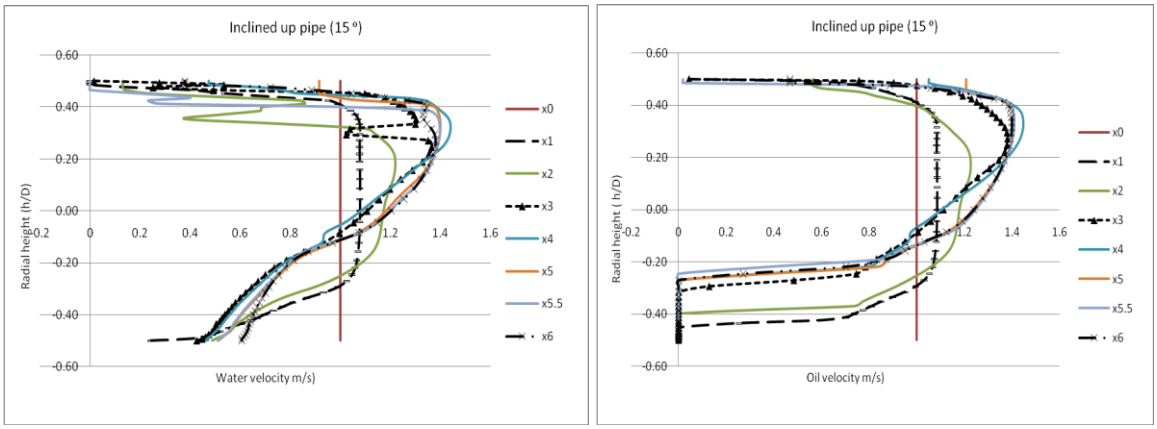

b) Water and oil radial velocity profile at $+15^o$

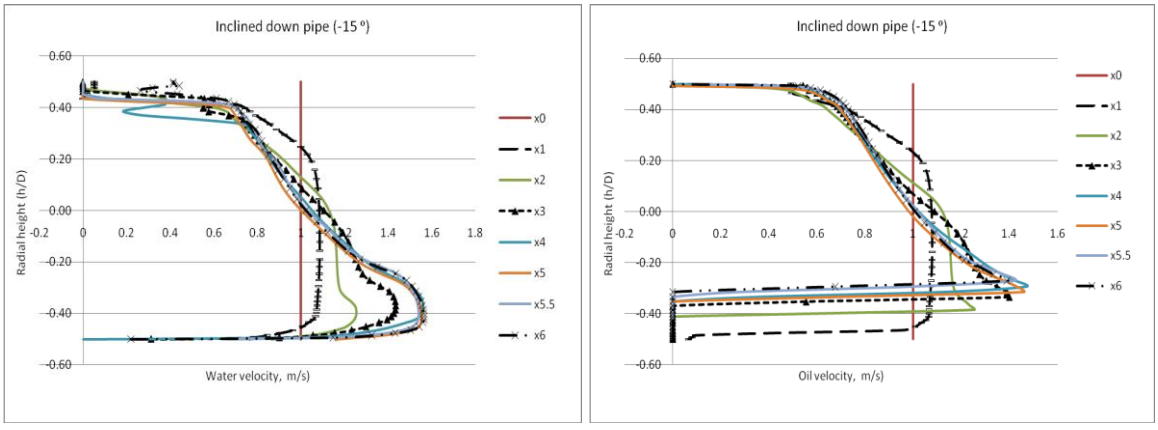

c) Water and oil radial velocity profile at -15^o

Figure 4.64: Velocity profile for water and oil at radial planes along different inclinations: a) 0^o, b)) $+15^o$,and c) -15^o

Referring to Figure 4.63 that compares the water contours at both cross section plane and the longitudinal vertical plane. In general, the figures show that as the pipe inclined up, flow pattern gets more water holdup and the down inclination reduces water holdup. The expected flow patterns map based on Figure 2.1 [Vedapuri et al. (1997)] is summarized as follows:

- At (0o) (horizontal) pipe: semi-segregated flow prevails as the flow pattern.
- At (+15o) (inclined up) pipe: semi-segregated flow prevails as the flow pattern.
- At (-15o) (inclined down) pipe: semi-segregated flow prevails as the flow pattern.

Figure 4.65 concentrates on the velocities profile at plane X5.5 which represents a comparison of velocities profile for oil and water in terms of changing the pipe inclinations. The parabolic velocity profile for water at horizontal pipe covers the complete cross-section of the pipe diameter while it is twisted in cases of inclined pipes with a reduction of the water velocity at the top. In case of inclined up, the water layer accumulates at the pipe bottom due to axial pulling back gravity force that resists the whole flow movement. Plugging the water to large cross-section area at the bottom causes the oil layer at the top to accelerate up while they are forced to shift up from the bottom. In case of inclined down, the water layer moves very fast forward the pipe outlet in the direction of both the axial gravity force and the flow direction that lead to low water accumulation at the bottom. The high movement of the water layer at the bottom increases pulling water from the top that enhances mixing or delay separation. The oil at the top moves slowly and resists the flow movement because it occupies large cross

section area. The high mixing for both oil and water shows wide range of both velocity profiles across the diameter. The oil layer approaches the pipe bottom in case of inclined down due to low water height. Figure 4.66 shows the drift velocity for inclined pipes at the plane X5.5. The figure shows that water holdup increases during inclined up and reduces as the pipe inclined down referring to the horizontal pipe. At the bottom, the drift velocities are very high due to high water velocity. At the top, the drift velocities are low due to less water amount and high oil velocity. The drift in inclined down shows the highest, then the horizontal pipe and inclined up pipe has the lowest drift at water separation.

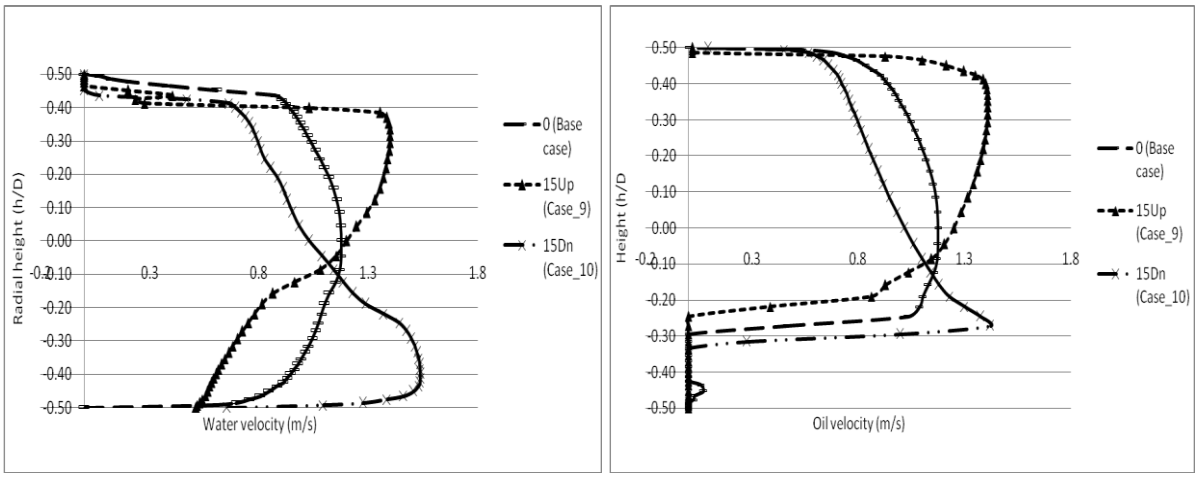

Figure 4.65: Comparison of radial water and oil velocity profiles for different pipe inclinations -15, 0, and +15^{o} at X5.5 (L/D = 35.7)

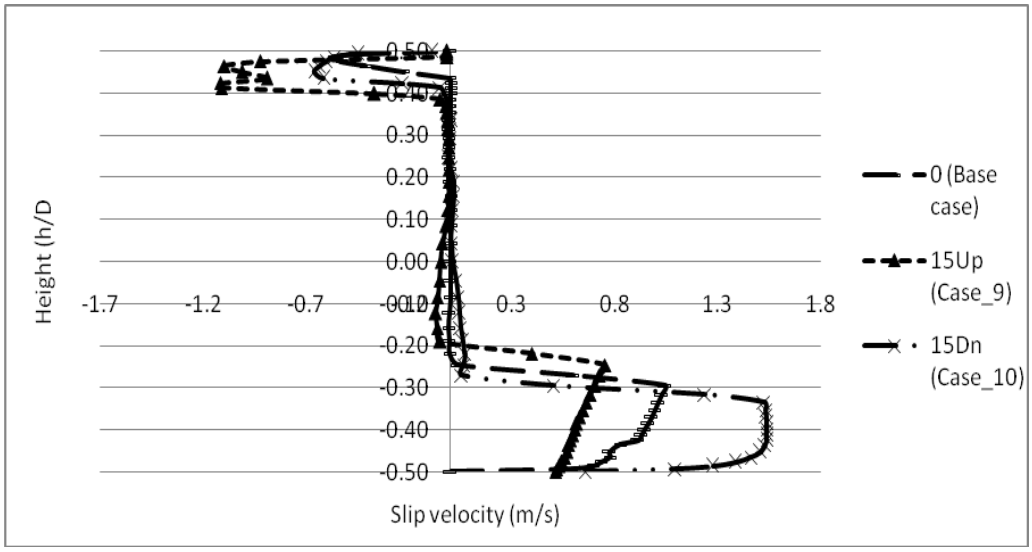

Figure 4.66: Comparison of radial oil/water drift velocity for different pipe inclinations (drift: -15, 0, and +15)

Figure 4.67 shows the effect of pipe inclinations on the water local concentration. It shows that during upper inclination separation rate reduces and during down inclination separation rate accelerates. Mixing of oil-water in inclined up pipe increases [Kumara et al. (2010)]. Figure 4.68 compares the influence of the pipe inclinations on the mixing zone at X5.5. The figure shows that all cases have almost the same separation rate. However, the water holdup height is shifted according to the case. The mixing range height of h/D is between (0.28 to 0.4) for horizontal pipe, (0.32 to 0.45) for inclined up, and (0.23 to 0.35) for inclined down pipe. The reason for the difference in water holdup based on pipe inclination is that the gravity force is more dominant at inclined pipes that act to accelerate or decelerate water.

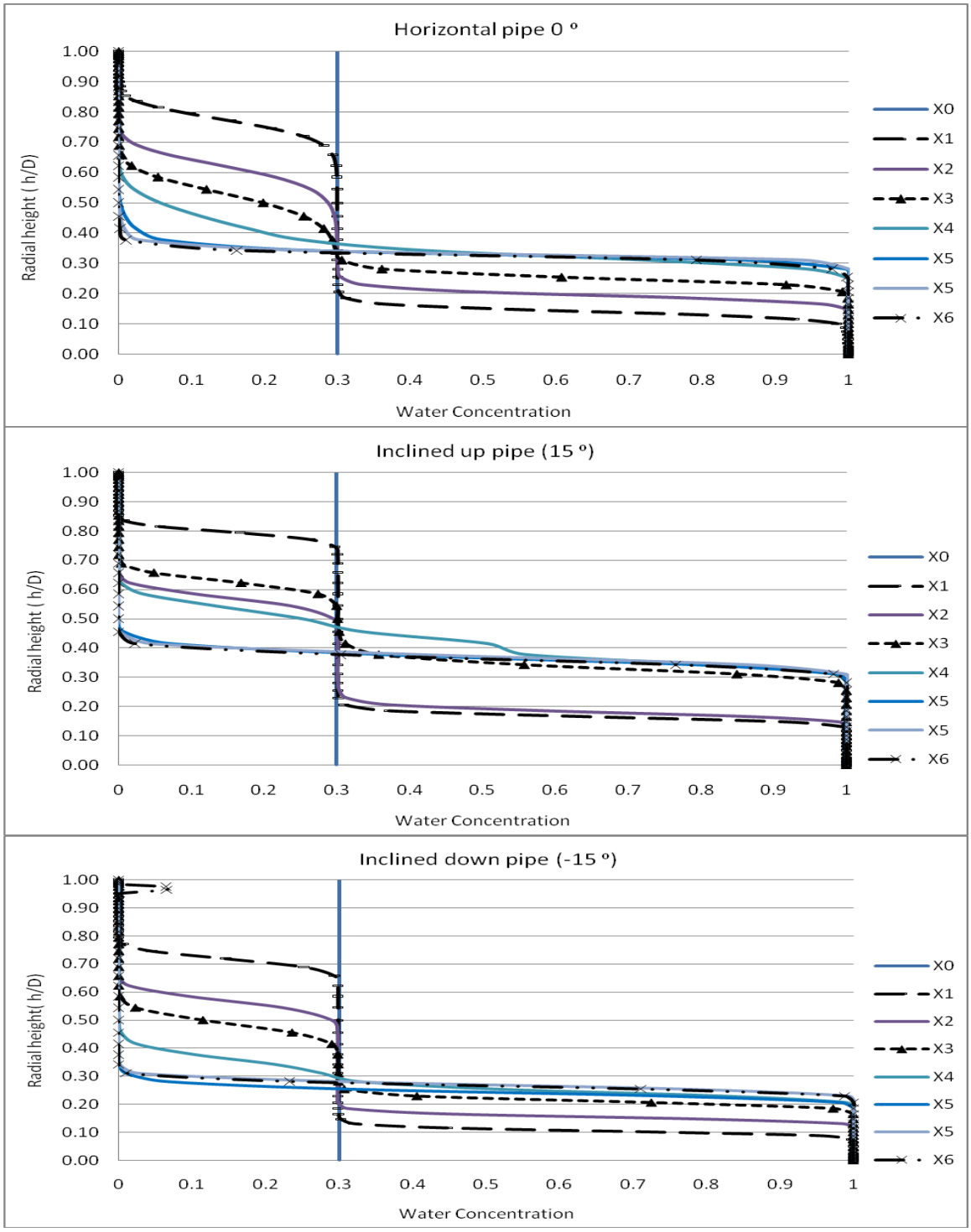

Figure 4.67: Variation of radial water concentration in vertical position of different Pipe inclinations

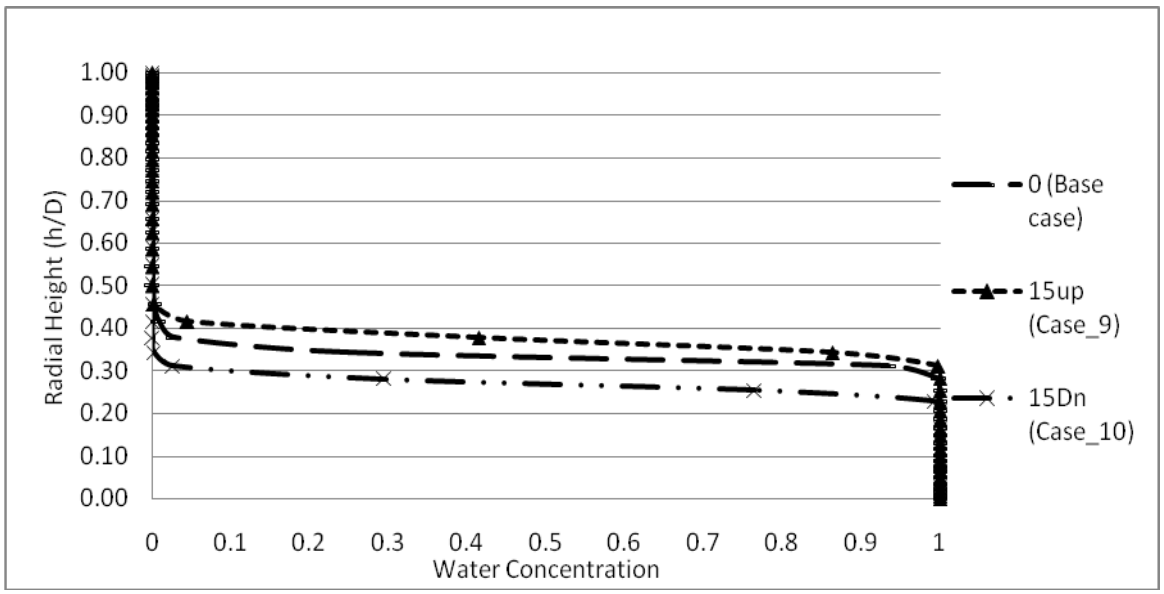

Figure 4.68: Variation of water concentration in vertical position for different pipe inclinations

The flow pattern outcome from different piping geometry changes can be summarized as follows and presented in Figure 4.69:

- Increasing pipe diameter results in increasing the mixing zone.
- Inclined up increases water holdup and inclined down reduces it.

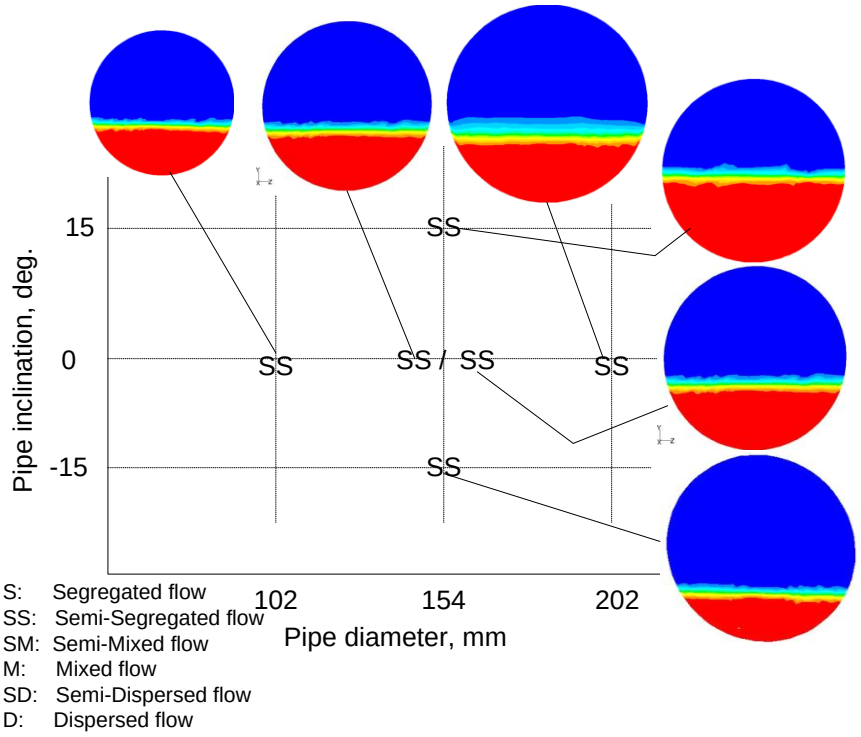

Figure 4.69: Observed flow patterns at different pipe diameters and pipe inclination

Slip ratio and water holdup

Water holdup is calculated based on the slip ratio factor calculation for different operation and design cases as per equations 1.3 and 3.6. The results are tabulated in Table 4.9. Moreover, the water holdup and slip ratio factor are presented in Figure 4.70. Both graphs perform in the same behavior. The slip ratio factor gives an indication of water holdup for different variables. If the ratio is unity, the velocity is equal for both phases and no water holdup. If the ratio is less than unity, that means water travels faster than oil and the opposite is true. If the ratio is greater than unity, it is an indication of high oil velocity and high water holdup. Referring to Figure 4.70, the followings are observed:

- ✓ The higher the mixture velocity, the higher the water holdup.
- ✓ With increasing of oil viscosity, there is a sudden drop in water holdup.
- ✓ Increasing pipe diameter, increases water holdup.
- ✓ The higher the water flow rate, the higher the water holdup.
- ✓ Upward inclination increases water holdup while downward inclination reduces the water holdup.
- ✓ Increasing oil to water density ratio, decreases water holdup.

Table 4.9: Water holdup evaluation

Variables	D	V_m	$\frac{WC}{100}$	μ_o	ρ_o	V_o	V_w	S	Hw
	mm	m/s	-	cP	Kg/m^3	m/s	m/s	-	-
Base case	154	1	0.3	2	830	1.17	1.07	1.09	0.32
Case 1(0.5 m/s)	154	0.5	0.3	2	830	0.6	0.58	1.04	0.31
Case 2 (2.0 m/s)	154	2	0.3	2	830	2.23	2.03	1.1	0.32
Case 3(15 cP)	154	1	0.3	15	830	1.02	1.16	0.88	0.27
Case 4 (30 cP)	154	1	0.3	30	830	0.85	1.17	0.73	0.24
Case 5(102 mm)	102	1	0.3	2	830	1.2	1.15	1.05	0.31
Case 6 (202 mm)	202	1	0.3	2	830	1.16	1.09	1.07	0.31
Case 7 (20 WC)	154	1	0.2	2	830	1.16	1.06	1.08	0.21
Case 8 (50 WC)	154	1	0.5	2	830	1.16	1.17	1.0	0.50
Case 9 (15 deg. Up)	154	1	0.3	2	830	1.25	0.81	1.54	0.40
Case 10 (15 deg. Dn)	154	1	0.3	2	830	1.1	1.48	0.75	0.24
Case 11 (998 kg/m^3)	154	1	0.3	2	998	1.0	1.0	1.0	0.30
Case 12 (662 kg/m^3)	154	1	0.3	2	662	1.18	1.15	1.03	0.31

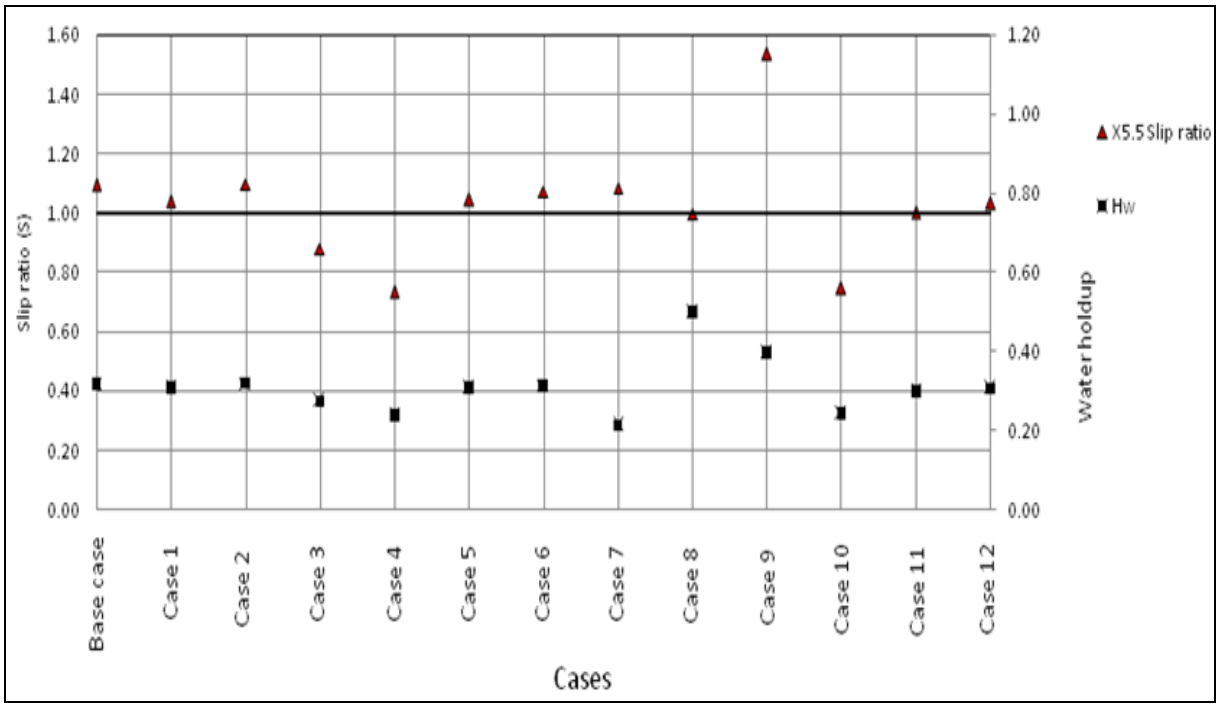

Figure 4.70: Water holdup and slip ratio monitoring

4.5.4 Corrosion Calculation

The corrosion calculation is not absolute for each case. It is a comparison based on each variable. By assuming corrosive environment for operation of different operation and design conditions, the internal corrosion can occur due to availability of free water layer. Accordingly, the expected corroded surface area that is covered by at least 90% free water layer, the corroded surface area is determined by locating the height of the water layer for each variable. The wetted surface area (A_{sw}) with at least 90% free water below the cord (c) and by calculating the corrosion rate referring to the base case per equation 3.12, the results are tabulated below for each variables.

Effect of inlet conditions

The inlet condition variables affect the corrosion rate as shown in Table 4.10. The corrosion based on the wetted-water surface area increases in two cases and reduces in two cases. By reducing the velocity to 0.5 m/s and increasing the inlet water contents to 50% WC, the wetted-water area increases by 1% and 26% respectively. By increasing the velocity to 2.0 m/s and reducing the inlet water contents to 20% WC, the corrosion rate reduces by 16% and 13% respectively.

Table 4.10: Corrosion of wetted-water surface area based on the inlet conditions

Cases	Diameter (D) (mm)	h_n Dim/less	CeS_n Dim/less	Note
Base case	154	0.311	1.00	Base wetted-water area
Case 1(0.5 m/s)	154	0.320	1.01	Increase by 1%.
Case 2 (2 m/s)	154	0.227	0.84	Reduce by 16%.
Case 7 (20% WC)	154	0.2434	0.87	Reduce by 13%.
Case 8 (50% WC)	154	0.4595	1.26	Increase by 26%.

Effect of oil properties

The corrosion with variable oil physical properties is different from inlet condition variables effect as shown in Table 4.11. The corrosion rate increases only in one case when oil density is less than water density to show a corrosion rate increase by 1%. In three cases, the corrosion rates reduce by 40%, 55% and 100% for 15 cP, 30 cP and 998.2 kg/m^3, respectively.

Table 4.11: Corrosion of wetted-water surface area based on the oil properties

Cases	Diameter (D) (mm)	h_n Dim/less	CeS_n Dim/less	Note
Base case	154	0.311	1.00	Base wetted-water area
Case 3(15 cP)	154	0.119	0.60	Reduce by 40%.
Case 4 (30 cP)	154	0.068	0.45	Reduce by 55%.
Case 11 (998.2 kg/m^3)	154	0	0.00	Reduce by 100%.
Case 12 (662 kg/m^3)	154	0.320	1.01	Increase by 1%.

Effect of piping geometry

The piping geometry variables affect the corrosion rate as shown in Table 4.12. The corrosion rate increases in two cases and reduces in two cases. By reducing the pipe diameter to 102 mm and having the pipe inclined 15 degrees up, the corrosion rate increases by 1% and 4% respectively. By increasing the pipe diameter to 202 mm and having the pipe inclined 15 degrees down, the corrosion rate reduces by 2% and 14% respectively.

Table 4.12: Corrosion of wetted-water surface area based on the piping geometry

Cases	Diameter (D) (mm)	h_n Dim/less	CeS_n Dim/less	Note
Base case	154	0.311	1.00	Base wetted-water area
Case 5 (102 mm)	102	0.3178	1.01	Increase by 1%.
Case 6 (202 mm)	202	0.3005	0.98	Reduce by 2%.
Case 9 (15 deg. Up)	154	0.3337	1.04	Increased by 4%.
Case 10 (15 deg. Down)	154	0.2389	0.86	Reduce by 14%.

CHAPTER 5

INTERNAL TURBULATOR DEVICES

5.1 Introduction

This is a preliminary work in the field of two-phase turbulator devices. The internal turbulator device is a new application in multiphase immiscible fluid. The device is installed inside a flanged spool, Figure 5.1. The spool can be inserted at certain locations along the production pipelines to control the flow patterns at certain locations. Two different designs of turbulator devices are selected, Type-A and Type-B showed in Figure 5.1 and 5.3 respectively. These two types are evaluated at two different operation conditions as per Table 5.1.

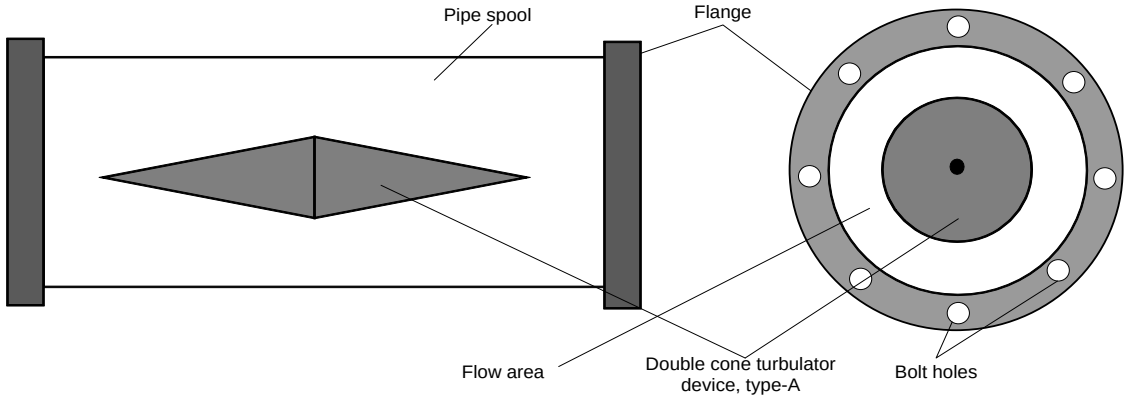

Figure 5.1: Pipe spool including turbulator device, type-A

The reported applications of the turbulator device are mainly limited for blending and mixing in the chemical process industry for polymer melt and additives. The scale of segregation between the liquids is greatly reduced by this process such that eventually diffusion can complete the mixing process [Cao, et al. (2003)]. The operation of the turbulent devices is covered in the following paragraph. However, the installation of the turbulator devices is not covered in this work. It requires support bars to fix the turbulator device inside the pipe spool fixed in certain design.

5.2 Operation Conditions

The operation conditions are subtracted from Table 4.1 and are shown in Table 5.1. The inlet flow is designed as a segregated flow of oil and water entering the pipe as shown in Figure 5.2. The partition exists only at the entrance and no longitudinal partition. The volume ratio is 20 % water and 80% oil for turbulator device A-type and 30% to 70% ratio for type-B turbulator device. Type-A is used with a pipe of 100 mm inner diameter and type-B is used with 154 mm inner diameter pipe. Both pipes operate at same operation conditions of 1.0 m/s for oil and water. The oil has a density of 830 kg/m3 and viscosity of 2 cp and the water has a density of 998.2 kg/m3 and viscosity of 1.0 cP.

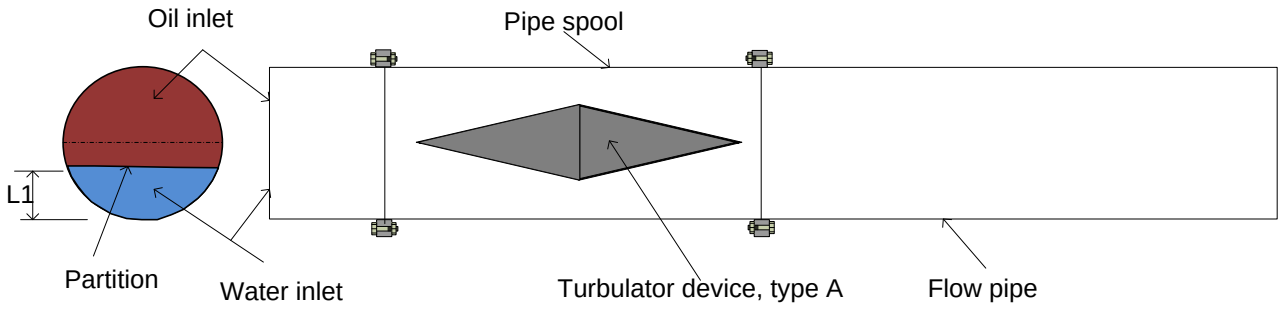

Figure 5.2: Entrance to pipe with a turbulator device

Table: 5.1: Operation condition for turbulator devices

Turbulator Devices Design (Case 13 & Case 14)	
Inlet flow pattern	Segregated Flow
Velocity (m/s): Oil/Water	1
Viscosity (cP): Oil/Water	2 / 1.002
Density (kg/m3): Oil/Water	830 / 998.2
Operating Press (MPa)	0.13
Operating temp (K)	298
Inner pipe Dia (mm): Oil/Water	100 or 154
WC%	20 or 30
Inclination (Degree)	0
Length (m)	6
Turbulator device	Type-A or Type-B

5.3 Turbulator Device System

The turbulator device system design consists of two parts: the design of the turbulator device and the design of the inlet flow for both fluids. The following sections cover these parts.

5.3.1 Turbulator Device Design

The present work includes two types of turbulator devices: Type-A and Type-B shown in Figure 5.1 and 5.3 respectively. These turbulators can be designed to provide certain velocities downstream the device. These velocities may assist to achieve certain flow patterns. The design of these two types is as follows.

Turbulator device: Type-A

The device, type-A, is shown in Figure 5.1. This type consists of a double cone. The turbulator device center is located at 1000 mm downstream the inlet for type-A. It can be designed so that the upstream velocity of 1.0 m/s can reach to 3.0 m/s at the device location to give a mixing that reduces water local contents to around 75%, per Figure 5.8.

The device A-type is sized based on the target flow pattern. For example, to get a mixture velocity of (V_2) of oil and water, per Table 5.1, flowing in a pipe of cross section area (A_1) that have oil and water as separated fluids each flows at velocity (V_1). By utilizing turbulator device A-type, the following steps are followed:

- Adjust the inlet of both oil and water to maintain same inlet velocity for both fluids based on the inlet volume fraction of each separated fluid and the fluid properties from Table 5.1 to fix the height (L_1). The adjustment of the inlet portions are covered in section 5.3.2.

By fixing the height, L_1, the target cross-section area is calculated based on the mixture target velocity, V_2:

  - Put the target velocity V_2, which is limited not to be more than V_1 by 2 m/s where $V_2 = V_1 + n$, $n \leq 2$.

  - $A_2 = A_1 \frac{V_1}{V_2}$

Now, the turbulator device is sized as follows:

The smallest flow cross section-area is at the middle of the double cones where both bases are attached. So the flow area is calculated based on the target velocity, V_2, then the cone base diameter, D_b, is identified:

$$D_b = \sqrt{\frac{4.(A - A_2)}{\pi}}$$

$$A_2 = A - A_b,\ A_b = \pi \frac{D_b^2}{4}$$

The base diameter, D_b, in this case is increased by 5% to have effective base diameter (D_{be}) and approximately equals 2/3 diameter of the pipe. The length of one cone in the flow direction equals the base diameter, D_b, adding to that a correction factor equals to the ratio of effective base diameter to the pipe diameter by the base diameter, (D_{be}/D)*D_b). Finally, the turbulator device, type-A, is designed as shown in Figure 5.2.

Turbulator device: Type B

Turbulator device, type-B, is shown in Figure 5.3. This type consists of a hollow cone. The cone base at type-B is located at 1000 mm downstream the inlet. It can be designed so that the upstream velocity of 1.0 m/s can reach to 3.0 m/s at the device location to give a mixing that reduces water local contents to 70% per Figure 5.9.

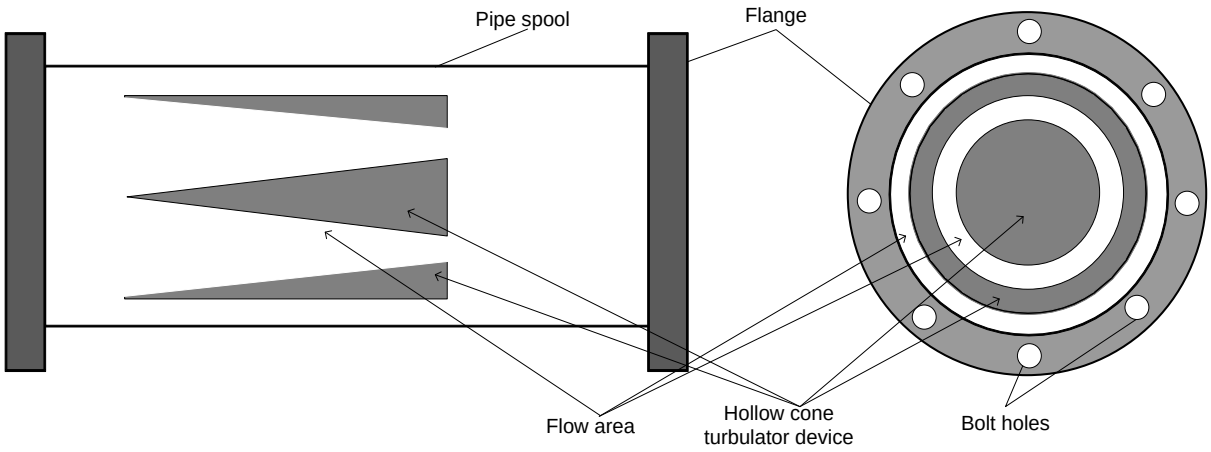

Figure 5.3: Type-B turbulator device

The turbulator device B-type is sized based on the target flow pattern. For example, to get a mixture velocity of (V_2) of oil and water, per Table 5.1, flowing in a pipe of cross section area (A_1) that have oil and water as separated fluids each flows at velocity (V_1) utilizing turbulator device B-type, the following steps are followed:

- Adjust the inlet of both oil and water to maintain same inlet velocity for both fluids based on the inlet volume fraction of each separated fluid and the fluids properties

from Table 5.1 to fix the height (L_1). The adjustment of the inlet portions are covered in section 5.3.2.

By fixing the height, L_1, the target cross-section area is calculated based on the mixture target velocity, V_2:

- Put V_2, where V2 = V_1 + n, n ≤ 2.
- $A_2 = A_1 \frac{V_1}{V_2}$

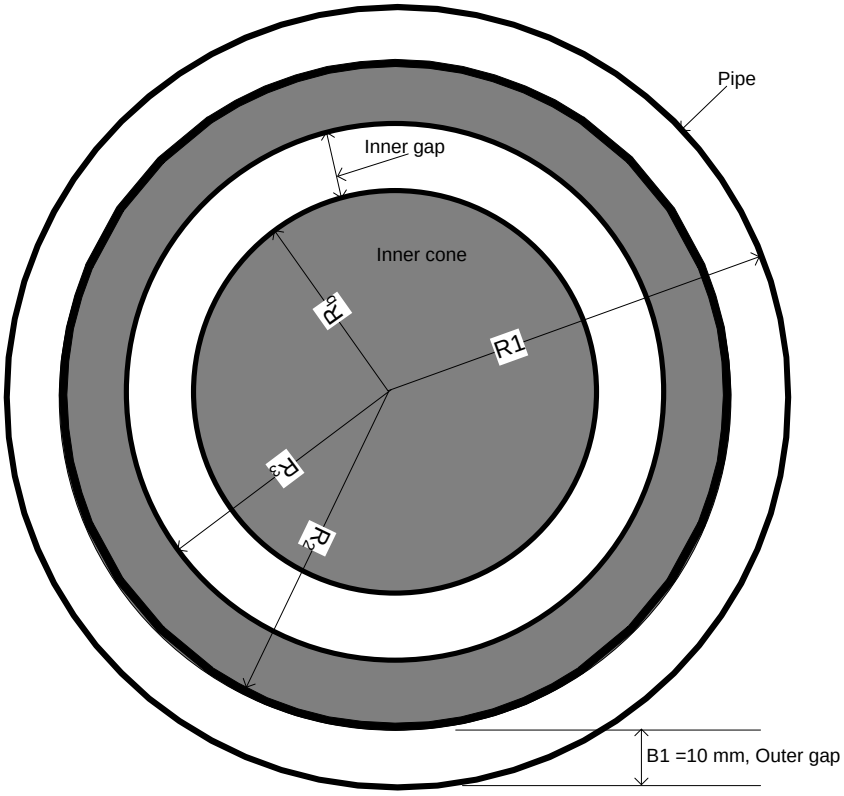

Figure 5.4: Type-B turbulator device gap detail

Now, the turbulator device is sized as follows:

The smallest flow area is at the base of the cone. So the flow area is calculated based on the target velocity, V_2, at the base:

$$A_2 = (A_{r3} - A_b) + (A - A_{r2}),\ A_b = \pi \frac{D_b^2}{4},\ A_{r2} = \pi \frac{D_{r2}^2}{4},\ A_{r3} = \pi \frac{D_{r3}^2}{4}$$

Referring to Figure 5.4:

Outer gap (B_1) is fixed to 10 mm and based on the inlet partition height of L_1 , the flowing relations are calculated:

$D_b = 2*R_1 - 2*L_1$, $Dr_2 = 2*R_1 - 2*B_1$, $D = 2R_1 = ID = 154$ mm,

$$D_{r3} = 2 * (\frac{A_2}{\pi} - R_1^2 + R_2^2 + R_b^2)^{0.5}$$

The diameter, D_{r3}, in this case is reduced by 5% to have effective diameter (D_{r3e}). The new required area is then calculated. The inner cone length in the opposite direction of the flow equals the effective diameter D_{r3}.

5.3.2 Inlet Flow Design

The flows enter as segregated flows (separated flows) at the inlet in a horizontal pipe by dividing the inlet to equivalent portions to the volume fractions. Oil enters through the upper portion while water enters from the lower portion. The two fluids move as stratified flows with some mixing at the interface that continue until they hit the existing turbulator device, type-A or B, downstream. The flows then get mixed with different degrees of mixing based on the turbulator device design and the operation conditions.

The inlet area is divided corresponding to the volume of each phase entering the pipe to make sure continuous separated flows before reaching the turbulent device. The inlet partition is design as follows:

The required inlet cross section-area is calculated for the separated fluid at velocity V1= 1.0 m/s entering the pipe based on the fluids properties from Table 5.1.

$$Q_w = V_w . A_w$$

$$A = \pi \frac{D^2}{4},\ A_o = A - A_w$$

$$A_w = 0.25 D^2 \{\pi - \cos^{-1}(2L_1 - 1) + (2L_1 - 1)[1 - (2L_1 - 1)^2]^{0.5}\}$$

Then by trial calculations based on the flow rates and the height, L_1, the calculations are repeated until getting the target volume fraction for both fluids as required of 20% WC for Type-A and 30% WC for Type-B. The mass flow rates, $\dot{m}_w$ and $\dot{m}_o$, and volume for both phase calculations are calculated per the following formulas:

$$W_w = V_w . \rho_w . A_w,\ W_o = V_o . \rho_o . A_w$$

$$Q_w = \frac{Q_w}{Q_w + Q_o}\%,\ Q_o = \frac{Q_o}{Q_w + Q_o}\%$$

5.4 Influence of Internal Turbulator Device

The water local contents or holdup is presented in longitudinal paths that are located at the pipe vertical center at different height, h, from the pipe bottom, per Figure 5.5. The paths are located at different heights as a percentage of the pipe diameter, D. The first and highest paths are very close to the pipe wall, where the first one, h = 0%D, is 2.0

mm above the wall and the highest one, h = 100%D, is 2.0 mm below the wall. The other paths are at 25%D, 50%D and 75%D. Two cross-section contours at Y-Z plane are located at 0.6 and 1.2 m downstream the inlet. The central vertical contour at X-Y plane presents the flow patterns along the pipe. One flow pattern type in noticed created at these two types of the turbulator devices. The created flow pattern is Oil and Dispersed Oil in Water (O&Do/w). Figure 5.6 and Figure 5.8 are related to type-A turbulator device. Figure 5.7 and Figure 5.9 are related to type-B turbulator device.

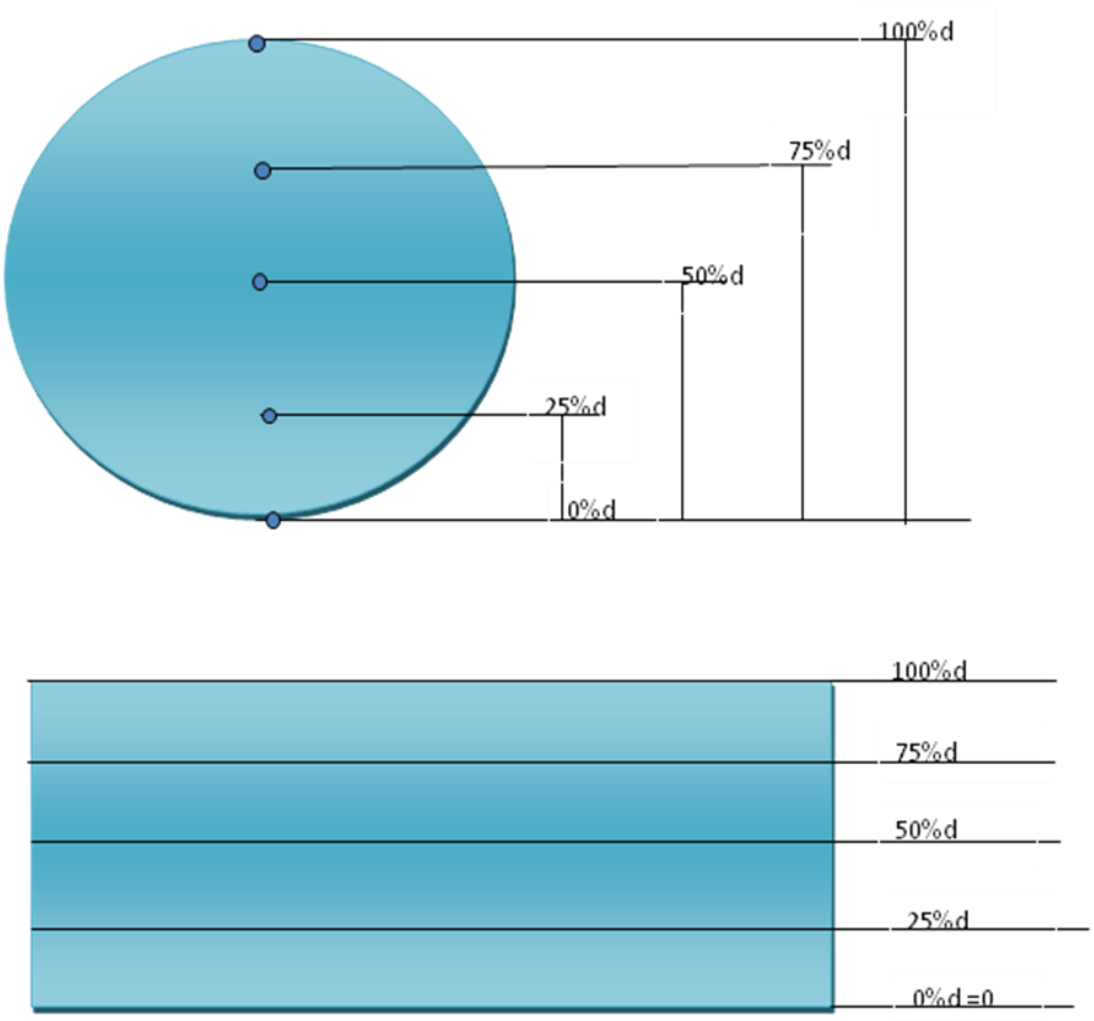

Figure 5.5: Radial and longitudinal pipe planes with longitudinal central lines at different height

Figure 5.6 shows water contours at cross-sections and longitudinal planes using type-A turbulator device. The cross section plans show two locations at 600 and 1200 mm downstream the inlet or X0.6 and X1.2 planes respectively. The X0.6 plane shows separated flows. The X1.2 plane shows mixed and pure phases. The mixed phase at the pipe bottom shows a mixture rising oil percentage at pipe bottom to around 25% oil. The upper phase is pure oil.

Figure 5.7 shows water contours at cross-sections and longitudinal planes using type-B turbulator device. The cross section plans show two locations at 600 and 1200 mm downstream the inlet or X0.6 and X1.2 planes respectively. The X0.6 plane shows separated flows. The X1.2 plane shows mixed and pure phases. The mixed phase at the pipe bottom shows a mixture rising oil percentage at pipe bottom to around 30% oil. The upper phase is pure oil.

Figure 5.8 shows water longitudinal concentration for turbulator type-A in a pipe of 100 mm diameter. It shows that there is no water available at the upper half (100%, 75% and 50%D). At level of 25%D, the water concentration jumps to around 62%. It then increases gradually to around 75% at the turbulator center, before it drops sharply to around 10%. The concentration increases fluctuating gradually to reach 100% at the exit. At pipe bottom (0%D), in general, the water concentration is 100% all over the pipe length. It has a drop in water concentration reaching to 75% in the range of L/D between 12 and 20 which is facing the change in 25%D level drop in concentration.

Figure 5.9 shows water longitudinal concentration for turbulator type-B in a pipe of 154 mm diameter. It shows that there is no water available at the upper half (100%, 75% and 50%D). At level of 25%D, the water concentration starts from around 30% and jumps to 100%. It drops gradually to 5% at L/D of 10 which is at the turbulator base. The concentration starts fluctuating in low range to reach zero% at the exit. At pipe bottom (0%D), the water concentration is 100% up to L/D = 25. Then there is a gradual drop in the concentration without any justification.

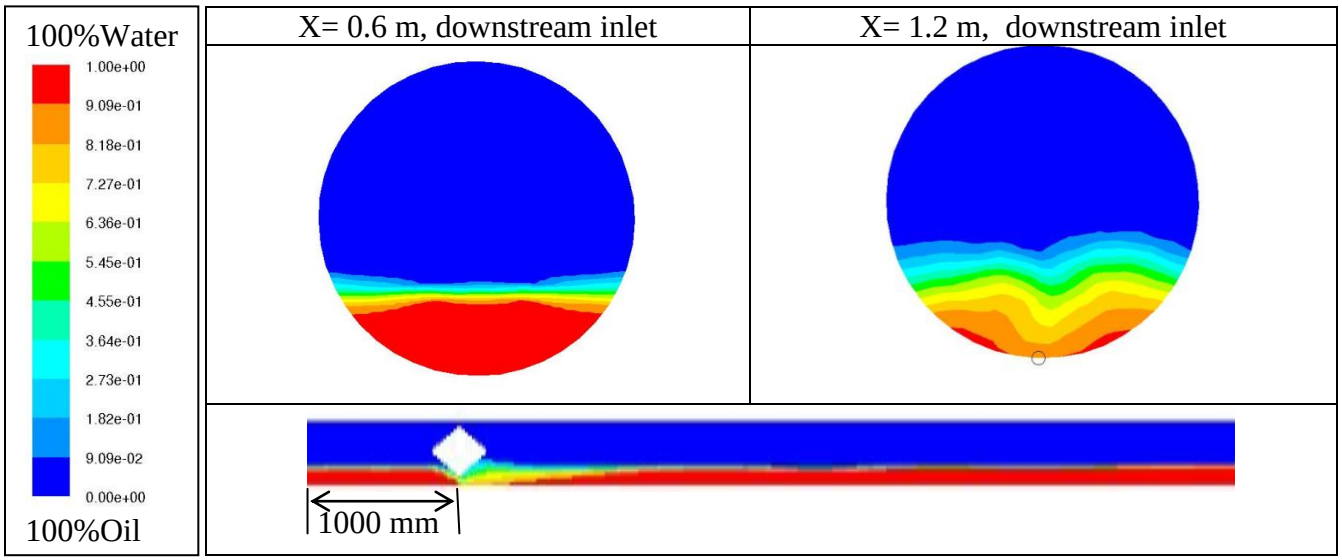

Figure 5.6: Water contours with Type-A turbulator device for different Y-Z-plane and X-Y-plane at 1.0 m/s and 20% WC

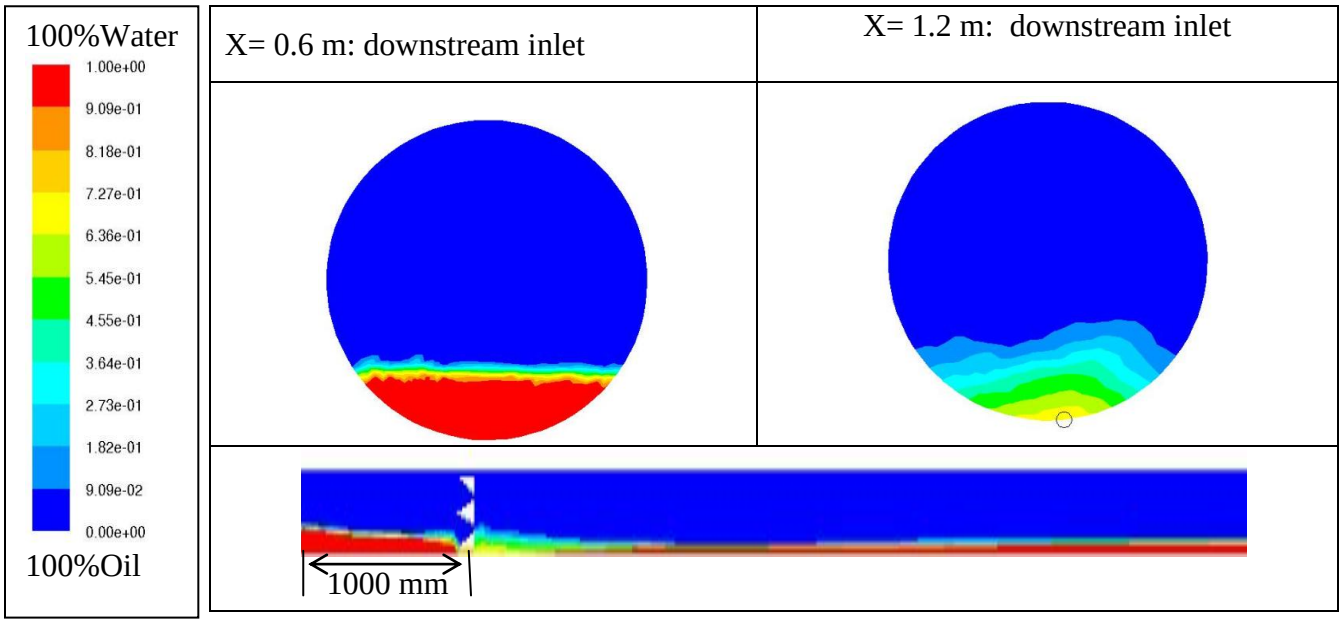

Figure 5.7: Water contours with Type-B turbulator device for different Y-Z-plane and X-Y-plane at 1.0 m/s and 30% WC

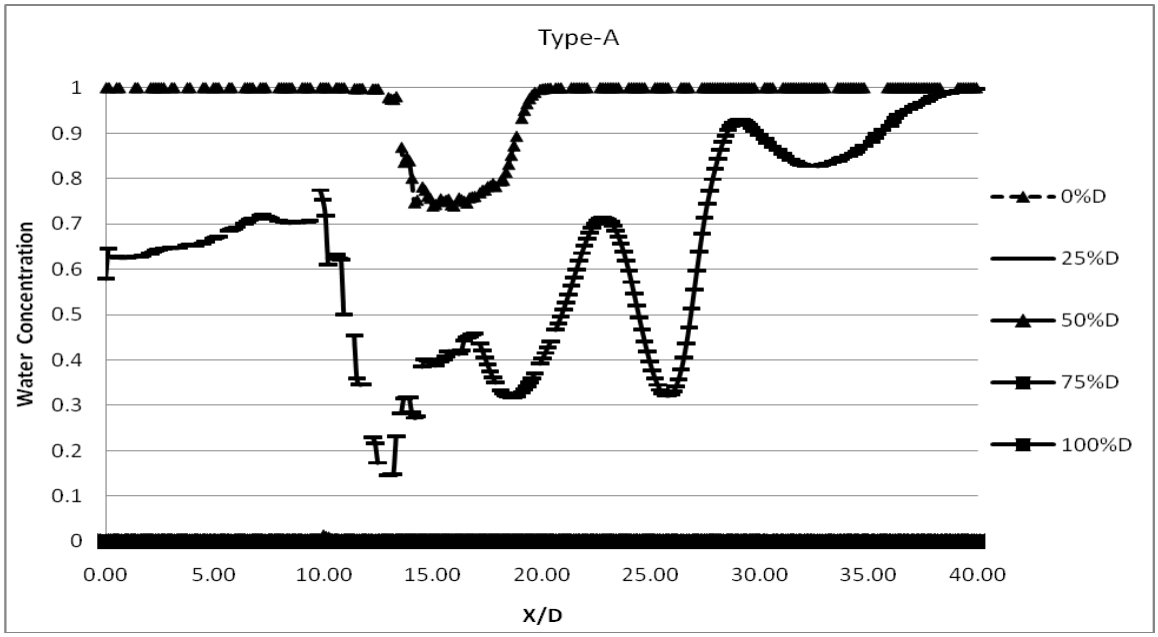

Figure 5.8: Comparison of water concentration along 100 mm inner diameter pipe with A-type turbulator device at different longitudinal centered heights for velocities of 1.0 and 20% WC (Case_13)

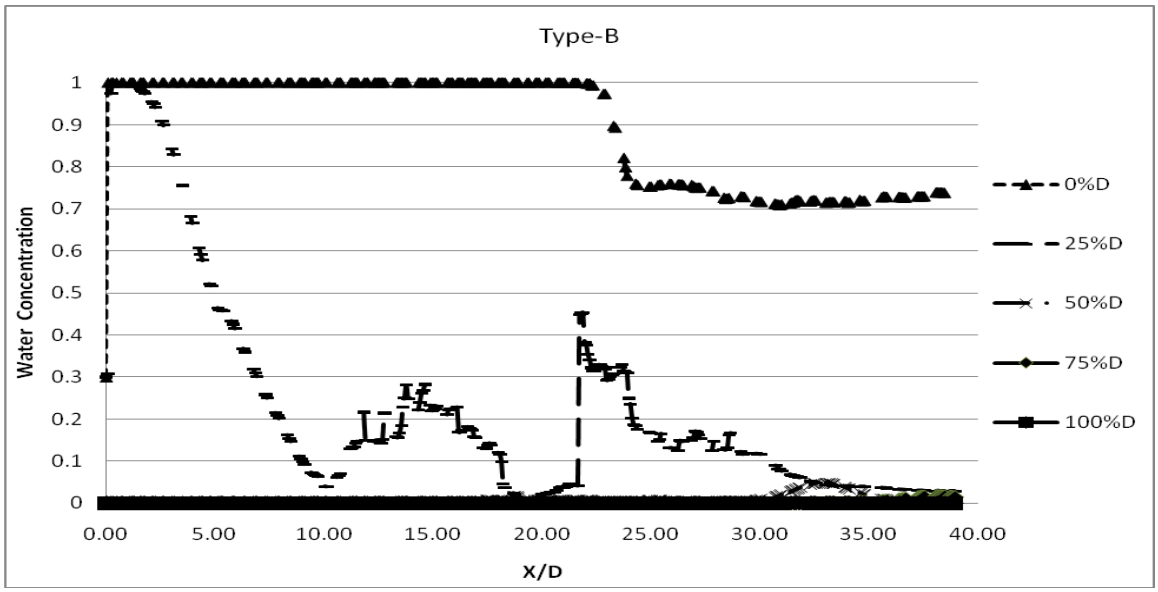

Figure 5.9: Comparison of water concentration along 154 mm inner diameter pipe with B-type turbulator device at different longitudinal centered heights for velocities of 1.0 and 30% WC (Case_14)

CHAPTER 6

CONCLUSIONS AND RECOMMENDATIONS

The following conclusions and recommendations can be reached based on the detailed study of the present work about different operation conditions of oil-water flow in horizontal and near horizontal pipes as per Table 4.1.

6.1 Conclusions

Several conclusions can be drawn from the result of the present work. These conclusions are applicable to the study of flow patterns and corrosion in multiphase pipelines.

General:

- The present work shows high matching to the previous experiments which reflects the model validity and practicality.
- It shows that the design conditions have significant effects on the change of the flow pattern that are immediately reflected in the corrosion rate change.
- The gravity impact changes as the design and operation conditions changes.

Effect of inlet conditions:

- The flow patterns change based on the operation conditions.
- As velocity increases, the phase separation is delayed.
- Water cut significantly affects the oil-water separation.
- Increasing inlet water contents leads to more water separation and less entrainment.
- By reducing the velocity to 0.5 m/s and increasing the inlet water contents to 50%, the corrosion rate increases by 1% and 26%, respectively, where gravity power is increases.
- By increasing the velocity to 2.0 m/s and reducing the inlet water cut to 20%, the corrosion rate reduces by 16% and 13%, respectively, where gravity force power is reduced.
- Even with identical water cut, the local water fraction (water holdup) can be very different dependent on the flow pattern existing in the pipe.

Effect of oil physical properties:

- Increasing the oil viscosity increasse its tendency to be more mixed and/or be dispersed flow. This result is also commented by Yeo et al. (2000).
- Increasing oil viscosity may cause oil layer holds up in the pipe top that leads to accelerate the water layer at the bottom.
- Oil-water mixing is directly proportional to the density difference between oil and water that is dominated by the gravity force.

- Reducing density difference between oil-and-water reduces the gravity affect and increases mixing range and the opposite is right. Large density differences increases the phases separation and that agrees with Yeo et al. (2000). Similar observation was reported by Charles et al. (1961) for their experimental work of equal density oil-water by noticing concentric water with oil flowing in the core.
- By increasing the oil density to 998.2 kg/m3, the flow pattern becomes dispersed.
- The corrosion rate increases only in one case when oil density is less than water density to show a corrosion rate increase by 1%. In the other three cases, the corrosion rate shows a reduction by 40%, 55% and 100% for 15 cP, 30 cP and 998.2 kg/m3 respectively.

Effect of piping geometry:

- Increasing pipe diameter increases mixing zone toward dispersion flow pattern to agree with Valle (1998).
- The degree of mixing largely depends on the pipe inclination where upward inclinations enhance the mixing zone due to high effect of gravity on the follow causing water back rolling.
- Upper inclination increase phase accumulation at pipe bottom due to water flow deceleration by gravity force acting back. This observation is in agreement with what was reported by Valle (1998) for 15^{o} upward inclined flow.
- Downward inclination reduces water accumulation at the pipe bottom due to flow acceleration by gravity force acting forward.

- The corrosion rate increases in both reducing the pipe diameter and having the pipe inclined up by 1% and 4%, respectively.
- By increasing the pipe diameter to 202 mm compare to the base case and having the pipe inclined 15 degrees down, the corrosion rate reduces by 2% and 14% respectively.

Effect of turbulator devices:

The turbulator devices based on the present work shows limited improvement in mixing zone. However, it could be a good tool to mitigate corrosion in pipelines.

- There is an uncertainty of using turbulator alone to mitigate corrosion in pipelines.
- It is expected to be very attractive using turbulator devices to create the suitable flow pattern to inject the right inhibitors at the right flow pattern.

6.2 Recommendations

The following are recommended future studies using the present work design and operating conditions.

Dimentional analysis:

i) Reynolds Number

The present work covers the Reynolds numbers (Re_m) for the mixture at the inlet of the pipe as tabulated in Table 6.1, 6.2 and 6.3 based on different variables. It is recommended to utilize the Re_m (7.97E+04) for all cases and calculate the required pipe diameter or inlet mixture velocities. So the target will be two variables: the inner diameter in case of investigating the inlet conditions and oil densities variables and inlet mixture velocity in case of investigating different inner pipe sizes. This work will generalize the picture for the flow pattern behavior by dealing with a common reference factor which is the Reynolds number at the mixture inlet.

Table 6.1: Change of pipe diameter based on inlet conditions

	Base	Inlet mixture velocity (m/s)		Water cut % (WC)	
Variable	1	0.5	2	20	50
Re_m (Calculated)	7.97E+04	3.99E+04	1.59E+05	7.39E+04	9.38E+04
Re_m (Recommended)	7.97E+04				
ID (mm) (Calculated)	154.0	308.0	77.0	166.2	130.9

Table 6.2: Change of pipe diameter based on oil physical properties

	Oil viscosity (cP)		Oil density (kg/m3)	
Variable	15	30	662	998.2
Re_m (Calculated)	1.26E+04	6.37E+03	6.91E+04	9.04E+04
Re_m (Recommended)	7.97E+04			
ID (mm) (Calculated)	977.9	1928.6	177.7	135.8

Table 6.3: Change of inlet mixture velocity based on pipe size

	Piping geometry		
Variable	102	202	154
Re_m (Calculated)	5.28E+04	1.53E+05	7.97E+04
Re_m (Recommended)	7.97E+04		
V_m (mm) (Calculated)	1.5	0.8	1.0

Turbulator devices

As the present work in the field of turbulator devices is preliminary, addition work is required. It could be a good idea to investigate using lower water droplets diameter and inject a stream to the oil-water two phase flows as a chemical inhibitor. The objective is to check the mixing effectiveness of the inhibitor using turbulator devices and find the best location of the injection nozzle.

REFERENCES

Abdulkadir, M. and Hernandez-Perez, V. "The Effect of Mixture Velocity and Droplet Diameter on Oil-water Separator using Computational Fluid Dynamics (CFD)." World Academy of Science, Engineering and Technology, 2010: 61.

Al-Wahaibi, T. and Angeli, P. "Droplet size and velocity in dual continuous horizontal oil–water flows." chemicalengineeringresearch and design 86 (2008): 83 – 93.

Al-Yaari, M., Soleimani, A., Abu-Sharkh, B., Al-Mubaiyedh, U., Al-sarkhi, A. "Effect of drag reducing polymers on oil–water flow in a horizontal pipe." International Journal of Multiphase Flow, 2009: V- 35, PP. 516–524.

Angeli, P., Hewitt, G.F. "Flow structure in horizontal oil-water Flow." International Journal of Multiphase Flow , 2000: V-26, PP. 1117-1140.

ANSYS, inc, 2002,"Fluent user guide",www.fluentusers.com.

Arirachakaran, S, Oglesby, K.D., Malinowsky, M. S., Shoham, O., Brill J. B. " "An Analysis of Oil/Water Flow Phenomena in Horizontal Pipes." SPE 18836, 1989.

Atmaca, S., Sarica, C., Zhang, H. –Q, and Al-Sarkhi, A. S. " Characterization of oil water flows in inclined pipes." SPE 115485, 2008.

Ayello, François; Li, Chong; Tang, Xuanping; Cai, Jiyong; Nešić, Srdjan; Cruz, C. Ivan T.; Al-Khamis, Jamal N. "Determination of Phase Wetting in Oil–Water Pipe Flows." (NACE International) Paper No.08566, no. Corrosion/2008 (2008).

Bannwart, A., Rodriguez O., Carvalho, C. ,Wang, I., Vara, R. " Flow Patterns in Heavy Crude Oil-Water Flow." Transactions of the ASME , Sep. 2004: P.184, Vol. 126.

Barth, T. J. and Jespersen, D., "The design and application of upwind schemes on unstructured meshes".Technical Report AIAA-89-0366, AIAA 27th Aerospace Sciences Meeting, Reno, Nevada, 1989.

Cai, J., Nesic, S. Li, C., and Waard, C. de; "Modeling of water wetting in oil water pipe flow", NACE 2004, Paper n. 04663, pp. 1-19, 2004.

Cao, Q, A. L. Ventresca, K.R. Sreenivas, and A. K. Prasad. "Instability due to Viscosity Stratification Downstream of a Centerline Injector." The Canadian Journal of Chemical Engineering 81 (Oct. 2003).

Charles, M.E., Govier, G.W. and Hodgson, G.W.: "The Horizontal Pipeline Flow of Equal Density Oil-Water Mixture," Can. J. Chem. Eng., 39, pp. 27-36 (1961).

Dayalan, E., de Moraes F. D., Shadley, J. R., Shirazi, S. A., and Rybicki, E. F. "CO2 corrosion prediction in pipe flow under FeCO3 scale-forming conditions." paper No. 51, NACE Corrosion/98, 1998.

Doyle, L., " the Independent / UK". "Oil Gushes into Arctic Ocean from BP Pipeline ." www.commondreams.org/headlines06/0321-06.htm, March 21, 2006.

Efird, K. D. and Jasinski, R. J. "Effect of the crude oil on corrosion of steel in crude oil/brine production." corrosion/89, 1989: Vol. 45, No-2.

Flores, J. G., Sarica, C., Chen, T. X., and Brill, J. P., "Investigation of Holdup and Pressure Drop Behavior for Oil-Water Flow in Vertical and Deviated Wells", ETCE-98, Paper No. 10797, 1997.

Habib, M.A., Said, S.A.M., Badr, H.M., Hussaini, I., and Al-Bagawi, J.J. "Effect of geometry on flow field and oil/water separation in vertical deadlegs." International Journal for Numerical Methods in Heat & Fluid Flow, 2005: Vol. 15 No. 4, pp. 348-3.

Hussain, S. A., Xu, X.Y., Hewitt, G. F. "Water Local Volume Fraction on Oil in Water Dispersion." Journal of Applied Fluid Mechanics, 2008: Vol. 1, No. 2, pp. 57-63.

Gao, H., Gu. Han-Yang, and Guo, Lie-Jin. "Numerical study of stratified oil–water two-phase turbulent flow in a horizontal tube." International Journal of Heat and Mass Transfer, 2003: V-46, PP. 749–754.

Kenics "www.kenics.com", Chemineer. "static mixing technology." Bulletin 800, 10M-BK-7, 1998.

Koch, Gerhardus H., Brongers, Michiel P.H., Thompson, Neil G., Virmani, Y. Paul and Payer, J.H. "Corrosion Costs and Preventive Strategies in the United States", PUBLICATION NO. FHWA-RD-01-156, 2001.

Kumara, W.A.S., Halvorsen, B.M., Melaaen, M.C. " Particle Image Velocimetry for Characterizing the Flow Structure of Oil–Water Flow in Horizontal and Slightly Inclined Pipes." Chemical Engineering Science, 2010: V-65, PP. 4332–4349.

Lovick, J. and Angeli, P.: "Experimental Studies on the Dual Continuous Flow Pattern in Oil-Water Flows," Int. J. Multiphase Flow, 30, pp. 139-157 (2004).

Lum, J.Y.-L.,Al-Wahaibi, T. ,Angeli, P. "Upward and downward inclination oil–water flows." Multiphase flow 32 (2006): 413–435.

Mandal, T. K., Chakrabarti, D.P., and Das, G. "Oil Water Flow through Different Diameter Pipes; Similarities and Differences." Trans IChemE, Part A, Chemical Engineering Research and Design, 2007: V- 85(A8), PP. 1123–1128.

Martinez, A.E., INTEVEP, S.A., Arirachakaran, S., Shoham, O., and J,P. Briil. " Prediction of Dispersion of Viscosity of Oil/Water Mixture Flow in Horizontal Pipes." SPE 18221, 1988.

Maxwell, J. B. "Data Book on Hydrocarbons", 9th edition by Huntington, N.Y. : R.E. Krieger Pub. Co., 1975, ©1950.

Morales, A. Rosanel. "Fluid Shear Effects of Centrifugal Pump On Oil-Water Flow" thesis, University of Tulsa, 2009.

Nadler, M., and Mewes, D. "Flow induced emulsification in the flow of two immiscible liquids in horizontal pipes." Int. J. Multiphase Flow , 1997: Vol. 23, No. 1, pp. 55-68.

Nesic´, Srdjan. "Key issues related to modelling of internal corrosion of oil and gas pipelines – A review." Corrosion Science 49 (Dec. 2007): 4308–4338.

Nyborge, R. "Controlling Internal Corrosion in Oil and Gas Pipelines ." Business briefing: Exploration & Production: the oil & gas review , 2005: 2005-issue 2.

Patankar, S. V., "Numerical Heat Transfer and Fluid Flow", Hemisphere Publishing corporation, 1980.

Patankar, S. V. and Spalding, D. B., "A Calculation Procedure for Heat, Mass and Momentum Transfer in Three-dimensional Parabolic Flows", International Journal of Heat and Mass Transfer, Vol. 15, pp. 1777-1787, 1972.

Rojas-Figueroa, A., and Fairuzov, Y. V. "Numerical Simulation of Corrosion Inhibitor Transport in Pipelines Carrying Oil-Water Mixtures." (Journal of Energy Resources Technology) 124 /239 (Dec. 2002).

Russell, T.W.R. Hodgsen, G.W. and Govier, G.W.: "Horizontal Pipeline Flow of Mixtures of Oil And Water," Can. J. Chem. Eng., 37, pp. 9-17 (1959).

Saudi Aramco Engineering Encyclopedia, 2005.

Shi, Hua. "A Study of Oil-Water Flows in Large Diameter Horizontal Pipelines" Thesis (Ohio University), Nov. 2001.

Shi, H., Wang, H., Jepson, W. P. " Predicting of Water Film Thickness and Velocity for Corrosion Rate Calculation in Oil-Water Flows." Corrosion/02, paper no 02500, 2002.

Stamixco "www.stamixco.com". " GV static mixer product bulletin." GV-2.2, 2006.

Tems, R.D. and Al Zahrani, A. "Cost of Corrosion in Oil Production and Refining, SAUDI Aramco Journal of Technology Summer, 2006.

Trallero, J. L., Cem Sarica, and J. P. Brill. "A Study of Oil/Water Flow Patterns in Horizontal Pipes." Society of Petroleum Engineering/SPE-36609, 1997.

Valle, A. "Multiphase Pipeline Flows in Hydrocarbon Recovery ." Multiphase Science and Technology, 1998: V-10, issue-1, pp 1–139.

Vedapuri, D., Bessette, D., and Jepson, W. P. "Segregated flow model to predict water layer thickness in oil-water flows in horizontal and slightly inclined pipelines." Multiphase-97/BHR Group, 1997.

Vielma, M., Atmaca, S., Sarica, C., & Zhang, H., "Characterization of Oil/Water Flows in Horizontal Pipes", SPE projects, facilities and construction (2008).

Wang, H. B., H. Shi, T. Hong, C. Kang, and W. P. Jepson. "Characterization of Inhibitor and Corrosion Product Film Using Electrochemical Impedance Spectroscopy (Eis)." Corrosion/2001, Paper No. 01023, 2001.

Xu, X-X. "Study on oil–water two-phase flow in horizontal pipelines." Journal of Petroleum Science and Engineering 59 (2007): 43-58.

Yeo, L. Y., Matar, O. K., Perez de Ortiz, and Hewitt, G. F. " Phase Inversion and Associated Phenomena." Multiphase Science and Technology, 2000: V-12, issue-1, pp 51-116.

Curriculum Vitae

Name:	Abdullah Misfer Al-Otaibi
Nationality:	Saudi Arabia
Address:	Al-Khubar, western region, Saudi Arabia P.O Box 12729 Dhahran, Saudi Arabia 31311
Telephone No.:	00966-55-383-0283
Email:	abuturki8@yahoo.com

Abdullah M. Al-Otaibi is a heat exchangers engineer at Saudi Aramco Oil Company, Consulting Services Department, Dhahran, Saudi Arabia. He received his B.S. degree in Mechanical Engineering in 2001 from King Fahd University of Petroleum & Minerals (KFUPM), Dhahran, Saudi Arabia.